ADDIS ABABA UNIVERSITY

INSTITUTE OF TECHNOLOGY

SCHOOL OF MECHANICAL AND INDUSTRIAL ENGINEERING

GRADUATE PROGRAM IN MECHANICAL ENGINEERING

Analysis of Mechanical Properties of Automotive Disc Brake by Finite Element of Method (FEM)

A Thesis Submitted to the Graduate School of Addis Ababa University

In Partial Fulfillment of the Requirements for the Degree of

Masters of Science in Mechanical Design

By

Oliyadi Dereje

Adviser: Dr. Daniel Tilahun

Co-Adviser: Mr. Muluken Maseresha

June, 2018

Addis Ababa, Ethiopia

Addis Ababa University
Addis Ababa Institute of Technology
School of Mechanical and Industrial Engineering

Analysis of Mechanical Properties of Automotive Disc Brake by Finite Element of Method (FEM)

By: Oliyadi Dereje

Approved by Board of examiners:

_____	_____	_____
Chair man of the school	Signature	Date
Daniel Tilahun (Associate Prof.)	_____	_____
Advisor	Signature	Date
Muluken Maseresha (MSc)	_____	_____
Co-Advisor	Signature	Date
Tadesse Nega (MSc)	_____	_____
Internal Examiner	Signature	Date
Dr. – Ir. Tamirat Tesfaye	_____	_____
External Examiner	Signature	Date

DECLARATION

I declare that this Thesis of **"Analysis of Mechanical Properties of Automotive Disc Brake by Finite Element of Method (FEM)"** is my original work and it does not worked by another person or has not been presented for degree of another university and I worked by my knowledge and experience.

Oliyadi Dereje	_____	_____
Student (MSc.)	Signature	Date
Daniel Tilahun (Associate prof.)	_____	_____
Advisor	Signature	Date
Muluken Maseresha (MSc)	_____	_____
Co-Advisor	Signature	Date

TABLE OF CONTENTS

ACKNOWLEDGEMENT

I would like to thanks my respective adviser **Dr. Daniel Tilahun** for Directing and supporting me by his long experience regarding to working varies research by Concept of mechanical design in mechanical engineering and also I gratitude my respective Co-adviser **Mr. Muluken Maseresha** for encouraging me through varies engineering concept and from his experience of working research by contacting in friendliness without any depression.

Finally, I would like to give thanks for **myself** in this period of working research for my activity to do this kind of research without any stress, depression, weakness and confusion. And I would like to give thanks for Addis Ababa institute of technology instructors of Mechanical Design in school of mechanical and industrial engineering and I would like to thanks all my friends of post graduate students of mechanical design and thermal engineering for exchanging engineering idea with me.

ABSTRACT

Excellent control of braking system in automobile is the essential for safety of braking performance. The brake disc is affected by type of friction material of brake pad. The determination of mechanical interaction that happen between brake disc of automobile and brake pads are very important in design consideration of braking system of automobiles.

For this investigation, the TOYOTA HIACE minibus taxi of 12 seats that used in Ethiopia City is taken as a sample. While, the problem occurred in this automobile is most of time failure of brake pads when braking is applied, and wear and fade of brake disc is occurred. Due to this kind of problem some time accident is happen; so the cause of this kind of problem happens in brake disc and brake pad of automobiles of TOYOTA HIACE minibus taxi that used in Ethiopian City is the idealization of selection of good performance friction material of brake pad with corresponding brake disc. Further, due to lack of consideration for selecting best friction material of brake pad with environmental friendliness, in the case of TOYOTA HIACE automobiles dust is produced from friction material of brake pad during braking time affect the aquatic life. Thus, the study of mechanical properties of brake disc with interface of brake pad by finite element method with the help of ANSYS software and experimental investigation of friction materials of brake disc used in local City taxi is very important regarding to best braking performance of automobiles and environmental protection.

Hence, as result obtain from analysis of finite element method with the help of software and experimental result of laboratory test; for safe environmental protection, reducing (or) free of Copper in brake pad of automobile especially in brake pad of TOYOTA-HIACE minibus 5L. And the use of Al-MMC brake disc with Ceramic brake pad is best for braking performance of automobiles rather than other interface.

Key words: Brake pad, Brake disc, Strength, Life cycle, ANSYS, Finite element method.

LIST OF FIGURE

LIST OF TABLE

NOMENCLATURE

t	time
L	liter
μ	Coefficient
g	gram
θ	angle
L	length
H	height
W	width
R_r	Effective Radius of Rotor
C_p	Specific Heat
W	vehicle weight
g	gravitational acceleration
D_x	linear deceleration
$-a_x$	linear deceleration
F_{xf}	Front axle braking force
F_{xr}	Rear axle braking force
D_A	Aerodynamic drag
Θ	uphill grade angle
F_d	Force on the disc
R_t	Radius of tire
R_r	Radius of rotor
R_e	Effective radius
r_o	Outer Radius of the pad
r_i	Inner Radius of the pad
t_s	time taken to stop the automobile
v_o	initial speed
F_{xt}	the total of all longitudinal deceleration force on the vehicle

V	forward velocity
R_{15}	diameter of wheel
F_b	Total brake force of front and rear wheels
T_W	Braking torque on wheel
F_C	Clamping force
D_t	Diameter of tyre
N	rotational speed
M	mass
C_p	Specific heat
Δt	Change of temperature
X_T	total stopping distance
C	Aerodynamic drag factor
A_{rf}	area of rubbing face
P	Power
A_c	contact area
f_s	sliding friction
w	linear wear
f_1	correction factor for motion
f_2	correction factor for environment
ε	strain
σ	Stress
v	Poisson ratio
E	Module of Elasticity
ω	angular velocity
σ_c	contact stress
r_1	minimum radii of the curvature
$\dot{r_1}$	Maximum radii of the curvature

σ_v	Von Mises stress
S_{sy}	yield strength in shear
S_y	Yield strength
σ_m	mean stress
σ_a	alternating stress
τ_{max}	shear stress
τ	frequency
U	strain energy
σ_F'	Fatigue strength coefficient
ε_F'	Fatigue ductility coefficient
b	Fatigue strength exponent
c	Fatigue ductility exponent
σ_{ut}	Ultimate strength
$\dot{k}$	Cyclic strength coefficient
$\dot{n}$	Cyclic strain hardening exponent
K_e	Element matrix
q	Vector of primary unknown quantities at the nodes of the element
Q	Vector of element nodal actions
P_{ext}	External pressure

LIST OF ABBREVIATION

FEM	Finite element method
FEA	Finite element analysis
3D	three dimensional
NVH	Noise, Vibration and Harshness
BTV	Brake Torque Variation
Al-MMC	Aluminum metal matrix composites
mph	miles per hour
TE	Total energy
KE	Kinetic energy
RE	Rotational energy

CHAPTER ONE: INTRODUCTION

1.1. Background

The idea of this title of thesis is basically concerned on the Mechanical interaction between disk brake and brake pad. Specifically, concerned on brake disc with brake pad of automotive in Ethiopian city taxi is taken as a sample. In addition, study the mechanical properties that occur between brake disk and brake pad, and develop their properties with available material to improve the performance of braking system by the help of FEM analysis.

Brakes are of two types: which are drum brakes and disc brakes. The drum brake is located inside a drum so that on application of the brakes, the brake lining is forced outward and pressed against the drum, while disc brakes operate in similar way except that they are exposed to the environment. The friction and wear mechanisms are altered under different temperatures. Normally, the brake disk is the rotation of wheel by pushing brake pad by the action of hydraulic pressure in the master cylinder of braking system with the effect of friction against brake disk with the arrangement of caliper stop the movement of vehicles. The brake system converts the kinetic energy of vehicle motion into heat. The friction materials used in brakes are required to provide a stable coefficient of friction and a lower wear rate at various operating speeds, pressures, temperatures and environmental conditions. The increase of friction moment is depends on the coefficient of friction, radius of rubbing path and forces that act on the pads.

Brake pads are steel backing plates with friction material bound to the surface that faces the disk brake rotor. The Brake pads convert the kinetic energy of the vehicle to thermal energy by the action friction. The two brake pads are contained in the brake caliper with their friction surfaces facing the rotor. When the brakes are hydraulically applied, the caliper clamps the two pads together into the spinning rotor to slow (or) stop the vehicle.

The most important components of an automotive braking system are brake pads with their arrangement of brake caliper. The brake pads are steel backing plates with friction materials bound to the surface facing the brake disc. That is used in the braking systems to control the speed of the automobile by converting the kinetic energy of the movement of automobile to thermal energy by friction and dissipating the heat energy produced to the surroundings.

The performance of brakes are depends definitely on the quality and fine composition of brake pads [**1**]**.**

At a low temperature, the hard asperities, small debris, and piece shape particles exist on the contact interface. The hard asperities may be embedded in a softer matrix, which results in plastic flowing and plowing called furrow effect with the increasing braking pressure and initial braking speed, the friction temperature will increase to result in several phenomena. The cavitations phenomenon causes granular or sheet debris fall off, which will reduce the braking torque. In general, with the increase in temperature, the friction coefficient decreases gradually. Nevertheless, after reaching a certain temperature, the friction coefficient may fall off suddenly. While the wear rate increases continuously as temperature increases. The wear will be more serious at a higher temperature [**2**]**.**

1.1.1. Classification of brakes based on transformation of energy

Hydraulic Brakes: The hydraulic brake is an arrangement of braking mechanism which uses brake fluid specially ethylene glycol to transfer pressure from the controlling unit to the actual brake mechanism of the vehicle. Parts of hydraulic brakes: Brake Pedal, Push rod, Master cylinder assembly and Brake caliper assembly.

Electrical Brakes: Electric brakes are actuator devices that use an electrical current or magnetic actuating force to slow or stop the motion of a rotating vehicle. There are two main types of electric brakes: those are magnetic and friction. The magnetic brakes are non-contact brakes that use magnetic fields to actuate the braking components such as Permanent magnetic brake, Electromagnetic brake, Eddy current brakes and Hysteresis powered brakes.

Mechanical Brakes: Mechanical brakes are assemblies consisting of mechanical elements for the slowing or stopping of vehicle. They use levers or linkages to transmit force from one point to another. There are several types of mechanical brakes. Band brakes, the simplest brake configuration, have a metal band lined with heat and wear resistant friction material. Drum brakes, which are commonly used on automobile rear wheels work when shoes press against a spinning surface called a drum. Disc brakes are constructed of brake pads, a caliper, and a rotor. During operation, the brake pads are squeezed against the rotor. Cone brakes are made with a cup and a cone, which is lined with heat and wear resistant material. During actuation, the cone is pressed against the mating cup surface [**3**]**.**

The mechanical brakes according to the direction of acting force may be sub divided into the following two groups:

1. Radial brakes
2. Axial brakes

Radial brakes: In these brakes the force acting on the brake drum is in radial direction. The radial brake may be subdivided into external brakes and internal brakes.

Axial brakes: In these brakes the force acting on the brake drum is only in the axial direction.

Example: - Disk brake, Cone brakes.

Disc brakes create braking power by forcing flat friction pads against sides of rotating disc. Higher applied forces can be used in disc brakes than in drum brakes, because the design of the rotor is stronger than the design of the drum.

Modern vehicles always equipped with disc brakes on at least the front two wheels. The main component of disk brakes are:-

Rotor: Spins with wheel. When used in conjunction with brake pads, slows vehicle.

Caliper: Holds pads and squeezes them against rotor.

Brake pads: Provide friction force when in contact with rotor. Works to slow or stop vehicle.

The schematic figure is shown below.

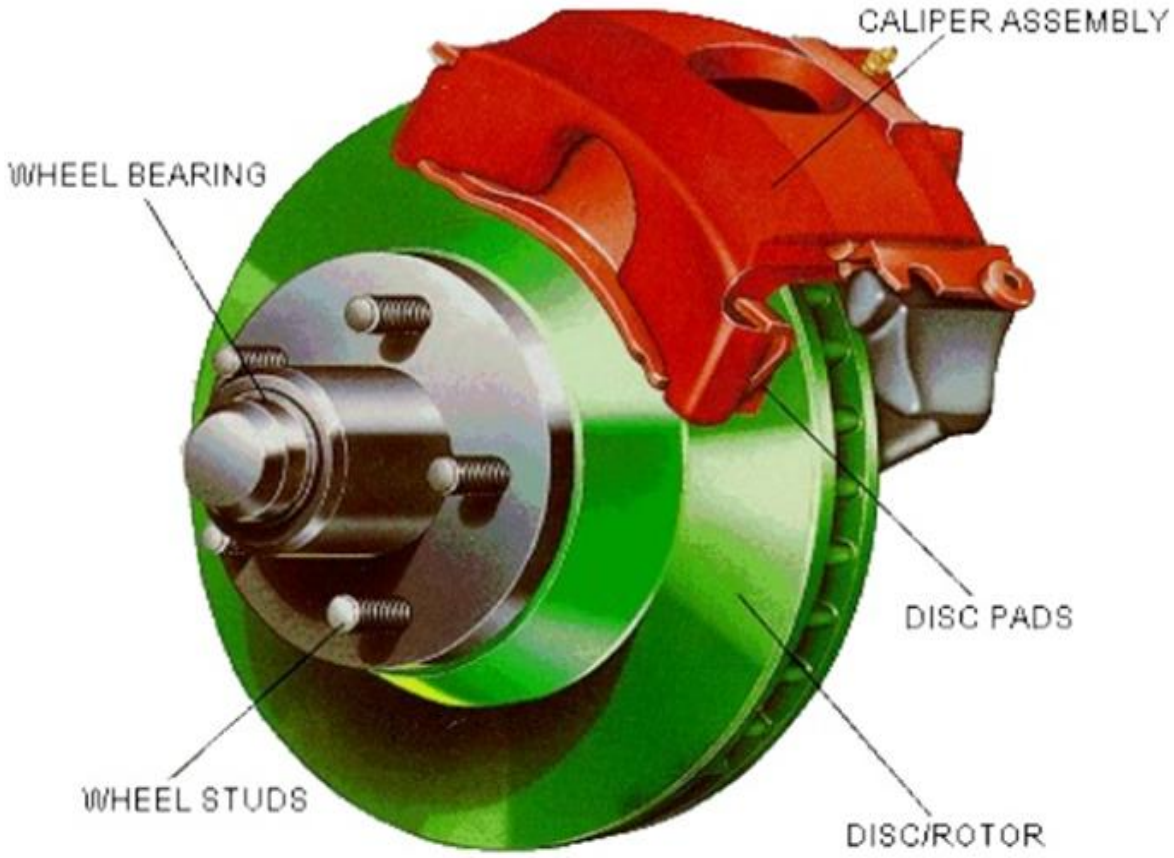

Figure1.1: Brake disk main Components

1.2. Motivation

Several automobiles brake pad is seriously damaged in short period of time. The friction characteristics of friction material are different based on type of material. Then, if the friction characteristics of brake disk material are different, the coefficient of friction is different. That means the coefficient of friction of metallic matrix, semi-metallic matrix and non-metallic matrix is different. Since, the capability of coefficient of friction of brake pad is measure the quality performance of braking system.

During the moving of automobiles and braking time, there is high heat dissipation in the interface of brake disk and brake pad, these heat dissipation between the interfaces, will deform the disk brake. Therefore, mathematical and software modeling and analyzing is important interpretation of problem in design of brake disk.

Due to environmental condition, the strength of brake pad is reduced and the wear of brake pad is increase. In warm area, the temperature is high during repeated braking and the brake pad is losing the physical properties due to hot and dry environmental condition. Thus, these studies try to know the mechanical properties or friction properties of brake pad materials at hot and cold environmental condition and protect environmental protection of dust produced from scratching of brake pad during repeated braking and mixed with water by movement of rainfall.

1.3. Statement of problem

During moving of Automobiles, braking is needed for certain purpose and to prevent accident, as this time the action of braking is measure the performance of vehicle. However, the friction material of brake pad that used in Ethiopian city taxi is semi metallic pad material with high content of copper in their composition; thus copper is naturally has high electric conductivity, high heat conductivity and it produce dust. When repeated braking is applied brake disc and brake pads must be strong enough to stop the vehicle with in minimum distance, well anti- fade characteristics and well anti wear properties. But, the friction surface of brake pad is damaged due to high heat dissipated between brake disk and brake pad. Then, as the result of the damaged brake pad, the moving vehicle is not stopped at required phenomena and it may be exposed by accident. Also, the result of high heat dissipated between that of interface is brings deformation of brake disk and wears disk brake, and during braking it produce noise. Further; the dust produced from copper is affect environment (affect aquatic life) by moving to the river (or) water way by the action of rainfall. Hence, to reduce such problem in braking system; the *first* hypothesis is use another alternative of brake pad like; ceramic brake pad, organic brake pad such as Kevlar brake pad. The *second* hypothesis is use the semi-metallic brake pad that contains more reduced composition of copper (or) free of copper composition content.

1.4. Objective of the study

1.4.1. General objective

The general objective of this study is to analysis the mechanical characteristics of automobile disc brake with interface of friction material of brake pad and damage of brake pad by FEM.

1.4.2. Specific objectives

- To determine mechanical strength of brake disc with brake pad (Ceramic AlO_3 brake pad, Kevlar brake pad, Aluminum alloy brake pad) of automotive that used for Ethiopian city taxi of minibus TOYOTA-HIACE by static analysis of ANSYS.
- To predict life span of brake disk and brake pad that used for automotive of Ethiopian city taxi.
- To find out the total heat flux generated in the brake disk when the process of repeated braking is applied by ANSYS software.
- To analyze the mechanical load of a brake disc using the finite element method (FEM).
- To specify type of brake pad composition that used in Ethiopian city taxi by testing in laboratory.

1.5. Scope of the study

- ✓ Introduce the brake disk and brake pad classification and explanation
- ✓ Mention the main and specific objective of the study
- ✓ Review of literature
- ✓ Study friction behavior of disk brake and brake pad
- ✓ Develop mathematical modeling and set boundary condition for brake pad materials
- ✓ Interpret the mechanical characteristics of friction material of brake pad
- ✓ Applying Finite element method (FEM) analysis By ANSYS software
- ✓ Construction 3D of brake disk and brake pad
- ✓ Method and Methodology for condition
- ✓ Interpretation and analyzing of condition
- ✓ Result and conclusion

1.6. Methodology

The methodology that used in this study is explained as following illustration. The initial method is reviewing literature and collects data from industries and different private organization that used for study, then writing governing equation, calculate boundary condition and writing report is up to the end of the research. Next identify material that used in this study that is disc brake material and brake pad material, for brake pad; types of friction of material that used in Ethiopian city taxi is not known which is import from outside country by trader so the type of

material is not clearly known. So in order to know friction material type take sample and test in the laboratory. After know friction material and choice best alternative brake disc material develop into software.

The next method is developing geometry of disc brake and brake bad by solid work software. Next export the assemble model of disc brake with brake pad to ANSYS software. Next finite element method (FEM) that is includes meshing, contact, applying boundary condition, analysis and solution. Next data collection from the ANSYS software result. Finally, plot the graph and interpret the result.

1.7. Organization of the research

The research is organized in five main parts. The first chapter is the introduction part, which covers the background of the research, statement of problem, the objective of the research, the scope of research, Methodology and organization of paper.

Chapter two is the literature review, that is discuss the review of literature on history of brake pad material, brake pad and brake disk material, types of friction material of brake disk and theories of basic friction.

In chapter three discusses on Material, Method and Condition. That is analytically or mathematically modeling of brake disk with brake pad and set the boundary condition. And also, the finite element method (FEM) is used, to develop 3-D model of disk brake with brake pad and applying the boundary condition for brake pad material and interpret the mechanical properties of materials.

In chapter four, summarize the output from finite element method analysis, which means summarizes the result obtain from ANSYS with the help of plotting of the graph, discussion and interpretation.

Finally, chapter five is give the conclusion that attain idea in the period of research working and assume the idea for feature work in this kind of research.

CHAPTER TWO: LITERATURE REVIEW

Dowson: from his experiments and calculations of published paper in 1998, he estimated that the frictional resistance of a body of rubbing surface is about ¼ of its weight. He furthermore discovered that the friction force between two rubbing surfaces is independent of the apparent and nominal contact area [**4**]**.**

The typical composition of brake pads are: - structural materials: metals, carbons, glass and/or Kevlar fibres, added to obtain the mechanical stability; matrix: in generally, phenolic resins are used, and sometime, different rubber type are used; filler: added to decrease the cost and/or to improve the manufacturability; some fillers may affect the friction characteristics of the material; frictional additives are added to control the coefficient of friction [**5**].

Bergman, s.a: considers that the brake squeal not be generated if the coefficient of friction is kept below some critical level. For the tested pad/disc combination the level find by the authors was found to be friction coefficient of 0.4. A small increase in the coefficient of friction in the close vicinity of the critical level causes a dramatic increase in squeal generation [**6**].

Nishiwaki: derived the equations of motion for a disc brake system using Lagrangian dynamics. Nishiwaki expanded the theory to suggest that all brake vibrations are generated by the same type of modal instability but at different modes depending on frictional input forces and modal displacements. The instability is generated due to a frictional force fluctuation as a result of normal force variations. The normal forces vary as a result of the in-tractions with the vibrating rotor and brake pads. The friction forces are used along with kinetic and potential energy expressions to develop the equations of motion using Lagrange's technique [**7**]**.**

Burckhardt et al.: this would lead to a slanted wear of the brake pads. Furthermore, a higher energy expenditure results on the positions with higher surface pressing which leads to higher temperatures. Further he suggested the comfort of the brake is also reduced, since sloping worn pads increase the squealing sensibility [**8**].

Raffaele Gilardi et al.: Noisy brakes are still the first problem reported by consumers and it has a big impact on the perceived quality of the vehicle. Particularly unpleasant noise levels are at frequencies higher than 1000 Hz (squealing). Squeals are induced by the friction due to contact between the brake pads and disc. Squeal during braking is a complex issue that covers a wide

field of dynamics at macroscopic scale (different components of the brake caliper) but also on a microscopic level (chemical composition of brake pads). While the coupling of vibration modes leading to squeal are now well understood and identified, the conditions that cause squeal occurrences remain poorly understood. This is mainly due to the complexity of the physical phenomena underlying the contact between the surfaces and the many factors that influence local friction. In order to improve brake NVH (Noise, Vibration and Harshness) performance, it is essential to understand which elements cause the squealing. Another focus of research in brake pads is generated by the new environmental regulations in the USA, aiming to reduce the amount of copper in brake pads initially to less that 5% and eventually to less than 0.5%. Copper has unique properties and functionalities in brake pads (friction stability, wear resistance, heat dissipation, noise damping). Among the 20 to 30 different ingredients contained in a typical brake pad formulation, there is no single material that can replace copper. As a consequence, in copper-free brake pads the formulations have to be readjusted and reinvented. Since some of the copper functionalities are similar to the functionality of graphite, it is likely that graphite can be considered as a possible substitute for copper [**9**].

Guoshun Wang and Rong Fu: The studies considered the impacts of brake pad shape, instantaneous angular velocity, radial position, and so forth but did not include the impact of the shape and structural layout of brake pad friction blocks upon brake disc temperature and stress. The structure differences of friction blocks of a brake pad can lead directly to differences in friction contact time and friction speed at each point on the brake disc surface, result in uneven temperature distribution on the brake disc surface, consequently cause high thermal stress, and therefore improve the brake disc thermal fatigue. It is an important topic to study the relationship between the structure of 2 Advances in Materials Science and Engineering the friction blocks of the brake pad and the temperature field of the brake disc. Starting from the relations between the friction block structural difference of the brake pad and the temperature and stress fields of brake disc, this paper establishes a connection between friction block structures of brake pad and temperature and stress distribution characteristics of brake disc, optimizes the structure and arrangement of the brake pad friction blocks, analyzes the variation of brake disc temperature and stress with the optimized brake pad, and finally validates the findings by sequential coupling simulations with ABAQUS6.8 finite element software. *According to his assumption,* Friction

braking is a complex process involving friction wear, deformation, vibration, and so forth. It is also a process of interactions of multiple physical, chemical, and mechanical changes [**10**].

G. P. Ostermeyer*:* His consideration was on the principal wear mechanism of brake pads which leads to a new type of differential equation of second order for the dynamic friction coefficient describing the stationary and transient friction behavior of brake pads. In brake systems characteristic structures are to be found in the contact area. With respect to wear equilibrium of flow of growing and destruction of hard patches is to be found on the contact surface. These patches modulate the friction power in the brake system. When the friction power density on a patch is not rather homogenously, the technical brake system seems to lose some of the performance:

- When the growing rate of the patches is too large, the patches aggregate to few but very large layers, which grind the metallic disc.
- When the growing rate is too small, the main energy dissipation channel of the system, that is the transformation of input power on the patches, is small and in addition the wear of the brake pad grows.

The friction layer on brake pads is characterized by growing and destruction of hard contact patches. These patches cause the main part of transformation of input power to friction power in the system. Friction coefficient μ has values between 0.1 and 0.9. It decreases with disk heat and friction power. In automotive cars the friction power ranges up to about 500 W/cm2 and the integral temperature in the contact zone can get values of 300 °C. The effect of decreasing friction coefficient with respect to growing friction power is sometimes called fading. Long time experiments show rather periodically changing hot bands on the disk. Another effect known from brake systems and also from clutch systems is a periodical change of μ itself with respect to time. The time periods of these vibrations varies from some seconds down to some minutes [**11**].

Prasanna Chowdary: He observed that higher pressure occurred on the leading side when the disc starts to slide, which again states that more wear appears on the leading side than the trailing side of the pad. So the study of dynamic pad pressure distribution helps in order to minimize and/or eliminate tapered wear in pads. Also the measurement of duration of speed reduction at 3MPa and 7MPa has been derived. With angular rotation at 10rad/sec dynamic pad pressure is obtained at 3MPa and 7Mpa pressure applied on to the Piston and Housing. As his thought a uniform pad wear and brake temperature, and more even friction coefficient could only be

achieved when pressure distributions between the pads and disc are uniform. In addition, unevenness of the pressure distribution causes uneven wear and consequently shortens the life of pads. This might lead to dissatisfaction to the customers who need to visit their garage more frequently in order to replace tapered wear pads. Also it has been speculated that a non-uniform pressure may promote disc brake squeal. One of the major improvements of both Pad wear and Brake Squeal is the change of the interface pressure distribution. Hence, higher and better the contact area of the pads, lower the squeal index and uneven Pad Wear [**12**].

During the same decade, North (1972) followed a similar line but started with an 8 degree of-freedom model.

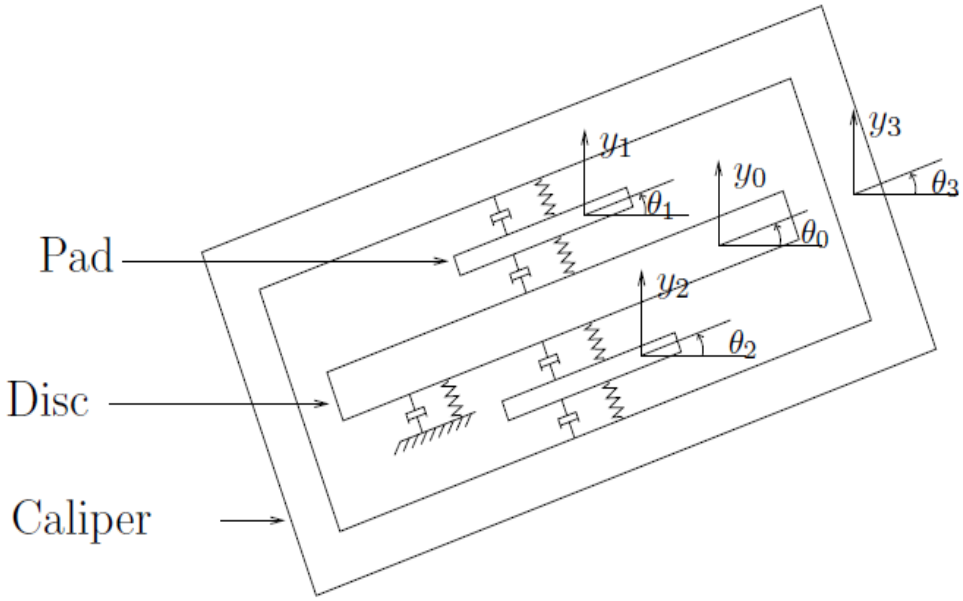

Figure 2.1: 8 degree-of-freedom model of a brake assembly

The model contains 4 rigid bodies: the disc, the caliper and two pads. Each is allowed to move in a transverse direction y and to rotate. This model comprises 4 parts: two pads, the disc and the caliper. Each of them is allowed to rotate and to have a transverse motion which makes 8 degrees of freedom. Once again after the equations of motions are derived, an eigenvalue analysis is carried out leading to some instability regions. The originality of North is first to suggest that the kind of instability observed in brakes might be similar to aircraft wing resounding, i:e: a coupling between a rotation and translation occurring when the two degrees of freedom have a certain phase shift (90 degrees for the wing). Second, he modeled the friction force as a so-called follower force". To illustrate this idea, consider the forces acting on the disc. North considers

that the forces of the pads on the disc are made up of a static compressive preload, N_0 augmented by an elastic term depending on the disc-pad separation. For instance, the force exerted by the top pad on the disc is written:

$N_1 = N_0 + K_{P1}(y_0 \_ y_1) + C_{P1}(\acute{y}_0 \_ \acute{y}_1)$;

Where K_{P1}, C_{P1} are the disc-top pad contact stiffness and damping coefficient respectively and y_0 and y_1 the upwards displacement of the disc and top pad. With similar notations, the force exerted by the bottom pad on the disc is;

$N_2 = N_0 \_ K_{P2}(y_0 \_ y_2) \_ C_{P2}(\acute{y}_0 \_ \acute{y}_2)$:

The concept of follower force is that the friction force instead of being modeled as remaining horizontal is allowed to follow the deflection of the disc. Here the rotation θ_0. Thus the friction force on the disc has the vertical component:

$F_y = \mu (N_1 + N_2) \sin(\theta_0) \approx \mu (N_1 + N_2)\theta_0$;

And its horizontal component is $\mu (N_1 + N_2) \cos(\theta_0) \approx \mu (N_1 + N_2)$.

Both ideas of resounding (noise) and follower forces have been taken up by numerous authors under different forms. It is now widely believed that brake squeal is expression of resounding instability [**13**].

Harshvardhan Zula et al.: This report deals with a systematic approach for manufacturing methods of friction pad as well as its wear characteristics Hardness and Density. Metal powder's types and characteristics play important role in manufacturing of friction pads. Manufacturing parameters i.e. molding temperature, molding pressure, and molding time required to be select properly to get good quality friction pads. In this study Taguchi technique has been used to study the parametric effect on quality. Friction pad wear reduce with increasing the sintering temperature and pressure. Quality of friction pad is predominately affected by molding pressure. Quality of friction pad has been checked using hardness, density, and its wear resistance. The objective of his study was concerned on: - study about the material composition and friction characteristics for manufacturing of friction pads, Fabrication/Production of Friction Pad by using Sintering of Powder metallurgy technique, Investigation the act of various manufacturing parameters on quality of friction pad using the Taguchi method, Measurement of wear Characteristics of the friction pads [**14**].

Degenstein et al.: his paper was consider on describing measuring device, that enables measuring the clamping forces acting during a braking process in the friction area between pad and disc. Thus the amount and the effective contact point of the clamping force are determined finger and piston-sided at the same time. State of research is the measurement of the distribution of clamping forces by means of pressure indication films. However, these are destroyed by shear stress or friction and in this way they can be only used with a stationary brake disc, that is, under no circumstances during a braking process. An analysis of the force lines in a caliper shows that the preferred position for the measurement of the clamping and tangential forces can be found in the friction material of the brake pads, since all forces which contribute to the braking process must be supported by the brake pad. As soon as these forces are induced in the back plate of the brake pad, a correct measurement becomes almost impossible because of the multitude of contact points with the caliper. The consideration of the point of application of load of the clamping force by a stationary brake disc causes a radial shifting to the brake disc's outer edge (this is primarily adjudged to the expansion of the caliper). During a braking process the acting tangential force causes a shifting in tangential direction. By reason of movement of the caliper during a braking process a visual measurement method was developed, which enables recording the movement of brake pads [**15**].

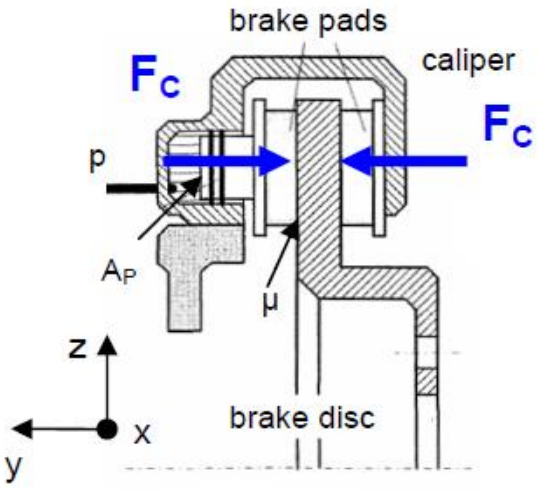

Figure 2.2: Forces acting on a disc brake

The following report and journals are the basic idea of Present work

Jaeho Kwak et al.: The suggestion of his paper was to develop in early design stage a reference model with relevant degrees of freedom. This model must describe the dynamic behavior of electromechanical brake components for the entire instrument range.

Also, since there was a wide range of efficiency on the brake actuator due to changing environmental conditions and the nonlinearities of its components. So, simplified models for future controller design and parameter estimator design were necessary. The rest of his paper was organized as into five Sections, those section were describes about: derives the complete nonlinear analytical model for an electromechanical brake system, natural frequencies and vibration modes were compared to capture the dominant frequency mode for the simplified model developed From the developed full degrees of freedom model, then two simplified models for clamping mode and gapping mode defined by contacting condition (braking status) are developed and finally, the simulation results for the characteristics of complete nonlinear model and the validity of two simplified models are presented [**16**].

Sadiq Sius LAWAL: He concluded that, the results of the research show that sawdust of 100μm particles size has properties that can effectively replace asbestos in brake pad manufacture, since it gives better brake pad properties. The properties such as compressive strength, hardness, density, ash-content and water absorption of the produced samples decreased with increasing particles size. The results showed that sawdust has properties comparable to that needed for use as brake pad material to replace asbestos in the manufacture of brake pads since it gave results which were within the range for brake pad manufacture. The materials used during the course of this work include sawdust, steel powder, silicon carbide, graphite and epoxy resin [**17**].

S. Oberst, J.C.S. Lai: the influence of the geometrical designs of brake pad on brake squeal is studied using a simplified brake setup consisting of an annular disc in contact with one brake pad. The various configurations of a brake pad studied here have been influenced by those used in the industrial testing of a full brake system. In this study, unstable vibration modes were first identified by the conventional complex eigenvalue analysis of a finite element model of the simplified brake system. Then, the acoustic power was calculated for a range of frequencies and friction coefficients using the acoustic boundary element method. It is shown that the performance of the various pads, in terms of brake squeal propensity caused by their geometric

differences, could be ranked based on contour plots of acoustic power with friction coefficient and frequency as the independent variables. These results indicate that the inclusion of acoustic power calculations, following a complex eigenvalue analysis of unstable vibration modes, provides improved prediction of brake squeal propensity [**18**].

A. Belhocine: His paper was investigating structural and contact behaviors of the disc brake and pads during the braking phase with and without thermal effects. His prediction result deduced that large deformations were occurred at the outer radius of the disc, the presence of grooves in the pads influences unfavorably the mechanical behavior of a brake and more uniform stress distribution was noticed for the pad without groove and with a double-piston loading. He suggests that temperature has a significant effect on the structure and contact behavior of the disc brake assembly, large deformation and high contact pressure was found in the disc-pad model with the thermal effect and the smoothness of the mesh increases the precision of the solution.

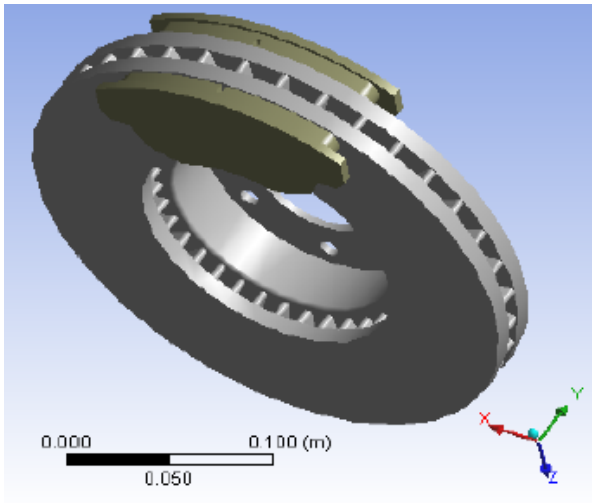

Figure 2.3: Brake disc with brake pad assembly

As his investigation the deformation of the disk is resulted due to the maximum temperature achieved on the tracks depends on the storage capacity the thermal energy in the disk, then the maximum displacement is localized on the slopes of friction, the fins and the outer ring. The maximum total deformation is occurred at the outer rim of the disc, which reaches 284.55 μm, at time t = 3.5 s. An increase in pressure and hence the temperature on a limited contact surface can create this phenomenon (heat deformation), local material fatigue and sometimes cracking of the disc [**19**].

Gil-hyoung Lee1et al.: In their study, Dynamic groan noise occurs when the Brake Torque Variation (BTV) between the disc and pads occur and also caused the vehicle when braking from repetitive thermal expansion of the disc and the pads surface conditions that occur due to changes in the analysis of dynamic groan noise. It is assumed to be equal to the number disc vane, the number of wave forms (BTV) is associated with each other and the shape of the surface of the pads and the disc of the thermal expansion and contraction during brake torque variation associated with the dynamic groan noise occurs. Therefore, the generation mechanism of dynamic groan noise, knew the progress in the order in which BTV occurs in the contact due to thermal deformation of the pad and the disc. This is to generate a dynamic groan noise. The Brake Torque Variation (BTV) is generated by contact via the thermal deformation of the disc and pad. Then, it Proceeds to generate a dynamic groan noise that sums up overall dynamic groan noise mechanism [**20**].

Samic and Sheridan: investigated the effects of friction on the pressure distribution between the rotor and the pads with a floating caliper using the finite element technique. The computational results without the friction forces (static case) revealed that the inboard and outboard pressure distributions varied because the locations of the normal forces acting on the pads were different on the piston and finger sides of the floating caliper. Furthermore, the pressure distributions with the friction forces taken into account were different from the static case due to the moment set up between the abutment and the friction interface [**21**].

Lee et al.: studied the pressure distribution between the rotor and the pads including the friction force with a floating caliper in order to investigate the motion at the friction interface that could be used to determine the onset of disc brake squeal using the finite element technique. The computed result revealed that the pressure distributions acting on the pads were different on the piston and finger sides of the floating caliper. Moreover, the axial displacements at the friction interface on the two sides were different [**22**].

CHAPTER THREE: MATERIAL, METHOD AND CONDITION

3.1. Brake disk and Bake pad material

3.1.1. Brake disk material

The brake disk type in this investigation is ventilated disc, vanes or pillars and provides a passage for the air to flow. The reason for using Ventilated brake discs is for the sake of increase the cooling rate and result in lower surface temperature. This lower temperature reduces the risk of brake fade and also helps in reducing wear of the disc and pad. Both of these designs are constructed with or without a mounting bell. A mounting bell increases the distance from the friction surface to axle and the surface area of the disc which improves cooling and therefore it helps to protect the wheel bearings from the high temperature generated due to braking operation [**23**].

Pearlitic matrix is the widely used material for brake discs. The benefits of using it as a disc material are good castability and machinability, high thermal conductivity and heat capacity, resistance to brake fade and lower cost. There is an interest in the industry to use lighter materials for the disc so that it contributes less to the overall weight of the vehicle and ultimately weight of the vehicle and ultimately improves the fuel consumption. Another reason for lighter disc is that the brake discs are part of the unsprung mass of the vehicle, so its reduction also adds to driving comfort. One way to reduce the weight is to use aluminum mounting bell and cast iron braking ring in a hybrid brake disc. These two parts can be connected with either integrally casted grey iron braking ring with aluminum bell or by mechanical connections e.g. integrating radial steel inlays. Friction ring is made of cast iron to take advantage of its superior friction and thermal properties while mounting bell is made of aluminum to reduce the overall weight. To reduce the weight further, lighter materials with suitable properties are required to be used as a braking ring. As the heat is generated at the surface of a disc due to frictional forces, it is desired that for a given heat input, material temperature rise is the minimum that means it should have maximum possible volumetric heat capacity (density× specific heat capacity). During a short braking this is very important as a significant amount of heat is stored. However during long braking, it also becomes important that this heat conducts to the core of the disc quickly from the friction surface i.e. disc material should have high thermal conductivity. Furthermore, during long and repeated braking it is also important that the heat conducts quickly relative to stored

heat. Which means it should have high thermal diffusivity (i.e. thermal conductivity/volumetric heat capacity). Other properties desired are friction stability, resistance to corrosion, low wear and lower coefficient of thermal expansion.

The light weight components in automobile sectors have led to the development of advanced material parts with improved performance and increasing demand of fuel efficiency. A specific class of metal matrix composites (MMCs) which has gained a lot of attention due to its potential is aluminum metal matrix composites (Al-MMCs). Aluminum metal matrix composites (Al-MMCs) have a great potential for several applications in automobile parts. For the case of just this performance application of high wear resistance and high specific mechanical properties, 67% lower density than cast iron and three times the thermal conductivity, thus Al-MMCs are ideal materials for the manufacture of lightweight automotive components initialization [**24**].

Table 3-1: Material properties of Al-MMCs and cast iron brake disc

S.n	**PROPERTY**	**Al-MMC**	**Cast Iron**
1	Tensile Strength (MPa)	484	207
2	Yield Strength (MPa)	437	330
3	Young's Modulus (GPa)	114	114
4	Poisson's Ratio	0.33	0.27
5	Density (gr/cm^{-3})	2.822	7.2
6	Thermal Conductivity (W/m.K)	140.2	45
7	Thermal Expansion Coefficient (C^{-1})	$(2.3) \times 10^{-5}$	$(1.2) \times 10^{-5}$
8	Specific Heat(J/kg.K)	800	510

The performance evaluation of the **Al-MMC** as the test condition followed the requirement of the Motorway Braking Check as recommended by Society of Automotive Engineers (SAE) with standard code: SAE J2522 with using the platform of Proton Wira 1.3L and curb mass of 1250kg the brake disk would be evaluated with vehicle initial velocity of 90% of its velocity maximum (180km/h), 50% of velocity maximum as final velocity (100km/h), deceleration of 0.3g and initial braking temperature of 150°C and having coefficient friction(μ=0.35).

3.1.2. Brake pad material

The brake pad material used in Automobiles is Asbestos, Semi-Metallic, Non-Asbestos materials, Low Steel, Carbon. **Asbestos:** is hydrated magnesium silicate Mg$Si205 (OH)d. When it is used, the content of asbestos in vehicle brakes varies between about 30-70%. According to Nicholson (1995), the positive characteristics of asbestos are: (i) asbestos is thermally stable to 500°C above which it produces silicates, (ii) asbestos helps regenerate the friction surface during use, (iii) silicates produced by asbestos are harder and more abrasive that asbestos, (iv) asbestos insulates thermally, (v) it processes well, (vi) it wears well, (vii) it is strong yet flexible, and (viii) asbestos is available at reasonable cost. The useful properties of asbestos are flexibility, high tensile strength, incombustibility, low thermal conductivity and resistance to chemical attack. There are six minerals included in this definition; those are chrysotile, is in the serpentine group of minerals, while the others, including amosite, crocidolite, anthophyllite, actinolite and tremolite belong to the amphibole group of minerals. The considerations use of asbestos in automobiles is good for absorbing and dissipating heat, average stopping power, legally regulate due to its carcinogenic properties [**25**].

Semi-Metallic Pads: Range from 30% to 65% metal and filler Different pads use Steel, Iron, and Copper. Harder material is very durable and has excellent heat resistance, creates more noise and dust; have a much higher thermal entrance due to metallic content; Still provide good cold bite; have a much wider operating temperature. The negative effects of this kind of brake pad are; have a tendency to be noisier than organic or ceramic pads, produce more brake dust, will wear brake disk more quickly, more expensive than organic pads.

Non-Asbestos Organic Pads: Typically contain nonferrous metals, inorganic and organic fibers, abrasives, lubricants and property modifiers such as glass, rubber, Kevlar and carbon. Typically used in high performance cars and referred to as “ceramics”. Low to medium-high coefficient of friction approaches to 0.33 –0.40, excellent wear at lower temperature less than 200C, good for wheel dust, relatively poor wear under heavy duty conditions and at higher friction levels, good noise & roughness characteristics, can have morning effectiveness noise – squealing noise on first couple of brake applies in the morning and its more expensive.

Low Steel Pads: Typically contain ferrous and nonferrous metals, inorganic and organic fibers, aggressive abrasives, lots of carbonaceous and sulfide lubricants. Replacing semi-metallic as the standard for passenger cars, have higher coefficient of friction levels closes to 0.38 –0.50, good pedal feel and braking confidence, good fade and high speed performance, have high pad or rotor wear, good for high speed wear, lots of wheel dust and inferior noise and life.

Carbon Pads: Composite materials reinforced with carbon fibers. Which are used for both pads and rotors, used in Formula one and other race cars, the major manufacturers include Hitco, Brembo and Carbon Industries, uses for light weight – rotors weigh less than 1kg, have high coefficient of friction - can decelerate an formula one car at over 5g, operating temperature is around 800-1000°C and extremely expensive to produce.

The candidate material selection for brake pad materials are organic brake pad such as Kevlar, ceramic brake pad and semi-metallic brake pad with free (or) a few content of copper composition, [**26**].

Some material properties of friction components are listed below, [**27**]**.**

Table 3-2: Material property of friction material component

S.n	**Friction component**	**Mass Density (kg/m^3)**	**Elastic Modulus (GPa)**	**Poisson ratio**
1	Aluminum Alloy	2700	69	0.33
2	Kevlar	1440	71	0.36
3	Ceramic Al_2O_3	3800	325	0.22

As research worked in California storm water quality association (CASQA) done by “Kelly D. Moran” on Topics of brake pad copper reduction- Metrics for tracking Progress; the California law requires near elimination copper (or) free of copper < 0.5% in vehicle brake pad in order to protect water quality, [**28**].

a) Sample preparation for testing composition of brake pad

The sample is produced by scratching a piece of brake pad and changing the scratched material in to fine particles, then the small fine particle is packed and taken to the laboratory to know the composition particle of brake pad that used in Ethiopian city taxes. The sample of brake pad is taken from the brake pad that used for TOYOTA-HIACE of 5L and tightened with six bolts.

Figure 3.1: Sample preparation for pad composition testing

b) Result obtain from laboratory

As the result of tested material obtain from laboratory of Ethiopian geological survey and tested under *base metal analysis report*, the analytical method is by four acid attacks (HCI, HNO_3, $HClO_4$, and HF), the sample preparation is 200 mesh and the analytical result is in part per million (ppm). And tested under *Complete Silicate Analysis Report* with analytical method of $LiBO_2$ fusion, HF attack, gravimeteric and colorimetric, the sample preparation under this category of test is the sample preparation is 200 meshes. The analytical result is given in percent. But, under this tested category the result is can't fit their procedure of laboratorial techniques. So, we take the result obtained under **base metal analysis report**. The laboratory result obtain from Ethiopian geological survey is illustrated in the table below.

Table 3-3: Experimental result of brake pad composition content

Collector's Code	Copper (ppm)	Zinc (ppm)	Lead (ppm)	Cobalt (ppm)	Nickel (ppm)
O.D-01	13360	686.4	<0.01	58.6	30

3.2. Modeling for brake disk and brake pad

3.2.1. Geometrical modeling of brake disk with brake pad

For analysis of mechanical properties of Automotive disc brake by finite element method, the dimension and specification of TOYOTA-HIACE minibus taxi of engine model of 2.5D4D95 is taken as sample, since among automotive that braking is repeated rather than other car. The detail specification is listed in appendix.

Figure 3.2: Automobile for City taxi

Table 3-4: Geometrical dimensions and important parameters of braking [**29**]**,** [**30**]**.**

Item	**Value**
Disk inner radius (mm)	195
Disk outer radius (mm)	295
Pad inner radius (mm)	207.5
Pad outer radius (mm)	282.5
Disk thickness (mm)	24
Cover angle of (θ) of pad	65
Size of pad(L x W x H mm)	75 x 150 x 69
Gross Vehicle Weight (kg)	2,800
Max speed (mph)of Automobile	91
Tire Size	195/70 R15
Effective Radius of Rotor, R_r	122.5
Mass of the disc (kg)	5
Specific Heat(J/kg.K), C_p	800
Acceleration 0-62mph (sec)	22.4

The 3-D Model of brake disc and brake pad is shown in the following figure 3.3.

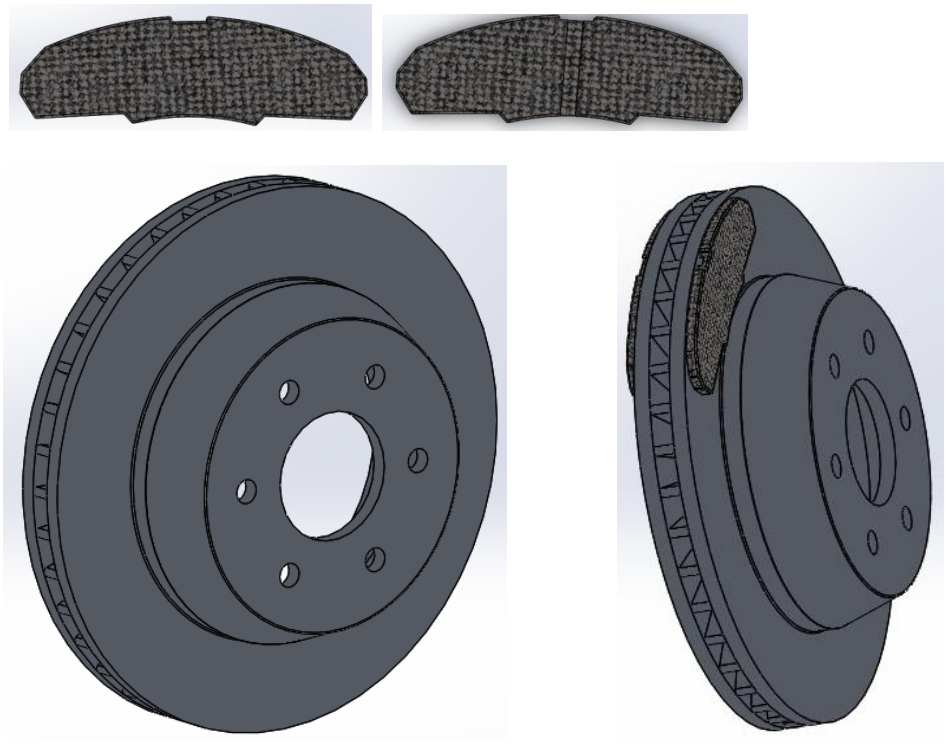

Figure 3.3: Brake disk with brake pad

3.2.2. Mathematical modeling

3.2.2.1. Equations for braking performance

As book published by society of automotive engineer on topics of Fundamental of vehicle dynamics prepared by "Thomas D.Gillespie", specific equations was taken from this book, so the general equations for braking performance can be obtained from Newton's second law written for the x-direction [**31**]. The force on the vehicle is generally typically shown in figure below.

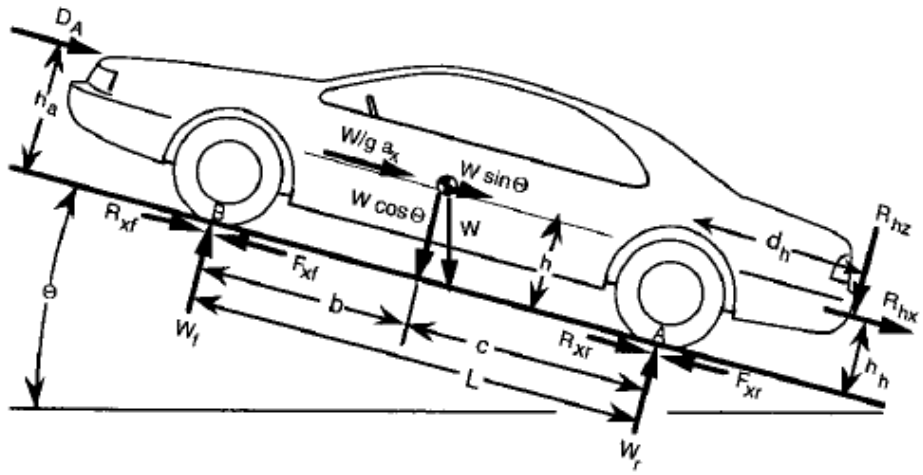

Figure 3.4: Arbitrary force acting on the vehicle

Then, Newton second law is;

$$Ma_x = -\frac{W}{g}D_x = F_{xf} - F_{xr} - D_A - w\sin\theta \quad \text{……..…….(3.1)}$$

Where;

W = vehicle weight

g = gravitational acceleration

$D_x = -a_x$ = linear deceleration

F_{xf} = Front axle braking force

F_{xr} = Rear axle braking force

D_A = Aerodynamic drag

Θ = uphill grade

F_d = Force on the disc

R_t = Radius of tire

R_r = Radius of rotor

R_e = Effective radius

r_o = Outer Radius of the pad

r_i = Inner Radius of the pad

t_s = time taken to stop the automobile

v_o= initial speed

a) Constant deceleration

The simple and fundamental relationships can be derived for the case where it is reasonable to assume that the force acting on the vehicle will be constant throughout a braking application. Then, from eqn. (3.1) we have;

$$D_x = \frac{F_{xt}}{M} = -\frac{dV}{dt} \quad \text{……..(3.2)}$$

Where;

F_{xt} = the total of all longitudinal deceleration force on the vehicle

V = forward velocity

This equation can be integrated for deceleration from initial velocity (V_o) to final velocity (V_f);

$$\int_{Vo}^{Vf} dV = -\frac{F_{xt}}{M}\int_{o}^{ts} dt \quad \text{……… (3.3)}$$

$$V_o - V_f = \frac{F_{xt}}{M} t_s \quad \text{……..(3.4)}$$

Thus, the time to stop is proportional to the velocity, where as the distance is proportional to the velocity squared (means doubling the velocity doubles the time to stop, but quadruples the distance required).

b) Tire size identification:

Tire size: $195/70R_{15}$;

195: width of the tire in mm,

19.5/2.54 = 7.677 inch, 1inch = 2.54cm,

70: aspect ratio in % is called section height,

Section height = 7.677 x 0.7 = 5.374 inch,

R_{15}: diameter of wheel,

Section height = section width x aspect ratio,

Therefore; Total diameter of tire = (section height x 2) + wheel diameter,

$R_t = D_t/2$ = 12.874 inch (or),

R_t = 32.7cm = 327mm = 0.327m (or),

D_t = 0.654m

By considering the speed of driving of TOYOTA HIACE 5L in Addis Ababa City Ethiopia;

The maximum speed is 50km/hr (or) 13.89m/s

The minimum speed is 20km/hr (or) 5.56m/s

The average or medium speed is 35km/hr (or) 9.7m/s

c) Kinetic energy of the vehicle:

KE *@**v** = 13.89m/s;* $KE = \frac{mv^2}{2} = \frac{(2800)(13.89)^2}{2}$ = 270.1kJ

KE *@**v** = 5.56m/s;* $KE = \frac{mv^2}{2} = \frac{(2800)(5.56)^2}{2}$ = 43.28kJ

KE @v =*9.7m/s;* $KE = \frac{mv^2}{2} = \frac{(2800)(9.7)^2}{2}$ = 131.73kJ

d) Maximum friction force (F),

F = μmg = 0.35 x 2800 x 9.8 = 9604N, where μ = 0.35,

e) Deceleration of the vehicle;

$-a_x = D_x = a = \frac{F_{xt}}{M} = \frac{F}{M} = \frac{9613.8}{2800} = 3.43\ \frac{m}{s^2}$

f) Time taken to stop the vehicle:

$t_s = \frac{V_o}{\frac{F_{xt}}{M}} = \frac{V_o}{Dx}$ …… (3.5)

t_s @ *v = 13.89m/s* $= \frac{v}{a} = \frac{13.89}{3.43}$ = 4 sec.

t_s @ *v = 5.55m/s* $= \frac{v}{a} = \frac{5.55}{3.43}$ = 1.6sec.

t_s @ *v = 9.7m/s* $= \frac{v}{a} = \frac{9.7}{3.43}$ = 2.8sec.

The maximum speed peed of the vehicle is 91mph (or),

146.44km/hr = 40.68m/s,

t_s = the times for the velocity change

because velocity and distance are related by V = $\frac{dx}{dt}$, we can substitute for"dt" in eqn. (3.2), integrate and obtain the relationship between velocity and distance:

$\frac{V_o{}^2 - V_f{}^2}{2} = \frac{F_{xt}}{M}X$ …… (3.6)

Where:

X = Distance travelled during the deceleration

In this case where the deceleration is full stop, then V_f is zero and,

g) X is stopping distance, SD.

Then: SD = X = $\frac{V_o{}^2}{2\frac{F_{xt}}{M}} = \frac{V_o{}^2}{2D_x}$ ……. (3.7)

X @ *v* = *13.89m/s* = $\frac{\boldsymbol{v_o{}^2}}{\boldsymbol{2D_x}} = \frac{\boldsymbol{v_o{}^2}}{\boldsymbol{2a}} = \frac{(\mathbf{13.89})^2}{\mathbf{2(3.43)}}$ = 28m

X @ *v* = *5.5m/s* = $\frac{\boldsymbol{v_o{}^2}}{\boldsymbol{2D_x}} = \frac{\boldsymbol{v_o{}^2}}{\boldsymbol{2a}} = \frac{(\mathbf{13.89})^2}{\mathbf{2(3.43)}}$ = 4.5m

X @ *v* = *9.7m/s* = $\frac{\boldsymbol{v_o{}^2}}{\boldsymbol{2D_x}} = \frac{\boldsymbol{v_o{}^2}}{\boldsymbol{2a}} = \frac{(\mathbf{13.89})^2}{\mathbf{2(3.43)}}$ = 13.7m

h) Deceleration with Wind Resistance

The Aerodynamic drag on vehicle is dependent on vehicle drag factors and the square of the speed. To determine stopping distance in such cases;

$\sum F_x = F_b + CV^2$ ……. (3.8)

Where:

F_b = Total brake force of front and rear wheels

C = Aerodynamic drag factor

Therefore:

$$\int_0^{SD} dx = M \int_{V_o}^{0} \frac{VdV}{F_b + CV^2} \quad \text{……. (3.9)}$$

Then, by integrating we obtain the stopping distance with aerodynamic drag is;

SD = $\frac{M}{2C} \ln[\frac{F_b + CV_o{}^2}{F_b}]$ ……..... (3.10)

Force required stopping vehicle within stopping distance (or) stopping time;

Use kinetic energy, KE at medium speed at *V = 35km/hr (or) 9.7m/s.*

Thus, Tangential braking force: $(F_b)_t = \frac{KE}{X} = \frac{131730}{13.7} = 9.615kN$

Tangential force on each wheel,

$F_t = \frac{(Fb)t}{4} = \frac{9615}{4} = 2.404kN$

$R_e = \frac{295+195}{4} = 122.5mm = 0.1225m$

i) Braking torque on wheel: $T_W = F_t \times R_t$, where R_t is radius of tire.

$T_w = 2404 \times 0.327 = 786Nm$

j) Braking torque on disk: $T_b = T_W X \frac{R_t}{R_0} = 786 \times \frac{0.327}{0.1475} = 1742.5Nm$

k) Clamping force: $F_C = \frac{T_b}{2 x \mu x R_e} = \frac{1742.5}{2 x 0.35 x 0.1225} = 20320.7N = 20.321kN$, is the force acting on each side of disk by caliper piston.

l) Angular velocity of disk:

Maximum speed of vehicle is 91mph = 146.44km/hr (or) 40.68m/s

But, in the case of addis Ababa City Ethiopia the medium driving speed of the driver is

35Km/hr (or) 9.7m/s.

Then, velocity (v) = ($\pi \times D_t \times N$)

$N = \frac{9.7}{\pi \times 0.654} = 4.7rps$; $\omega = \frac{v}{R_t} = \frac{9.7}{0.327} = 29.66rad/s$

m) Heat flux:

Take the mass of disk is 5 kg,

Heat generated when applying braking action on disk brake = kinetic energy

Heat generated (Hg) = KE

But, heat generated is, $Hg = mC_p\Delta t$

$Hg = 131730J = 5kg \times 800J/kg.k \times \Delta t$

$\Delta t = \frac{131730}{5 \times 800} = 33k = -240^oC$

$\Delta t = t_i - t_f$

$t_f = t_i - \Delta t;$

$t_f = t_i - \Delta t = 22^oC + 240^oC =$ **262^oC**, where, $t_i = 22^oC$ is room temperature

n) Restoration energy (RE) of the vehicle is given by;

$RE = 3\%\ KE$ …….. (3.11)

$RE = 0.03 \times 131730J = 3952J$

So, total energy (TE) given as;

$TE = KE + RE$ …….. (3.12)

$TE = 131730 + 3952 = 135682J$

Area of rubbing face of the disk is given by;

$A_{rf} = TE \times (r_o - r_i)$ ……(3.13)

$A_{rf} = 135682 \times (0.2825 - 0.2075) = 10176m^2$

o) Power (p):

The power produced during braking is, $p = \frac{KE}{t_s} = \frac{131730}{2.8} = 47046W = 47.046kw$

Hence, the power produced on each front wheel is;

$P = \frac{47}{2} = 23.5\ kW$

Disc useable area:

Disk useable area (A) = $\frac{\pi}{4}\ (r_o{}^2 - r_i{}^2)$

A = $\frac{\pi}{4}\ [(0.2825)^2 - (0.2075)^2]$ = 0.02886 m^2

Contact area of piston of caliper;

A_c = 2 x contact area of piston of caliper,

= 2 x $\frac{\pi}{4}\ [(D_O)^2 - (\frac{D_O+D_i}{2})^2]$

= 2 x $\frac{\pi}{4}\ [(0.295)^2 - (\frac{0.295+0.195}{2})^2]$

= 0.0424 m^2

For each front wheel = $\frac{0.0424}{2}$ = 0.0212 m^2

External pressure between disc and pad:

External pressure = $\frac{F_{clamp}}{A_c} = \frac{20320.7}{0.0212}$ = 958523.6 N/m^2

P_{ext} = 0.96 MPa

3.2.2.2. Linear Sliding wear

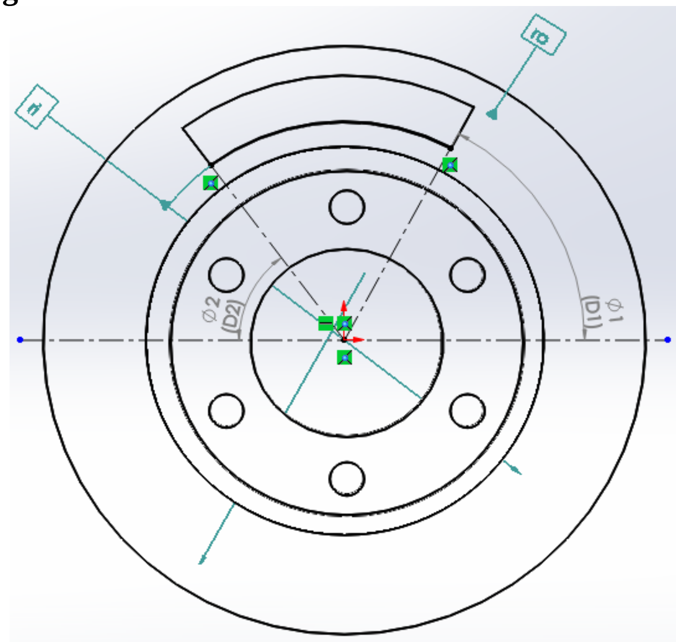

Figure 3.5: Parameter of Disc Brake

Considering a block with surface area A, sliding over fixed surface with contact pressure P, where the co-efficient of sliding friction f_s & define a linear wear measure w. The work done by frictional force (f_sPA) during displacement S is f_sPAS or f_sPAVt (where V is velocity & & t is time). The volumes of material removed because of wear (V = wA) is proportional to the work (wA α f_sPAVt) i.e. wA = KPAVt Where, K is proportionality factor which includes the co-efficient of friction f_s, [**32**]. The SI unit of K is m^3.s / (N.m.s).

w = KPVt

Additional correction factors f_1 & f_2 can be included such that:

$w = f_1f_2KPVt$

Where, f_1 correction factor for motion type

f_2 correction factor for environment

Then the Force and the torque equations are given as,

$$w = f_1f_2KPVt \quad \ldots\ldots (3.14)$$

$$F = \int_{\theta_1}^{\theta_2}\int_{r_i}^{r_0} Pr.dr.d\theta \quad \ldots\ldots (3.15)$$

$(\theta_2 - \theta_1) \int_{r_i}^{r_0} Pr.dr$ ……(3.16)

$$T = \int_{\theta_1}^{\theta_2} \int_{r_i}^{r_0} f.Pr^2.dr.d\theta$$

$= (\theta_2 - \theta_1) f \int_{r_i}^{r_0} Pr^2.dr$ ……(3.17)

$$r_e = \frac{T}{fF} = \frac{\int_{r_i}^{r_0} pr^2.dr}{\int_{r_i}^{r_0} pr.dr} \quad \text{……(3.18)}$$

$$M_x = F\bar{r} = \int_{\theta_1}^{\theta_2} \int_{r_i}^{r_0} \Pr(r\sin\theta).dr.d\theta$$

$= (\cos\theta_1 - \cos\theta_2) \int_{r_i}^{r_0} pr^2\, dr$ ……(3.19)

$$\bar{r} = \frac{M_x}{F} = \frac{(\cos\theta_1 - \cos\theta_2)}{\theta_2 - \theta_1} r_e \quad \text{……(3.20)}$$

Again these equations are applied for uniform wear condition and uniform pressure condition

a) Uniform Wear Condition

$\boldsymbol{F} = (\theta_2 - \theta_1) P_a.r_i(r_o - r_i)$ …….. (3.21)

$T = (\theta_2 - \theta_1) f.P_a.r_i \int_{ri}^{ro} r.dr$

$= \frac{1}{2}(\theta_2 - \theta_1) f.P_a.r_i(r_o^2 - r_i^2)$ ……(3.22)

$$= \frac{r_0^2 - r_i^2}{2} \frac{1}{r_o - r_i} = \frac{r_0 + r_i}{2}$$

$$r_e = \frac{P_a r_i \int_{r_i}^{r_o} r.dr}{P_a r_i \int_{r_i}^{r_o} dr} \quad \text{……(3.23)}$$

$$\bar{r} = \frac{(\cos\theta_1 - \cos\theta_2)}{\theta_2 - \theta_1} \frac{r_o + r_i}{2} \quad \text{……(3.24)}$$

b) Uniform Pressure Condition

$F = (\theta_2 - \theta_1)P_a \int_{ri}^{ro} r.dr$

$= \frac{1}{2}(\theta_2 - \theta_1)P_a(r_o^2 - r_i^2)$ ……(3.25)

$T = (\theta_2 - \theta_1) f P_a \int_{r_i}^{r_o} r^2 . dr$

$= \frac{1}{3}(\theta_2 - \theta_1) f . P_a(r_o^3 - r_i^3)$ ……(3.26)

$$r_e = \frac{p_a \int_{r_i}^{r_o} r^2 . dr}{p_a \int_{r_i}^{r_o} r . dr} \quad \text{……(3.27)}$$

$$= \frac{r_o^3 - r_i^3}{3} \frac{2}{r_o^2 - r_i^2} = \frac{2}{3} \frac{r_o^3 - r_i^3}{r_o^2 - r_i^2} \quad \text{……(3.28)}$$

$$\bar{r} = \frac{\cos\theta_1 - \cos\theta_2}{\theta_2 - \theta_1} \frac{2}{3} \frac{r_o^3 - r_i^3}{r_o^2 - r^2 i}$$

$$= \frac{2}{3} \frac{r_o^3 - r_i^3}{r_o^2 - r_i^2} \frac{\cos\theta_1 - \cos\theta_2}{\theta_2 - \theta_1} \quad \text{……(3.29)}$$

3.2.2.3. Stress in brake disk

a) Stiffness Matrix [C] for General Material

The stiffness matrix [C] has 36 constants, [**33**].

$$\begin{bmatrix} \sigma_1 \\ \sigma_2 \\ \sigma_3 \\ \tau_{23} \\ \tau_{31} \\ \tau_{12} \end{bmatrix} = \begin{bmatrix} C_{11} & C_{12} & C_{13} & C_{14} & C_{15} & C_{16} \\ C_{21} & C_{22} & C_{23} & C_{24} & C_{25} & C_{26} \\ C_{31} & C_{32} & C_{33} & C_{34} & C_{35} & C_{36} \\ C_{41} & C_{42} & C_{43} & C_{44} & C_{45} & C_{46} \\ C_{51} & C_{52} & C_{53} & C_{54} & C_{55} & C_{56} \\ C_{61} & C_{62} & C_{63} & C_{64} & C_{65} & C_{66} \end{bmatrix} \begin{bmatrix} \varepsilon_1 \\ \varepsilon_2 \\ \varepsilon_3 \\ \gamma_{23} \\ \gamma_{31} \\ \gamma_{12} \end{bmatrix}$$

b) Stiffness Matrix [C] for Isotropic Materials

$$\begin{bmatrix} \varepsilon_1 \\ \varepsilon_2 \\ \varepsilon_3 \\ \gamma_{23} \\ \gamma_{31} \\ \gamma_{12} \end{bmatrix} = \begin{bmatrix} C_{11} & C_{12} & C_{12} & 0 & 0 & 0 \\ C_{12} & C_{11} & C_{12} & 0 & 0 & 0 \\ C_{12} & C_{12} & C_{11} & 0 & 0 & 0 \\ 0 & 0 & 0 & 2(C_{11} - C_{12}) & 0 & 0 \\ 0 & 0 & 0 & 0 & 2(C_{11} - C_{12}) & 0 \\ 0 & 0 & 0 & 0 & 0 & 2(C_{11} - C_{12}) \end{bmatrix} \begin{bmatrix} \sigma_1 \\ \sigma_2 \\ \sigma_3 \\ \tau_{23} \\ \tau_{31} \\ \tau_{12} \end{bmatrix}$$

Therefore, the relationship between stain and stress can be expressed as;

$$\begin{bmatrix}\sigma_x\\ \sigma_y\\ \sigma_z\\ \tau_{yz}\\ \tau_{zx}\\ \tau_{xy}\end{bmatrix}=\begin{bmatrix}\frac{E(1-\nu)}{(1-2\nu)(1+\nu)} & \frac{\nu E}{(1-2\nu)(1+\nu)} & \frac{\nu E}{(1-2\nu)(1+\nu)} & 0 & 0 & 0\\ \frac{\nu E}{(1-2\nu)(1+\nu)} & \frac{E(1-\nu)}{(1-2\nu)(1+\nu)} & \frac{\nu E}{(1-2\nu)(1+\nu)} & 0 & 0 & 0\\ \frac{\nu E}{(1-2\nu)(1+\nu)} & \frac{\nu E}{(1-2\nu)(1+\nu)} & \frac{E(1-\nu)}{(1-2\nu)(1+\nu)} & 0 & 0 & 0\\ 0 & 0 & 0 & G & 0 & 0\\ 0 & 0 & 0 & 0 & G & 0\\ 0 & 0 & 0 & 0 & 0 & G\end{bmatrix}\begin{bmatrix}\varepsilon_x\\ \varepsilon_y\\ \varepsilon_z\\ \gamma_{yz}\\ \gamma_{zx}\\ \gamma_{xy}\end{bmatrix},$$

The Equilibrium equations in polar coordinate are given as;

$$\frac{\partial\sigma_{rr}}{\partial r}+\frac{1}{r}\frac{\partial\sigma_{r\theta}}{\partial\theta}+\frac{1}{r}(\sigma_{rr}-\sigma_{\theta\theta}) = 0$$

$$\frac{\partial\sigma_{r\theta}}{\partial r}+\frac{1}{r}\frac{\partial\sigma_{\theta\theta}}{\partial\theta}+\frac{2\sigma_{r\theta}}{r} = 0 \quad \ldots\ldots\ldots\ldots\ldots\ldots\ldots\ldots\ldots\ldots\ldots\ldots\ldots\ldots\ldots.(3.30)$$

Hooks law in the stress-strain relations in polar coordinates are given by;

$\varepsilon_{rr} = \frac{1}{E}[\sigma_{rr}-v\sigma_{\theta\theta}]$, $\varepsilon_{\theta\theta} = \frac{1}{E}[\sigma_{\theta\theta}-v\sigma_{rr}]$, $\varepsilon_{r\theta} = \frac{1+v}{E}\sigma_{r\theta}$,

$\varepsilon_{zz} = -\frac{v}{E}(\sigma_{rr}+\sigma_{\theta\theta})$, Hook's law (plane stress) ………….(3.31)

And, $\varepsilon_{rr} = \frac{1+v}{E}[(1-v)\sigma_{rr}-v\sigma_{\theta\theta}]$, $\varepsilon_{\theta\theta} = \frac{1+v}{E}[(1-v)\sigma_{\theta\theta}-v\sigma_{rr}]$,

$\varepsilon_{r\theta} = \frac{1+v}{E}\sigma_{r\theta}$, Hook's law (plane strain) ……………………(3.32)

2-D Strain-Displacement Expressions Relations and Hooke's Law,

$$\varepsilon_{rr} = \frac{\partial u_r}{\partial r}$$

$$\varepsilon_{\theta\theta} = \frac{1}{r}\frac{\partial u_\theta}{\partial\theta}+\frac{u_r}{r}$$

$$\varepsilon_{r\theta} = \frac{1}{2}\left(\frac{1}{r}\frac{\partial u_r}{\partial\theta}+\frac{u_\theta}{\partial r}-\frac{u_r}{r}\right) \quad \ldots\ldots\ldots\ldots\ldots\ldots\ldots\ldots\ldots\ldots\ldots.(3.33)$$

This can be simplified that the displacement, u_θ = *constant*, $\frac{\partial u_\theta}{\partial\theta} = 0$

Then reduced to;

$$\varepsilon_{rr} = \frac{\partial u_r}{\partial r}$$

$$\varepsilon_{\theta\theta} = \frac{u_r}{r}$$

$$\varepsilon_{r\theta} = \frac{1}{2}\left(\frac{\partial u_\theta}{\partial r} - \frac{u_\theta}{r}\right) \quad \ldots\ldots\ldots\ldots\ldots\ldots\ldots\ldots\ldots\ldots\ldots\ldots\ldots\ldots (3.33)$$

The equations (3.33) is reduced by assuming the displacement, $u_\theta = 0$

$$\varepsilon_{rr} = \frac{\partial u_r}{\partial r}, \quad \varepsilon_{\theta\theta} = \frac{u_r}{r}, \quad \varepsilon_{r\theta} = 0 \quad \ldots\ldots\ldots\ldots\ldots\ldots\ldots\ldots\ldots\ldots\ldots\ldots\ldots\ldots\ldots\ldots\ldots (3.34)$$

It follows from Hooke's law that $\sigma_{r\theta} = 0$. The non-zero stresses are illustrated in figure below.

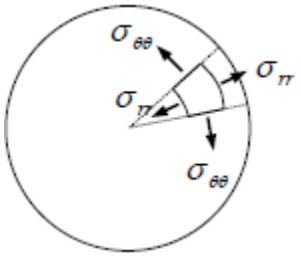

Figure 3.6: Stress components in plane axisymmetric

Only two stress components remain, and Hooke's law (3.31) reads

$$\varepsilon_{rr} = \frac{1}{E}\left[\sigma_{rr} - v\sigma_{\theta\theta}\right],$$

$$\varepsilon_{\theta\theta} = \frac{1}{E}\left[\sigma_{\theta\theta} - v\sigma_{rr}\right], \quad \text{or}$$

$$\sigma_{rr} = \frac{E}{1-v^2}\left[\varepsilon_{rr} + v\varepsilon_{\theta\theta}\right]$$

$$\sigma_{\theta\theta} = \frac{E}{1-v^2}\left[\varepsilon_{\theta\theta} + v\varepsilon_{rr}\right] \quad \ldots\ldots\ldots\ldots\ldots\ldots\ldots\ldots\ldots\ldots\ldots\ldots\ldots\ldots (3.35)$$

With $\varepsilon_{zz} = \frac{-v}{E}\left[\sigma_{rr} + \sigma_{\theta\theta}\right]$, $\quad \varepsilon_{zr} = \varepsilon_{z\theta} = 0$ and $\sigma_{zz} = 0$.

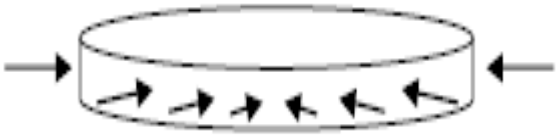

Figure 3.7: plane stress axisymmetric

The equations governing the plane axisymmetric are the equations of equilibrium (3.30) which reduce to the single equation;

$$\frac{\partial \sigma_{rr}}{\partial r} + \frac{1}{r}(\sigma_{rr} - \sigma_{\theta\theta}) = 0 \quad \ldots\ldots\ldots\ldots\ldots\ldots\ldots\ldots\ldots\ldots\ldots\ldots\ldots\ldots\ldots\ldots\ldots\ldots (3.36)$$

Taking the plane stress case, substituting (3.34) into the second of (3.35) and then substituting the result into (3.36) lead to (with a similar result for plane strain)

$$\frac{d^2u}{dr^2}+\frac{du}{rdr}-\frac{u}{r^2}=0 \quad \ldots\ldots\ldots\ldots\ldots\ldots\ldots\ldots\ldots\ldots\ldots\ldots\ldots\ldots\ldots\ldots\ldots\ldots\ldots\ldots..(3.37)$$

This is Navier's equation for plane axisymmetric. It is an "Euler-type" ordinary differential equation which can be solved exactly and given by;

$u = C_1 r\ C_2\frac{1}{r}$ ………………………………………………………………………… (3.38)

With the displacement known, the stresses and strains can be evaluated, and the full solution is;

$$u = C_1 r\ C_2\frac{1}{r}$$

$$\varepsilon_{rr}=C_1-C_2\frac{1}{r^2}\ ,\varepsilon_{\theta\theta}=C_1+C_2\frac{1}{r^2}$$

$$\sigma_{rr}=\frac{E}{1-v}C_1-\frac{E}{1+v}C_2\frac{1}{r^2}$$

$$\sigma_{\theta\theta}=\frac{E}{1-v}C_1+\frac{E}{1+v}C_2\frac{1}{r^2} \quad \ldots\ldots\ldots\ldots\ldots\ldots\ldots\ldots\ldots\ldots\ldots\ldots\ldots\ldots\ldots\ldots\ldots\ldots\ (3.39)$$

For problem involving stress boundary conditions, it is best to have simplest expressions for the stress so; introducing new constants,

A$=\frac{-EC_2}{1+v}\ and\ C=\frac{EC_1}{2(1-v)}$ ……………………………………………….(3.40)

The solutions can be re-written as;

$$\sigma_{rr}=+A\frac{1}{r^2}+2C,\ \sigma_{\theta\theta}=-A\frac{1}{r^2}+2C,\ \varepsilon_{rr}=+\frac{(1+v)A}{Er^2}+\frac{2(1-v)C}{E},\ \varepsilon_{\theta\theta}=-\frac{(1+v)A}{Er^2}+\frac{2(1-v)C}{E},\ \varepsilon_{zz}=-\frac{4vC}{E},\quad u=-\frac{(1+v)A}{Er}+\frac{2(1-v)C}{E},$$

Plane stress axisymmetric solutions, …………………………………………………........(3.41)

By substituting equations (3.40) into (3.41) the stress are now;

$$\sigma_{rr}=\frac{E}{(1+v)+(1-2v)}\left[-(1-2v)C_2\frac{1}{r^2}+C_1\right],$$

$$\sigma_{\theta\theta}=\frac{E}{(1+v)+(1-2v)}[+(1-2v)C_2\frac{1}{r^2}+C_1] \quad \ldots\ldots\ldots\ldots\ldots\ldots\ldots\ldots\ldots\ldots\ldots\ldots\ldots.. (3.42)$$

Then with A = $\frac{-EC_2}{1+v}\ and\ C=\frac{EC_1}{2(1+v)(1-2v)}$, the solutions can be re-written as;

$$\sigma_{rr}=+A\frac{1}{r^2}+2C,\qquad \sigma_{\theta\theta}=-A\frac{1}{r^2}+2C,\qquad \sigma_{zz}=4vC,$$

$\varepsilon_{rr} = \frac{1+v}{E}\left[+\frac{A}{r^2} + 2(1-2v)C\right]$, $\varepsilon_{\theta\theta} = \frac{1+v}{E}\left[-\frac{A}{r^2} + 2(1-2v)C\right]$,

$u = \frac{(1+v)}{E}\left[-A\frac{1}{r} + 2(1-2v)Cr\right]$, Plane strain axisymmetric solutions, ……..(3.43)

The solutions (3.41) and (3.43) involve two constants. When there is a solid body one boundary, A must be zero in order to ensure finite-valued stresses and strains; C can be determined from the boundary condition.

The mechanical properties of material are determined by standard governing;

Bulk modulus, $K = \frac{E}{3(1-2v)}$

Shear Modulus, $\mu = \frac{E}{2(1+v)}$

Lame Modulus, $\lambda = \frac{vE}{(1+v)(1-2v)}$ …….. (3.44)

Since, by considering a thin disc rotating with constant angular velocity (ω) from the following figure, the material particles are subjected to a centripetal acceleration $a_r = -r\omega^2$. The subscript *r* indicates acceleration in the radial direction and the minus sign indicates that the particles are accelerating towards the centre of the disc [**34**].

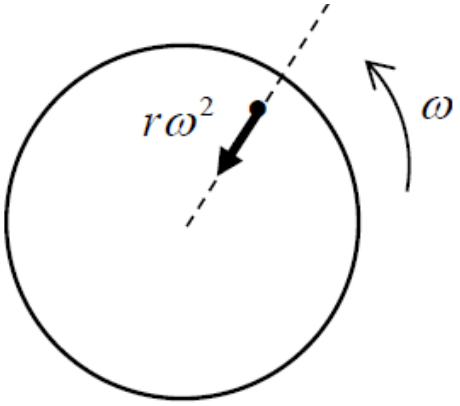

Figure 3.8: The rotating disc

The accelerations lead to an inertial force (per unit volume) $F_a = -pr\omega^2$ which in turn leads to stresses in the disc. The inertial force is an axis symmetric "loading" and so this is an axis symmetric problem. The axis symmetric equation of equilibrium is given by equation (3.35), adding in the acceleration term gives the corresponding equation of motion:

$$\frac{\partial \sigma_{rr}}{\partial r} + \frac{1}{2}(\sigma_{rr} - \sigma_{\theta\theta}) = -pr\omega^2$$

This can be express as;

$$\frac{\partial \sigma_{rr}}{\partial r} + \frac{1}{2}(\sigma_{rr} - \sigma_{\theta\theta}) = -\mathrm{pr}\omega^2 + \mathrm{b_r} = 0 \quad \ldots\ldots\ldots\ldots\ldots\ldots\ldots\ldots\ldots\ldots\ldots\ldots\ldots\ldots\ldots\ldots\ldots\ldots (3.45)$$

Where $b_r = pr\omega^2$. Thus the dynamic rotating disc problem has been converted into an equivalent static problem of a disc subjected to a known body force.

Using the strain-displacement relations (3.34) and the plane stress Hooke's law (3.35) then leads to the differential equation.

$$\frac{d^2u}{dr^2} + \frac{du}{rdr} - \frac{u}{r^2} = -\frac{1-v^2}{E} pr\omega^2 \quad \ldots\ldots\ldots\ldots\ldots\ldots\ldots\ldots\ldots\ldots\ldots\ldots\ldots\ldots\ldots\ldots\ldots\ldots (3.46)$$

This is equation (3.37) with a non-homogeneous term. The equation is derived as;

$$U = C_1 r + {}_2\frac{1}{Cr} - \frac{1}{8}\frac{1-v^2}{E} pr^3\omega^2 \quad \ldots\ldots\ldots\ldots\ldots\ldots\ldots\ldots\ldots\ldots\ldots\ldots\ldots\ldots\ldots\ldots\ldots\ldots (3.47)$$

Substitute equations (3.40) in equations (3.34) and (3.35), the full general governing equation are given as;

$$\sigma_{rr} = +A\frac{1}{r^2} + 2C - \frac{1}{8}(3+v)pr^2\omega^2 \quad \ldots\ldots\ldots\ldots\ldots\ldots\ldots\ldots\ldots\ldots\ldots\ldots\ldots\ldots\ldots\ldots\ldots\ldots (3.48)(xxb)$$

$$\sigma_{\theta\theta} = -A\frac{1}{r^2} + 2c - \frac{1}{8}(1+3v)pr^2\omega^2$$

$$\varepsilon_{rr} = \frac{1}{E}[+(1+v)\frac{A}{r^2} + 2(1-v)C - \frac{3}{8}(1-v^2)pr^2\omega^2] \quad \ldots\ldots\ldots\ldots\ldots\ldots\ldots\ldots\ldots\ldots\ldots\ldots (3.49)$$

$$\varepsilon_{\theta\theta} = \frac{1}{E}[-(1+v)\frac{A}{r^2} + 2(1-v)C - \frac{1}{8}(1-v^2)pr^2\omega^2]$$

$$u = \frac{1}{E}[-(1+v)\frac{A}{r} + 2(1-v)C_r - \frac{1}{8}(1-v^2)pr^3\omega^2]$$

Which reduce to (3.41) when, ω = 0

For a hollow Disc the boundary conditions are;

$$\sigma_{rr}(a) = 0, \qquad \sigma_{rr}(b) = 0 \quad \ldots\ldots\ldots\ldots\ldots\ldots\ldots\ldots\ldots\ldots\ldots\ldots\ldots\ldots\ldots\ldots\ldots\ldots (3.50)$$

Where *a* and *b* are the inner and outer radii respectively. It follows from (3.49) that;

$$A = -\frac{1}{8}(3+v)pa^2b^2\omega^2, \qquad C = \frac{1}{16}(3+v)p\omega^2(a^2+b^2) \quad \ldots\ldots\ldots\ldots\ldots\ldots\ldots\ldots\ldots\ldots (3.51)$$

And the stresses and displacement are;

$$\sigma_{rr}(r) = \frac{3+v}{8}\mathrm{p}\omega^2[\mathrm{a}^2 + \mathrm{b}^2 - \mathrm{r}^2 - \frac{a^2b^2}{r^2}]$$

$$\sigma_{\theta\theta}(r) = \frac{3+v}{8}\mathrm{p}\omega^2[\mathrm{a}^2 + \mathrm{b}^2 - \frac{1+3v}{3+v}\mathrm{r}^2 + \frac{a^2b^2}{r^2}] \quad \ldots\ldots\ldots\ldots\ldots\ldots\ldots\ldots\ldots\ldots\ldots\ldots (3.52)$$

$$u(r) = \frac{3+v}{8} p\omega^2 \frac{1-v^2}{E} r[a^2 + b^2 - \frac{1+v}{3+v} r^2 + \frac{1+v}{1-v} \frac{a^2 b^2}{r^2}]$$

Dimensionless stress and displacement are plotted in figure below, for the case of v = 0.3 and $\frac{a}{b}$ = 0.2. The maximum stress occurs at the inner surface, where; [**35**].

$$\sigma_{\theta\theta}(0) = \frac{3+v}{4} p\omega^2 b^2 \left[1 + \frac{1-v}{3+v}\left(\frac{a}{b^2}\right)\right] \quad \ldots\ldots\ldots\ldots\ldots\ldots\ldots\ldots\ldots\ldots\ldots\ldots (3.53)$$

This is approximately twice the solid-disc maximum stress.

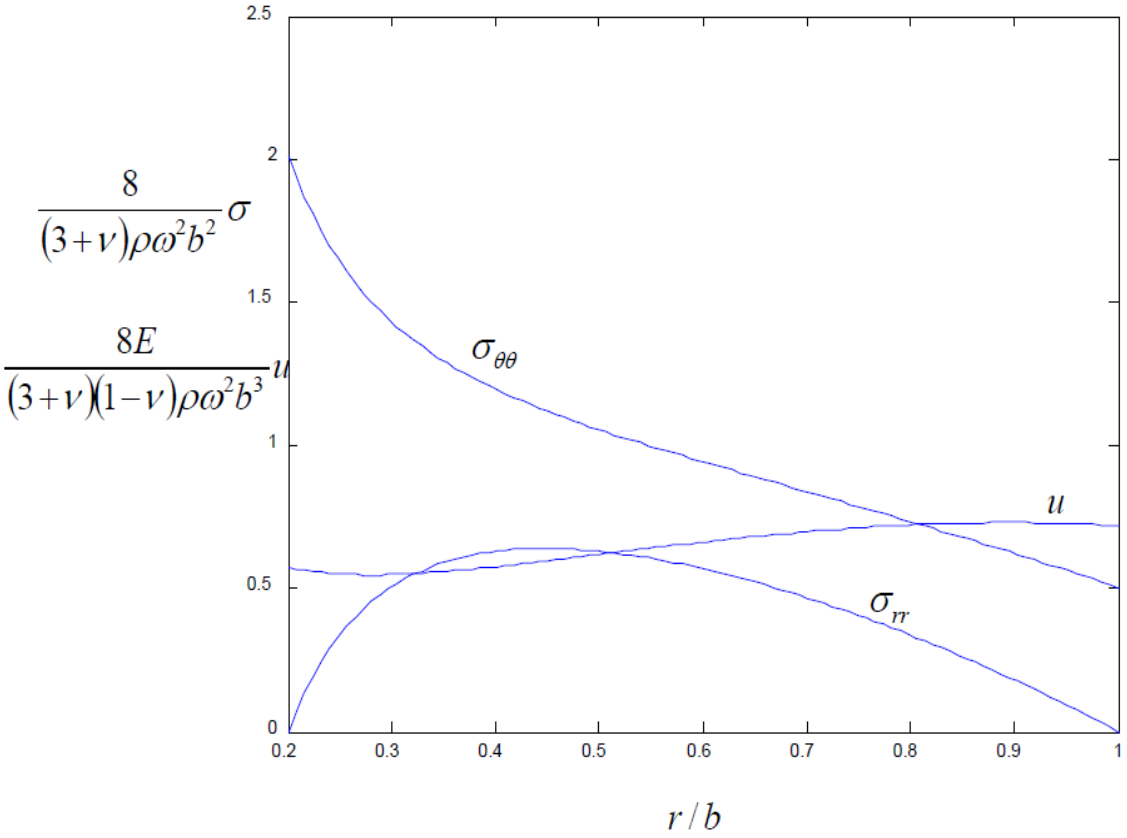

Figure 3.9: Stresses and displacements in the hollow rotating disc

3.2.2.4. Contact stress between the brake disk and brake pad

The following assumptions are generally made in the solution of the contact problem. Those are;

1) The contacting bodies are isotropic and elastic.
2) The contact areas are essentially flat and small relative to the radii of the curvature of the unreformed bodies in the vicinity of the interface.
3) The contact bodies are perfectly smooth, and therefore only normal pressures need to taken into account.

The contact pressures vary from zero at the side of contact area to maximum value to the contact stress (σ_c) at its center.

Then now by considering two rigid bodies of equal elastic module E, compressed by force P for curved surfaced of different radii.

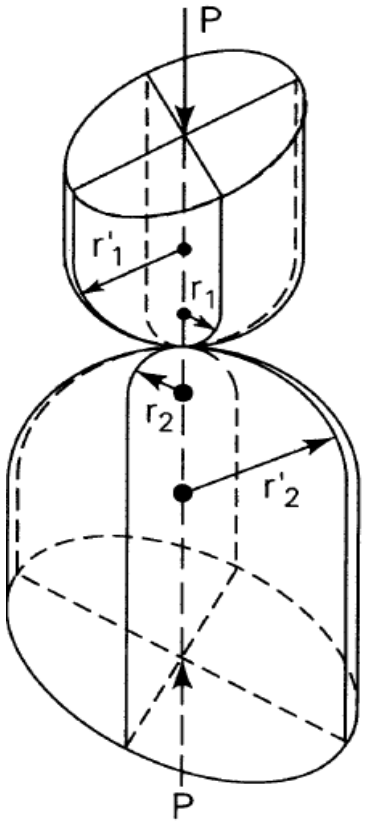

Figure 3.10: Surfaces of two bodies compressed by force P

The minimum and maximum radii of the curvature of the surface of the upper body are r_1 and $r_{1'}$; those of the lower bodies are r_2 and $r_{2'}$ at the point of contact. Thus $1/r_1$, $1/r_{1'}$, $1/r_2$ and $1/r_{2'}$ are the principal curvature. The sign convention of the curvature is positive if the corresponding center of curvature is inside the body and negative if the center of curvature is outside. Let θ be the angle between normal planes in which radii r_1 and r_2 lie and subsequent to loading, the area of contact will be an ellipse an ellipse with semi-axis *a* and *b*. Then, the maximum contact pressure, maximum contact stress or maximum principal stress is given by:

$$\sigma_{c=1.5}\frac{P}{\pi ab} \quad \text{.....(3.54)}$$

Where;

$$a = C_a \sqrt[3]{\frac{pm}{n}}$$

$$b = C_b \sqrt[3]{\frac{pm}{n}} \quad \textit{and;}$$

$$m = \frac{4}{\frac{1}{r_1}+\frac{1}{r_{1'}}+\frac{1}{r_2}+\frac{1}{r_{2'}}}$$

$$n = \frac{4E}{3(1-v^3)} \qquad \text{……..(3.55)}$$

But, for brake disk and brake pad but $r_{1'}$ and $r_{2'}$ are mutually perpendicular. So $r_{1'}$ and $r_{2'}$ are zero. So the above equations the value of *m* is reduced to;

$$m = \frac{4}{\frac{1}{r_1}++\frac{1}{r_2}} \quad ; n = \frac{4E}{3(1-v^3)}$$

The contact C_a and C_b are read in the table, the first column of table lists value of α.

Then, α is calculated as

$$\text{Cos}(\alpha) = \frac{B}{A}$$

Where;

$$A = \frac{1}{2}\left(\frac{1}{r_1} + \frac{1}{r_2}\right)$$

$$B = \pm\frac{1}{2}\left(\frac{1}{r_1} - \frac{1}{r_2}\right)$$

$$\text{So, Cos}(\alpha) = \pm\frac{1}{2}\left(\frac{\frac{1}{r_1}-\frac{1}{r_2}}{\frac{1}{r_1}+\frac{1}{r_2}}\right) \qquad \text{……(3.56)}$$

$$\sigma_{c = 1.5}\frac{P}{\pi ab} \qquad \text{……(3.57)}$$

Table 3-5: The constant of contact C_a and C_b

α (degrees)	c_a	c_b
20	3.778	0.408
30	2.731	0.493
35	2.397	0.530
40	2.136	0.567
45	1.926	0.604
50	1.754	0.641
55	1.611	0.678
60	1.486	0.717
65	1.378	0.759
70	1.284	0.802
75	1.202	0.846
80	1.128	0.893
85	1.061	0.944
90	1.000	1.000

3.2.2.5. Von Mises theory analysis

The von Mises stress criterion, the maximum shear stress criterion and the maximum normal stress criterion are a yield function to check whether the stress state is beyond the elastic region. Maximum shear stress (Tresca) and von Mises are applied when the structural material is ductile. The von Mises theory obviously predicts failure and the Tresca theory is often used in design, because it is simpler to apply. The Maximum Shear Stress theory states that failure occurs when the maximum shear stress from a combination of principal stresses equals or exceeds the value obtained for the shear stress at yielding in the uni-axial tensile test [**36**].

The general simplified equations of von Mises are;

$$\sigma_v = \sqrt{\frac{[(\sigma_{11} - \sigma_{22})^2 + (\sigma_{22} - \sigma_{33})^2 + (\sigma_{33} - \sigma_{11})^2 + 6(\sigma_{12}{}^2 + \sigma_{23}{}^2 + \sigma_{31}{}^2)^2]}{2}}$$

……..(3.58)

Where: the subscripts 1, 2, 3 can be replaced with x, y, z, or other orthogonal coordinate system. For uniaxial or simple tension, σ_1 =0 and (σ_2 , σ_3 , σ_{12} , σ_{23} , σ_{31} = 0), then von Mises criterion simply reduced to: $\sigma_1 = \sigma_y$. Which means the materials starts to yield when σ_1 reaches the yield strength of the materials by σ_y and is in agreement with the definition of tensile (or) compressive yield strength.

The von-Mises effective stress (σ_e) also sometimes referred to as equivalent stress is defined as the uniaxial tensile stress that would create the same distortion energy as is created by the actual combination of applied stresses.

$\sigma_e = [\sigma_1^2 + \sigma_2^2 + \sigma_3^2 - \sigma_1\sigma_2 - \sigma_2\sigma_3 - \sigma_3\sigma_1]^{1/2}$

$\sigma_e = [\sigma_1^2 + \sigma_3^2 - \sigma_3\sigma_1]^{1/2}$; for two dimensional stress $\sigma_2 = 0$.

In terms of applied stresses in coordinate directions expressed as;

$\sigma_e = [\sigma_{xx}^2 + \sigma_{yy}^2 - \sigma_{xx}\sigma_{yy} + 3\tau_{xy}]^{1/2}$

The von Mises theory (or) distortion energy of the strain energy is given by:

$$U_d = \left(\frac{1+v}{3E}\right)\frac{(\sigma_1-\sigma_2)^2+(\sigma_2-\sigma_3)^2+(\sigma_3-\sigma_1)^2}{2} \quad \text{.....(3.59)}$$

And when express distortion energy interims of equivalent stress.

$$U_d = \left(\frac{1+v}{3E}\right)\sigma_{vm}^2 \quad \text{.....(3.60)}$$

The von Mises stress is defined in terms of principal stresses as;

$$\sigma_{vm} = \sqrt{\frac{[(\sigma_1 - \sigma_2)^2 + (\sigma_2 - \sigma_3)^2 + (\sigma_3 - \sigma_1)^2]}{2}}$$

At yielding, in a uni-axial test, the principal stresses are:

$\sigma_1 = S_y$ and $\sigma_2 = \sigma_3 = 0$.

Therefore; the shear strength at yielding;

$$S_{sy} = \frac{[\sigma_1 - (\sigma_2 \text{ or } \sigma_3 = 0)]}{2}\text{; then: } S_{sy} = \frac{S_y}{2} \quad \text{..... (3.61)}$$

Where:

S_{sy} is yield strength in shear

S_y is yield strength

According to the maximum principal stress theory, a brittle material ruptures when the maximum principal stress in the specimen reaches some limiting value for the material. Again, this critical value can be inferred as the tensile strength measured using a uniaxial tension test.

The maximum shear stress governing equation is given as by computing three principal stresses (σ_1, σ_2, σ_3).

$$\tau_{max} = \frac{\sigma_1 - \sigma_2}{2} = \frac{\sigma_{p}max - \sigma_{p}min}{2} \quad \text{.....(3.62)}$$

Since, compare the maximum shear stress to the failure criterion.

$\tau_{max} \leq S_{sy}$ (or) $\frac{\sigma_{p}max - \sigma_{p}min}{2} \leq S_{sy}$

The safety factor for the maximum shear stress theory [**37**], is given by:

$$f = \frac{S_{sy}}{\tau_{max}}$$

3.2.2.6. Fatigue life time estimation

Fatigue is weakening of the structure caused by applied cyclic loading. The damage appears after a certain number of load cycles at nominal stress level that is usually far below the static tensile strength of the material. Material fatigue is classified into two: Those are high-cycle fatigue and low-cycle fatigue. The high-cycle fatigue is defined as low stress and high number of loading cycle to failure; as well as low-cycle fatigue is defined as high stress and low number of loading cycle to failure.

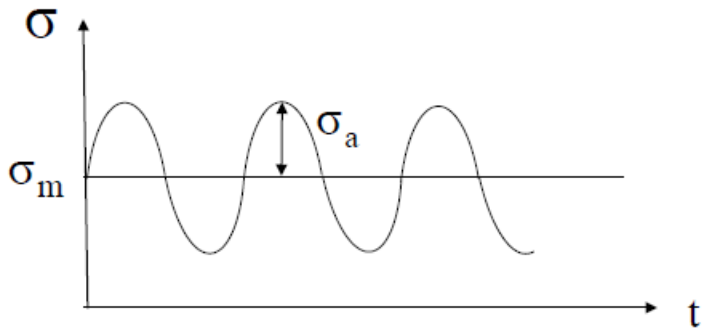

Figure 3.11: Fatigue life cycle

$\sigma(t) = \sigma_m + \sigma_a \sin\omega t$ …….(3.62)

Stress amplitude:

$\sigma_a = \frac{1}{2}(\sigma_{max} - \sigma_{min})$ ……(3.63)

Mean stress:

$\sigma_m = \frac{1}{2}(\sigma_{max} + \sigma_{min})$ …….(3.64)

Where:

$\sigma_{max} = \sigma_m + \sigma_a$

$\sigma_{min} = \sigma_m - \sigma_a$

N = $\frac{t}{\tau} = \frac{\omega t}{2\pi}$, number of loading cycles ……..(3.65)

Cycle loading

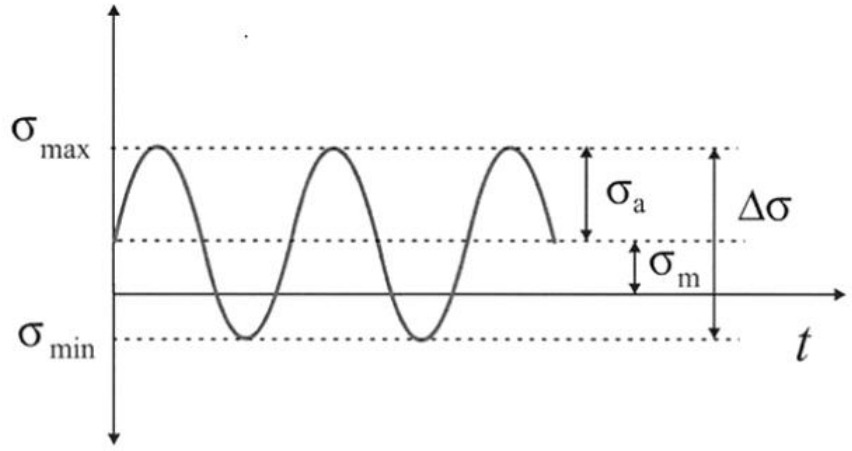

Figure 3.12: Cycle loading

Strain Energy: Assuming that the stress-strain curve is essentially linear up to the yield point, we can express the total strain energy at any point in that range as;

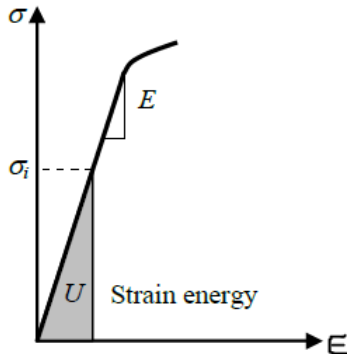

Figure 3.13: Strain-stress curve and strain energy

A strain energy equation is given by:

U = $\frac{1}{2}\sigma\varepsilon$ …… (3.66)

Extending this equation in to three dimensional cases;

$\frac{1}{2}(\sigma_1\varepsilon_1 + \sigma_2\varepsilon_2 + \sigma_3\varepsilon_3)$ …….. (3.67)

Where: (σ_1, σ_2 and σ_3) are principal stress and (ε_1, ε_2 and ε_3) are principal strain.

Expressing strain interims of stresses as;

$\varepsilon_1 = \frac{1}{E}[\sigma_1 - \nu(\sigma_2 + \sigma_3)]$

$\varepsilon_2 = \frac{1}{E}[\sigma_2 - \nu(\sigma_1 + \sigma_3)]$ …… (3.68)

$\varepsilon_1 = \frac{1}{E}[\sigma_3 - \nu(\sigma_2 + \sigma_1)]$

The total energy of the three dimensional case is given by equating above two equations;

$U = (\frac{1}{2E})[\sigma_1^2 + \sigma_2^2 + \sigma_3^2 - 2\nu(\sigma_1\sigma_2 + \sigma_2\sigma_3 + \sigma_3\sigma_1)]$ ……(3.69)

3.2.2.7. Boundary condition and engineering data aspect

For Fatigue life time estimation, in the cyclic stress- strain and strain life relationships have been introduced with four fatigue properties. Those are:

σ_F' - Fatigue strength coefficient

ε_F' - Fatigue ductility coefficient

b - Fatigue strength exponent

c - Fatigue ductility exponent

The fatigue strength exponent 'b' values varies from (-0.05 to -0.12). But, for the most metals with an average of (-0.085 $\simeq$ -0.09). For fairly ductility metals (where $\varepsilon_F = 1$) have average value of 'c' = -0.6. For strong metals (where $\varepsilon_F = 0.5$) a value of fatigue ductility exponent 'c' = -0.5 is probably more reasonable. Fatigue ductility coefficient 'ε_F' ' $\simeq$ ε_F (monotonic fracture ductility) [**38**], [**39**]. In general, the fatigue life estimation equation can be expressed as;

$\sigma_a = \sigma_F'(2N_f)^b$ ……..(3.70)

Where: $\sigma_F' = 1.6\,\sigma_u$

Since, high cycle fatigue is expressed as ($\geq 10^4$) and low cycle fatigue is expressed as ($\leq 10^4$). The cycle strength coefficient, k' and cyclic strain hardening exponent, n' are obtained from fitting stable stress amplitude versus plastic strain amplitude data. Rough estimates of k' and n' can be calculated from the low cycle fatigue properties by using:

$k' = \frac{\sigma_F'}{(\varepsilon_F')^{b/c}}$, $n' = b/c$

The strain life equation is expressed as;

$\frac{\Delta\varepsilon}{2} = \varepsilon_a = \frac{\Delta\varepsilon_c}{2} + \frac{\Delta\varepsilon_p}{2} = \frac{\sigma_F'}{2E}(2N_f)^b + \varepsilon_F'(2N_f)^c$ ……..(3.71)

The stable cyclic stress-strain curve can be represented by the following equation for several metals [**40**].

$\varepsilon_a = \frac{\Delta\varepsilon}{2} = \frac{\Delta\varepsilon_2}{2} + \frac{\Delta\varepsilon_p}{2} = \frac{\Delta\sigma}{2E} + (\frac{\Delta\sigma}{2k'})^{1/n'} = \frac{\sigma_a}{E} + (\frac{\sigma_a}{k'})^{1/n'}$ ……..(3.72)

Where: k' and n' are material cyclic deformation properties.

As "TALAT lecture" prepared by "L. Froyen, University of Leuven. Verlinden, University of Leuven, Belgium"**;** the aluminum metal matrix composite (Al-MMC) with Al_2O_3 of volume percent of (20%) type 2014-T6 approximately, the ultimate strength is, σ_{ut} = 483Mpa.

Boundary condition estimation:

$n' = \frac{b}{c} = \frac{-0.09}{-0.5} = 0.18 = 0.2$

$\sigma'_F = 1.6\sigma_{ut} = 1.6 \times 483 = 772.8$ MPa

$k' = \frac{\sigma'_F}{(\varepsilon'_F)^{b/c}} = \frac{772.8}{(0.5)^{0.2}} = \frac{772.8}{0.87} = 888.3$Mpa

Table 3-6: Parameters that used for estimating fatigue life time of Al-MMC

σ'_F (MPa)	ε_F	k' (MPa)	n'	b	c
772.8	0.5	888.3	0.2	-0.09	-0.5

3.2.3. Finite Element Modeling and analysis

3.2.3.1. Introduction to Finite element analysis and ANSYS

The Finite Element Analysis (FEA) is a numerical method for solving problems of engineering and mathematical physics. It's useful for problems with complicated geometries, loadings and material properties. Further, the concept of Finite element analysis is a method of solving unknown variable by approximately in certain problems in engineering and science. The solved certain problem by FEA is mainly not exact solution. This method of analysis is required for complicated element that cannot really solved in analytical and different shapes like deformation, strain, displacement, stress, other load, etc. can be solved approximately by FEA. This certain problem solved in FEA is by splitting up into a number of smaller areas or volumes, which is named as Finite element and the two dimensional model of spanner to be divided is named as discretization and the assembly of the elements is named as Mesh. The discretization of elements can be of various shapes, in two dimensions can be quadrilateral or triangular, and in three-dimensions can be brick-shaped (hexahedral), Wedge-shaped (pentahedral) or tetrahedral.

Finite Element analysis procedure

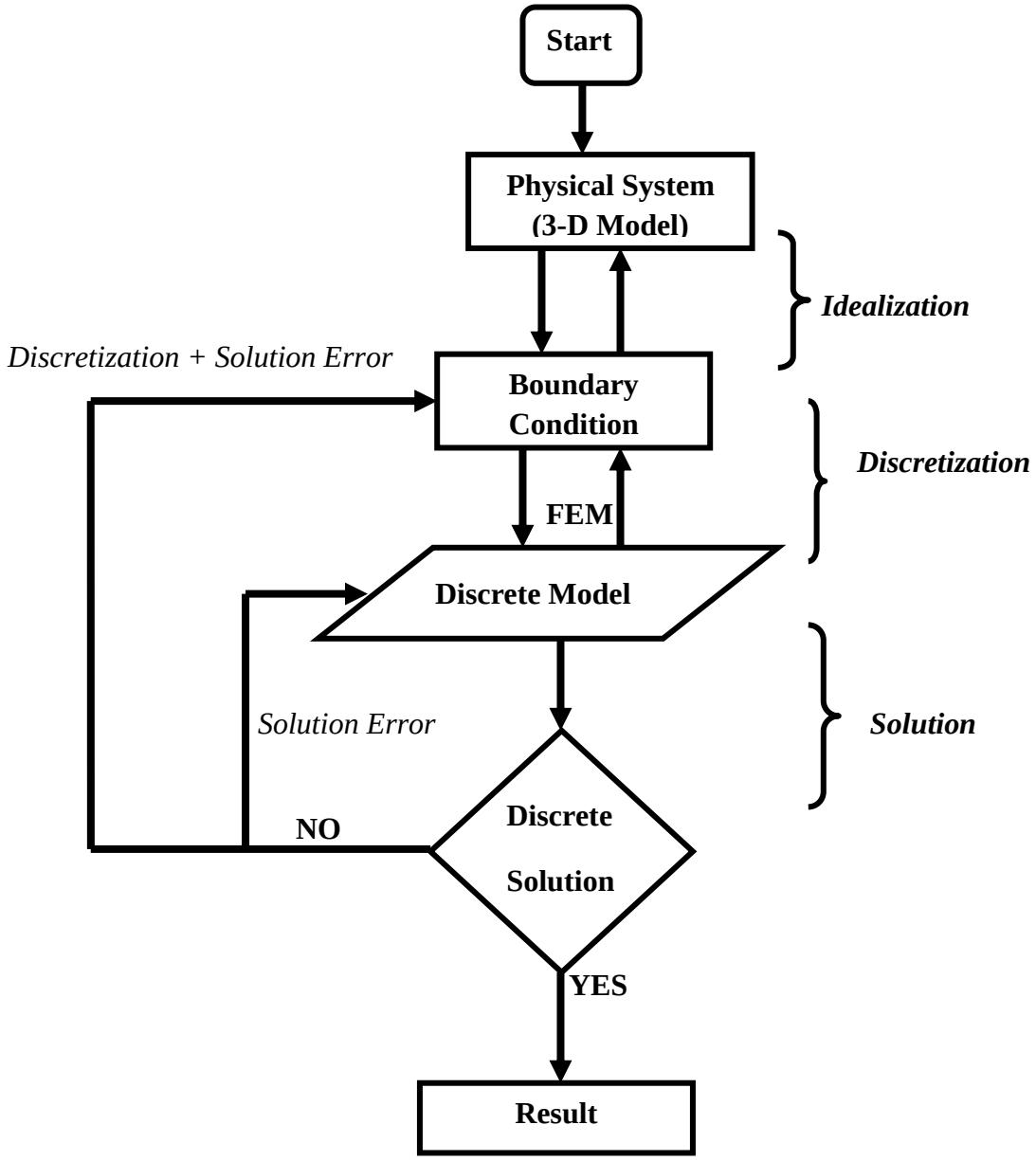

Figure 3.14: Finite Element analysis procedure

a) Physical System

Physical system of finite element analysis model needs extensive use of software packages that implement the accurate finite element method for solving equations considered along with the appropriate initial and boundary conditions and physical system is useful for predicting the performance and behavior of the design. The physical model of the object is shown below.

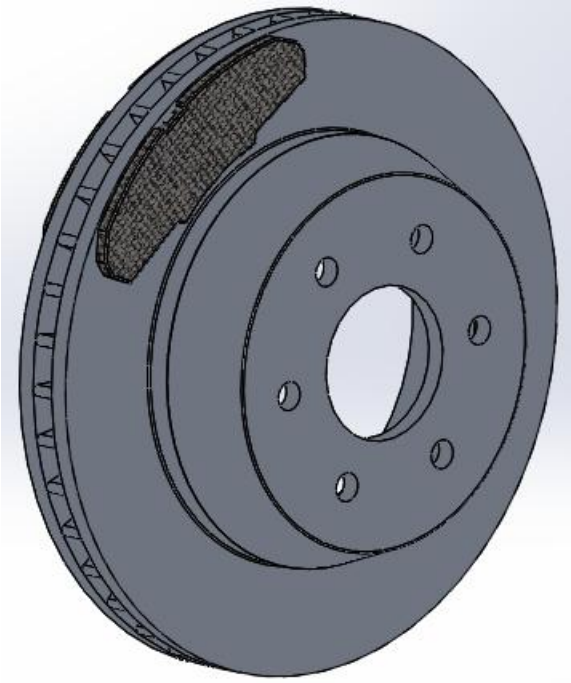

Figure 3.15: Physical model of Brake disc with brake pad

b) Boundary Condition

The Boundary condition of finite element analysis is includes structural load likes applied load, pressure, support, temperature, velocity, etc. are can be modeled and the equation for the system is prepared to analyzed by finite element method to discrete the model. The mathematical model assigning initial and condition is shown below.

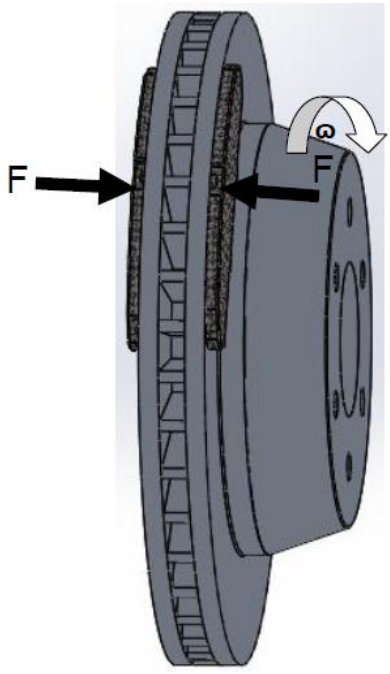

Figure 3.16: Boundary condition applied

c) Discrete Model

The discrete model of finite element method is a model body by dividing it into an equivalent system of many smaller bodies or units that are finite element interconnected at points common to two or more elements that are nodes or nodal points and boundary lines or surfaces. The discretization element is the triangular plate element, because the geometry is solid.

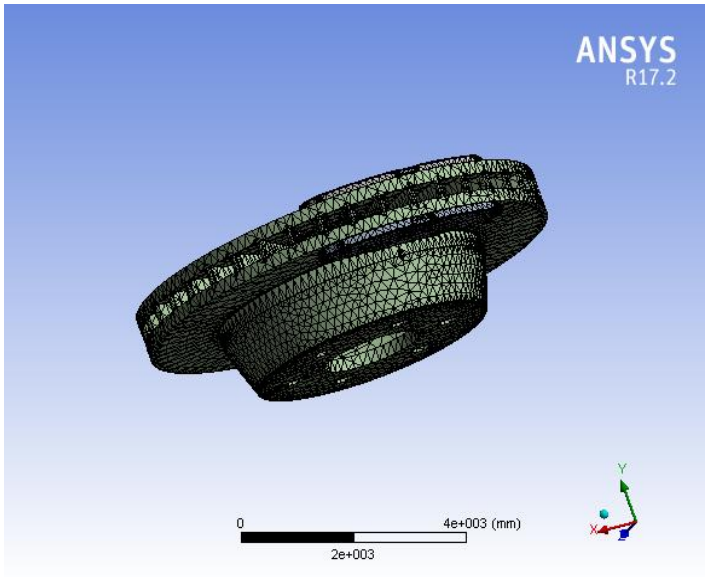

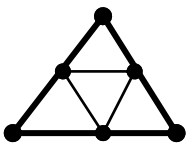

Figure 3.17: Discrete model

d) Discrete solution

The discrete solution of the model is analyzed as setting of the initial and boundary condition. The parameter to be solved by discretization is stated as follow:

- Total deformation
- Equivalent elastic strain
- Equivalent Stress
- Strain Energy
- Maximum principal stress
- Minimum principal stress
- Maximum principal elastic strain
- Minimum principal Elastic strain
- Life cycle
- Damage
- Safety factor
- Equivalent alternating Stress
- Temperature that produce in the contact of brake disk and brake pad
- Total heat flux that generate between brake disk and brake pad

Therefore, Based on the discrete solution, if the solution is approximately discrete correctly import the solution. And if the discrete solution is not correctly discrete in approximate, return the process to the back and set and analysis again. The type of commercial software to analysis the finite element method is ANSYS software for structural analysis allows you to solve your most complex structural engineering projects and make superior design decisions more quickly. Finite element analysis (FEA) software from ANSYS provides engineers the ability to automate and customize simulations and even parameterize them for many design application. The finite element method is analyzed on ANSYS Workbench 17.2. The project schematic on workbench is shown below.

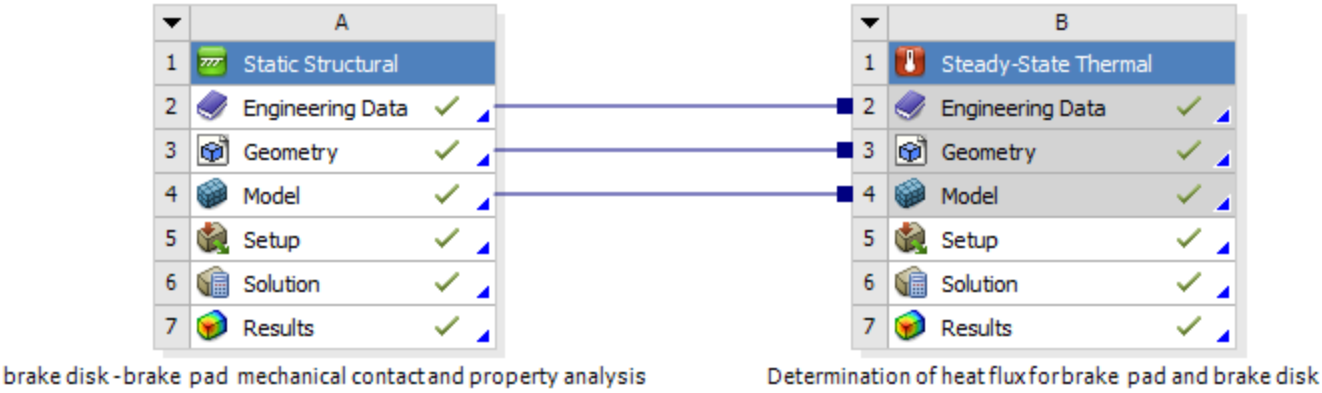

Figure 3.18: Schematic static structure and steady-state thermal analysis

3.3. Methods of Finite Element Analysis

The method of finite element analysis is a numerical method for solving problems of engineering and mathematical physics to solve the problem; it subdivided a large problem into smaller, simpler parts. The simple equations that model these finite elements are then assembled into a larger system of equations that models the entire problem. Then, the finite element method uses variation methods from calculus of variations to approximate a solution by minimizing an associated error function.

3.3.1. Analysis order of finite element

1. Discretization of structure (or) real continuum

In this process of analysis the finite element mesh is established. The shape of element for discretization is triangular plate elements and the commercial finite element code process is *automatic mesh generator* together with built in element library. Further, establish the mesh with set coordinates, element numbers and node numbers.

2. Identify primary unknown quantity

Element displacements for stress analysis and Element temperature for heat conduction analysis

In the stress analysis, the primary unknowns are nodal displacements, but secondary unknown quantities include: strains in elements can be obtained by the strain-displacement relations, and the unknown stresses in the elements by the stress-strain relations (the Hooke's law).

3. Interpolation functions and derivation of Interpolation functions

It is very important to derive a function that can relate the element quantities with the same quantities at the corresponding nodes. The interpolation function in finite element method relates the Element quantity $\phi(x, y, z)$. Mathematical expressions of interpolation functions:

$$\{\phi(r)\} = \{N(r)\}\{\phi\}$$

Where $\{\phi(\mathbf{r})\}$ = Element quantity, $\{\phi\}$ = nodal quantity, $N(\mathbf{r})$ = interpolation function with $\mathbf{r}$ = coordinates.

The interpolation functions can be expressed to relate the corresponding nodes in the following way:

Element quantity $\phi(x, y)$ = Interpolation function $\{N_1(x, y)\ N2(x, y)\ N3(x, y)\}$ x nodal quantity.

$\{\phi\}^T = \{\phi_1\ \phi2\ \phi3\}$ for plate elements with 3 nodes.

4. Derivation of Element equation

The derivation of element equation under this process is Rayleigh-Ritz method for stress analysis of solid structure using the potential energy in deformed solids as the functional to be minimized.

Element equations of the form: $[K_e]\{q\} = \{Q\}$

Where; $[K_e]$ = Element matrix

$\{q\}$ = Vector of primary unknown quantities at the nodes of the element

$\{Q\}$ = Vector of element nodal actions, like Force.

5. Derive Overall Stiffness Equation

Under this process, assembles all individual element equations derived in process 4 to provide the Stiffness equations for the entire medium. Mathematically, this equation has the form:

$$[K]\{q\} = \{R\}$$

Where; $[K]$ = overall stiffness matrix = $\sum_1^m [K_e]$

M = q = total number of elements in the discrete

$\{R\}$ = assemblage of resultant vector of nodal actions

6. Solve for primary unknowns

Use the inverse matrix method to solve the primary unknown quantities $\{q\}$ at all the nodes from the overall stiffness equations $\{q\} = [K]^{-1}\{R\}$

7. Solve for secondary unknowns

For secondary unknowns in stress analysis by FEM:

The primary unknowns = {q} = {u} = displacement components at all nodes in the FE model

Secondary unknowns: strains in element {ε} from the strain – displacement relations that are derived from theory of elasticity, stresses in element {σ} from the stress-strain relation: which is derived from the Hooke's law for simple uni-axial stress case generalized Hooke's law by theory of elasticity.

8. Display and Interpretation of Results

Present results of FEA by the following forms: a) tabulations, b) graphics. The present of result by graphics is shown into two ways; those are static and animation to interpretation of results.

In general, the method of finite method is analyzed by three stages. Those are;

A) Preprocessing

Define geometric domain: The geometric model of brake disk and brake pad is model by solid work software and imported the IGES save file to the ansys work bench working space.

Define element type: In two-dimensional case with a single field variable φ(x, y), The type of element in this kind of analysis is triangular element is described that said to have 3 degrees of freedom, as three nodal values of the field variable are required to describe the field variable everywhere in the element.

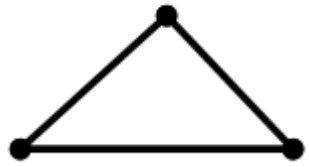

The function of single field variable is given as;

$$\varphi(x, y) = N_1(x, y)\,\varphi_1 + N_2(x, y)\,\varphi_2 + N_3(x, y)\,\varphi_3$$

In general, the number of degrees of freedom associated with a finite element is equal to the product of the number of nodes and the number of values of the field variable which is possible for its derivatives that must be computed at each node.

Define Material: the material selected for analysis is aluminum metal matrix composite (Al-MMC) for Disc material and Semi-metallic for brake pad. The friction materials of the current use of Ethiopian city taxes and other alternative friction material is analyzed.

Material properties of brake disc (Al-MMC)

Table 3.7: Material properties of brake disc (Al-MMC)

S.n	**PROPERTY**	**Al-MMC**
1	Tensile Strength (MPa)	484
2	Yield Strength (MPa)	437
3	Young's Modulus (GPa)	114
4	Poisson's Ratio	0.33
5	Density (gr/cm^{-3})	2.822
6	Thermal Conductivity (W/m.K)	140.2
7	Thermal Expansion Coefficient (C^{-1})	$(2.3) \times 10^{-5}$
8	Specific Heat(J/kg.K)	800

Material Properties of brake pad

Table 3.8: Material Properties of brake pads

S.n	**Friction component**	**Mass Density (kg/m^3)**	**Elastic Modulus (GPa)**	**Poisson ratio**
1	Aluminum Alloy	2700	69	0.33
2	Kevlar	1440	71	0.36
3	Ceramic Al_2O_3	3800	325	0.22

Meshing: The basic concept in finite element method is to analysis structure that is an assembly of discrete piece which means element and node that is connected together at finite number of points. So the network of these elements is called mesh and also the finite element that for meshing were triangular shapes. The number of element generated in the mesh is 74784 nodes and 41847 elements.

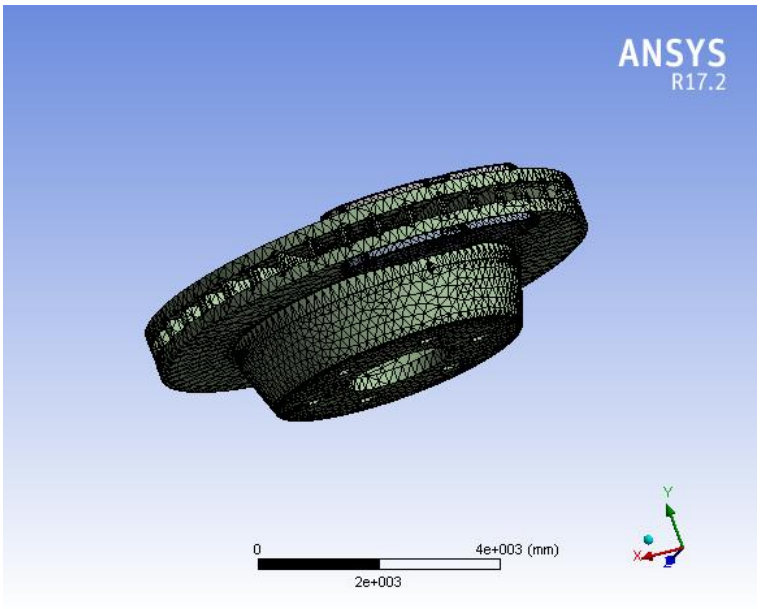

Figure 3.19: Meshing

3.3.2. Mechanical Load, Thermal load and boundary condition

The mechanical load clamped on brake disc by the action of brake pad hydraulic pressure of caliper is 20321N is applied on front brake disc of the car. And the temperature generated during braking at the initial and final braking is room temperature 22^{o}C and 262^{o}C respectively and also the coefficient of friction at different condition on ANSYS is 0.2. The figure below is show the mechanical load and thermal load applied on brake disc.

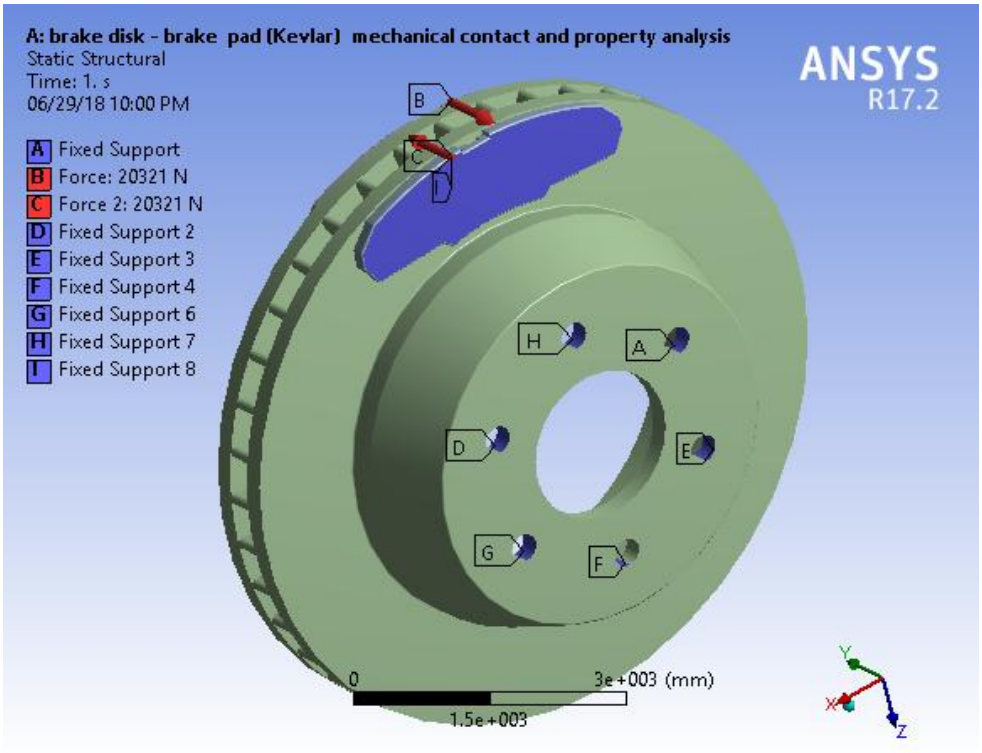

Figure 3.20: Mechanical load

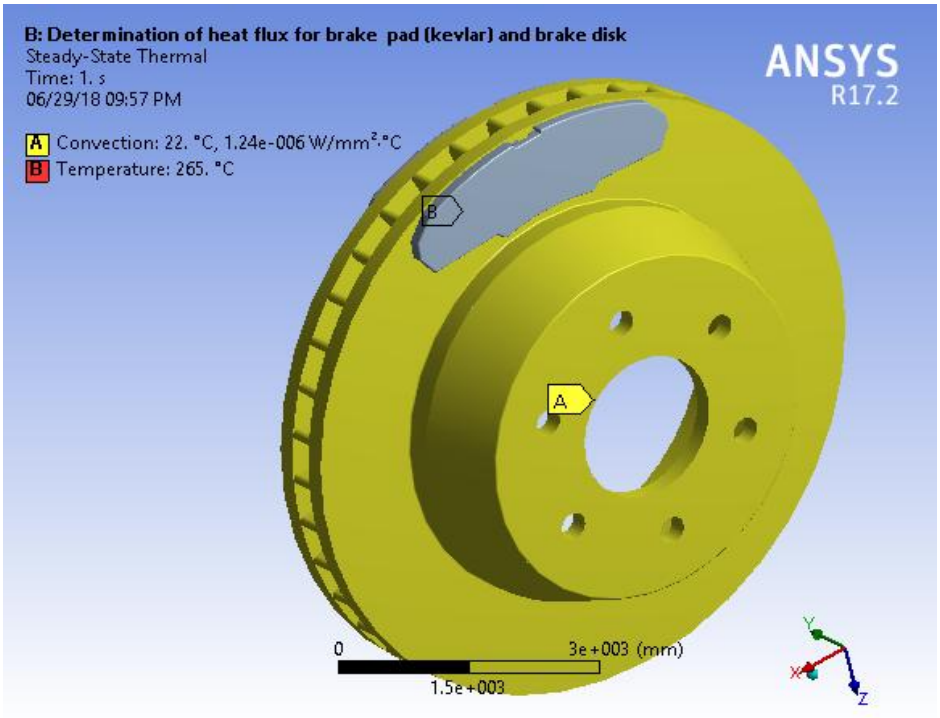

Figure 3.21: Thermal load

B) Process

Conduct numerical analysis in computer system and solve the boundary value problem. Compute the values are can be used by back substitution to compute additional, derived variables, such as reaction forces, element stresses, and heat flow.

C) Post processing

In the post processing, see the results in tabulation, graphs and animation. And select the result from finite element solution, like deformation, stress, strain, temperature, fatigue tools, etc. the result obtain in this process is illustrated in appendix I.

CHAPTER FOUR: RESULT AND DISCUSSION

In this section result and discussion of the study is presented in the mode of table, graph, etc. the mechanical properties of the material is discussed as the result obtain from the soft ware of ANSYS; and the result obtain in this investigation by reviewing varies data sources are presented. In addition, the condition of braking system in automotive is performed depending on the result obtain in this kind of investigation.

4.1. Content of brake pad composition in Ethiopian city taxi

The Composition of brake pad that use in Ethiopian city taxi is stated with the high amount of copper in their semi-metallic brake pad composition; thus this high amount of copper content is affect the brake pad by generating high heat during braking application, then the high heat dissipation is bring the wear of brake pad. As result obtains from Ethiopian geological survey laboratory, from the result listed in table 3.3 and the amount of ingredient in composition is shown by graph description in **figure 4.1.**

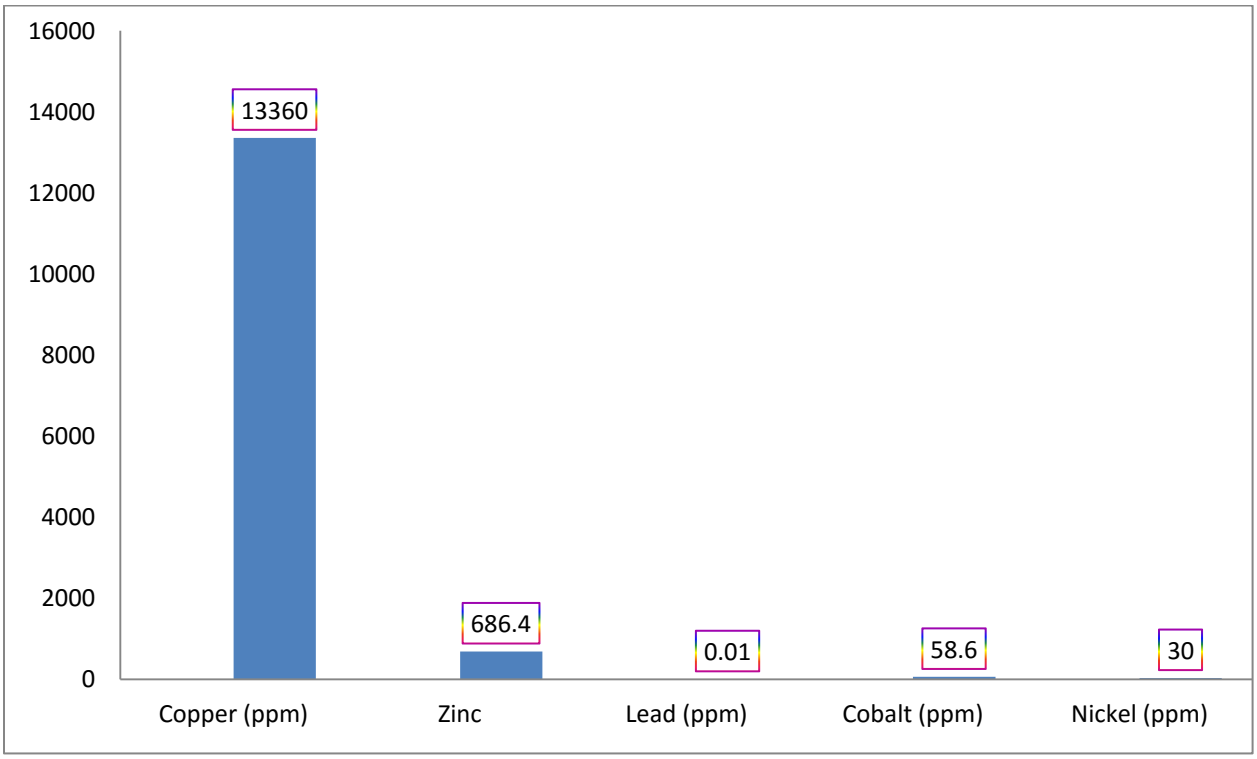

Figure 4.1: Composition of brake pad ingridient that used in Ethiopian City taxi

Further, the copper in brake pad is produce dust, those dustiest are removed on roads when braking is applied, the removed dust on road is moved by rainfall mixed with river or lakes, thus copper is toxic metal that can be affect organism. Hence, the brake pad that used in Ethiopian city taxi is contain more amount of composition of copper; then the reduction of copper in composition of semi-metallic brake pad distinctly that used in Ethiopian automotive city taxi vehicle is reduce the environmental pollution of Ethiopia for saving the life of organism that live in water (river, lakes etc).

4.2. Mechanical Result

A) Mechanical Result of Al-MMC brake disc with Kevlar brake pad

The analysis of mechanical result of Al-MMC brake disc with Kevlar brake pad obtained under ANSYS software is illustrated in the tabulation form in table 4.1.

Table 4-1: Mechanical Result of Al-MMC brake disc with Kevlar brake pad

Object Name	Minimum	Maximum
Total Deformation(mm)	0	$1.7553x10^{-12}$
Equivalent Elastic Strain (mm/mm)	$1.0804x10^{-19}$	$2.3519x10^{-14}$
Equivalent Stress (Mpa)	$3.8052x10^{-15}$	$8.4974x10^{-10}$
Strain Energy (mJ)	$5.6321x10^{-30}$	$7.5897x10^{-18}$
Maximum Principal Stress (Mpa)	$-4.2114x10^{-10}$	$7.6336x10^{-10}$
Minimum Principal Stress (Mpa)	$-1.2987x10^{-9}$	$1.0181x10^{-10}$
Maximum Principal Elastic Strain (mm/mm)	$-1.3098x10^{-17}$	$9.7057x10^{-15}$
Minimum Principal Elastic Strain(mm/mm)	$-1.3723x10^{-14}$	$1.0397x10^{-17}$

B) Mechanical Result of Al-MMC brake disc with Ceramic brake pad

The analysis of mechanical result of Al-MMC brake disc with Ceramic brake pad obtained under ANSYS software is illustrated in the tabulation form in table 4.2.

Table 4-2: Mechanical Result of Al-MMC brake disc with Ceramic brake pad

Object Name	Minimum	Maximum
Total Deformation(mm)	0	$1.5832x10^{-12}$
Equivalent Elastic Strain (mm/mm)	$1.0846x10^{-19}$	$1.9199x10^{-14}$
Equivalent Stress (Mpa)	$4.1973x10^{-15}$	$3.1627x10^{-9}$
Strain Energy (mJ)	$1.0749x10^{-29}$	$1.3465x10^{-17}$
Maximum Principal Stress (Mpa)	$-1.0621x10^{-9}$	$2.1063x10^{-9}$
Minimum Principal Stress (Mpa)	$-4.4507x10^{-9}$	$2.62x10^{-10}$
Maximum Principal Elastic Strain (mm/mm)	$-1.9437x10^{-16}$	$7.7092x10^{-15}$
Minimum Principal Elastic Strain(mm/mm)	$-1.1908x10^{-14}$	$8.8278x10^{-17}$

C) Mechanical Result of Al-MMC brake disc with Aluminum alloy brake pad

The analysis of mechanical result of Al-MMC brake disc with Aluminum alloy brake pad obtained under ANSYS software is illustrated in the tabulation form in table 4.3.

Table 4-3: Mechanical Result of Al-MMC brake disc with Aluminum alloy brake pad

Object Name	Minimum	Maximum
Total Deformation(mm)	0	$1.7787x10^{-12}$
Equivalent Elastic Strain (mm/mm)	$1.0038x10^{-19}$	$2.4039x10^{-14}$
Equivalent Stress (Mpa)	$4.0774x10^{-15}$	$8.3353x10^{-10}$
Strain Energy (mJ)	$5.2945 x10^{-30}$	$7.5389x10^{-18}$
Maximum Principal Stress (Mpa)	$-3.8447x10^{-10}$	$7.1502x10^{-10}$
Minimum Principal Stress (Mpa)	$-1.2478x10^{-9}$	$8.894x10^{-11}$
Maximum Principal Elastic Strain (mm/mm)	$-1.7003x10^{-17}$	$9.6626x10^{-15}$
Minimum Principal Elastic Strain(mm/mm)	$-1.4104x10^{-14}$	$8.7101x10^{-18}$

D) Total deformation of Al-MMC disc brake and brake pads with braking time

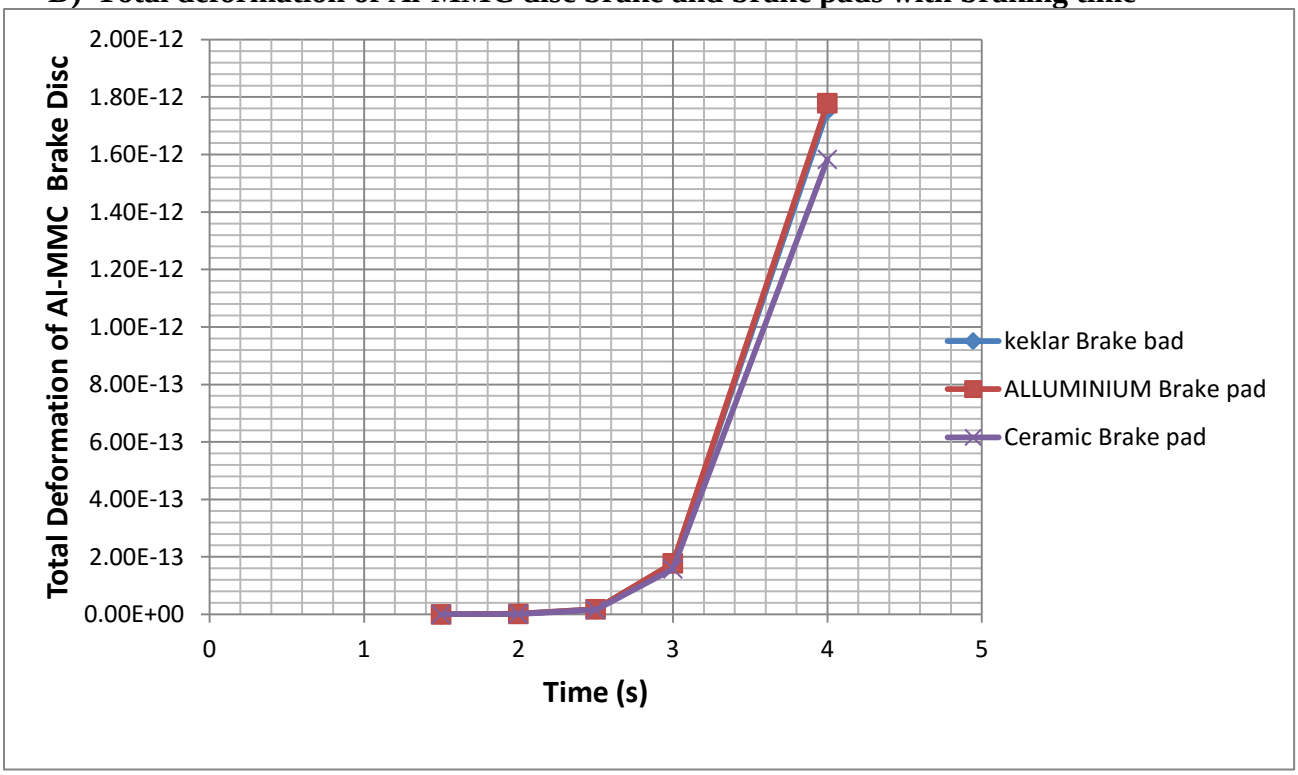

Figure 4.2: Total deformation versus time

From the graph description the maximum deformation is occurred at inner side of the disc that the center of brake pad contact and the minimum deformation is occurred at inner side of the disc that end of contact of brake pad. Among the three brake pad interface with disc the aluminum brake pad has maximum deformations.

E) Von-Mises stress of Al-MMC brake disc and pads with braking time

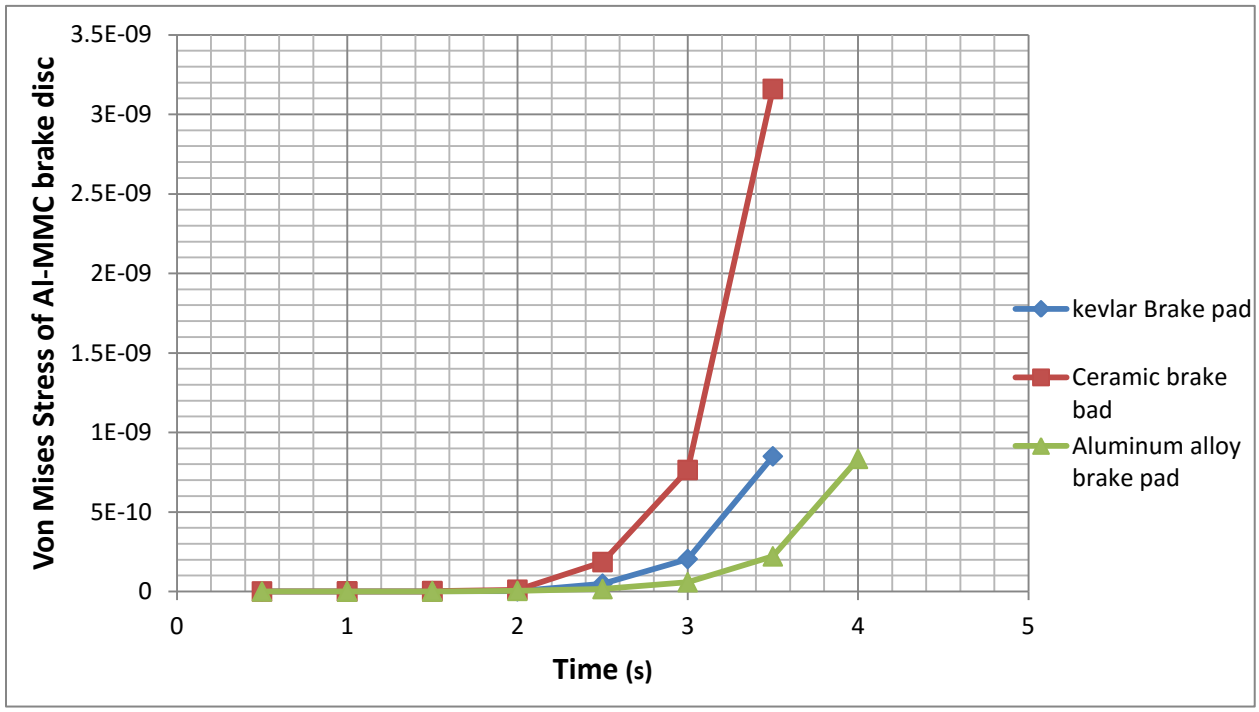

Figure 4.3: Von Mises stress versus time

From the graph the maximum stress is occurred at inside surface of disc and the minimum stress is occurred at outer surface of the disc. And also when the disc is interface with ceramic brake pad has high stress.

4.3. Mechanical properties of Stress - strain relationship

As the result obtains from software analysis of brake disc with friction materials of three brake pad types; the equivalent stress that describes the mechanical property of the materials among all three kind of brake pad material the equivalent stress of brake disc with brake pad of ceramic is the highest. The equivalent (von-Mises) stress of this material is must be below yield stress to avoid plastic deformation and kept below ultimate stress of the material in order to avoid structure failure. Thus, the equivalent stress of this material is below its yield stress and ultimate stress, and then it's safe. The result is presented shown in the table 4.4 and figure 4.4.

Table 4-4: Mechanical properties of Stress - strain relationship

Equivalent stress			Equivalent Strain
Brake disc with Ceramic brake pad	Brake disc with Aluminum brake pad	Brake disc with Kevlar brake pad	
$4.20x10^{-15}$	$4.08x10^{-15}$	$3.81x10^{-15}$	$1.00x10^{-19}$
$3.51x10^{-10}$	$9.26x10^{-11}$	$9.44x10^{-11}$	$2.67x10^{-15}$
$7.03x10^{-10}$	$1.85x10^{-10}$	$1.89x10^{-10}$	$5.34x10^{-15}$
$1.05x10^{-09}$	$2.78x10^{-10}$	$2.83x10^{-10}$	$8.01x10^{-15}$
$1.45x10^{-09}$	$3.70x10^{-10}$	$3.78x10^{-10}$	$1.07x10^{-14}$
$1.76x10^{-09}$	$4.63x10^{-10}$	$4.72x10^{-10}$	$1.34x10^{-14}$
$2.11x10^{-09}$	5.56x10-^{10}	$5.66x10^{-10}$	$1.60x10^{-14}$
$2.46x10^{-09}$	$6.48x10^{-10}$	$6.61x10^{-10}$	$1.87x10^{-14}$
$2.81x10^{-09}$	$7.41x10^{-10}$	$7.55x10^{-10}$	$2.14x10^{-14}$
$3.16x10^{-09}$	$8.34x10^{-10}$	$8.50x10^{-10}$	$2.40x10^{-14}$

Stress- strain linear graph for brake pad interface with brake disc:

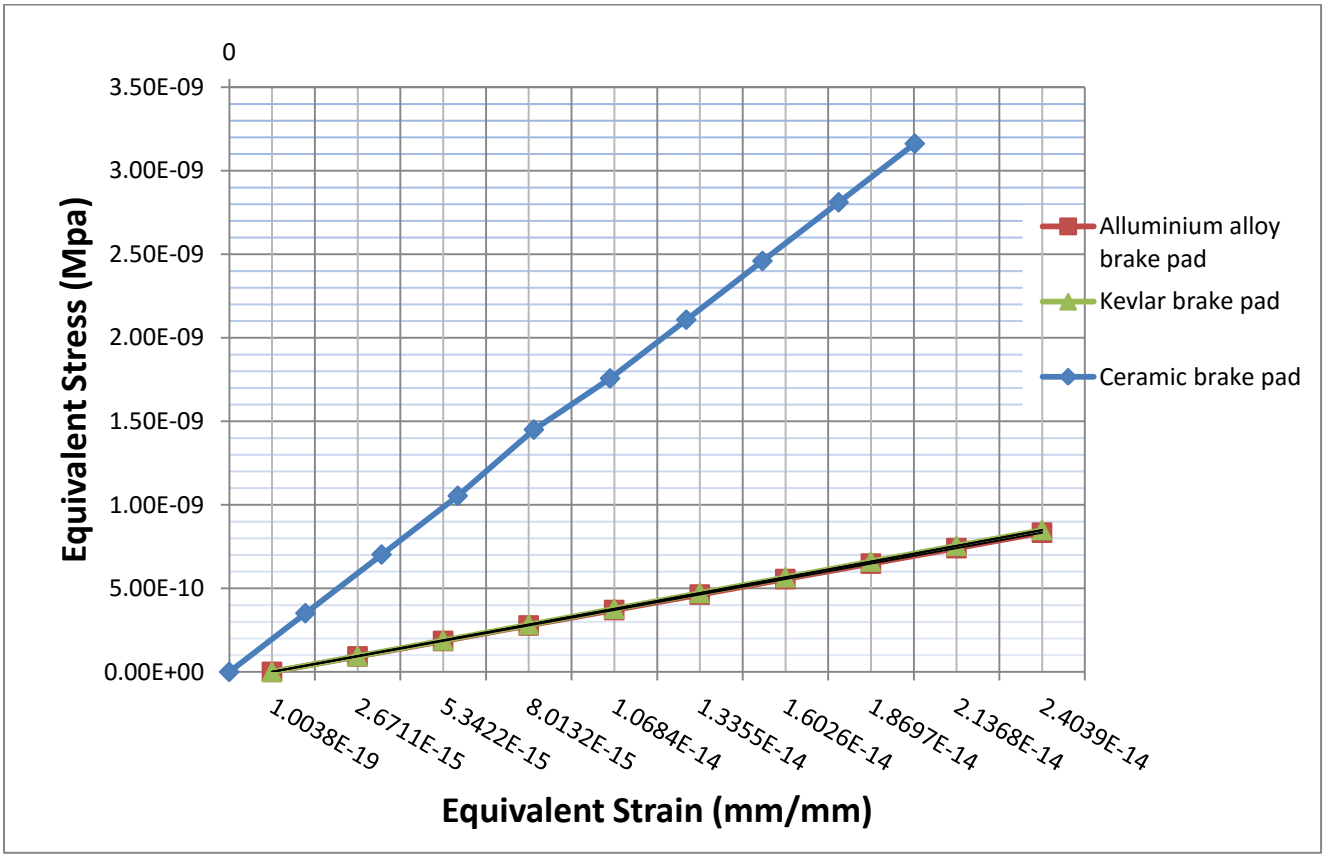

Figure 4.4: Stress- strain linear graph for brake pad interface with brake disc

4.4. Mechanical properties of Contact stress

The contact stress between brake disc and brake pad of alternative friction material is interpreted; among contact stress between brake disc with brake pad of Ceramic brake pad, Kevlar brake pad and aluminum alloy brake pad, thus the contact stress applied between brake discs with brake pad of Ceramic is highest. The interpretation is shown by the graph in figure 4.5 from result presented on table 4.5.

Table 4-5: Mechanical properties of Contact stress

Contact stress	Al-MMC brake disc with Ceramic brake pad	Al-MMC brake disc with Kevlar brake pad	Al-MMC brake disc with Aluminum brake pad
Maximum Principal stress	2.1063 x10^{-9} MPa	7.6336x10^{-10} MPa	7.1502x10^{-10} MPa

Interpretation of contact stress of brake pads with brake disc interface by chart description:

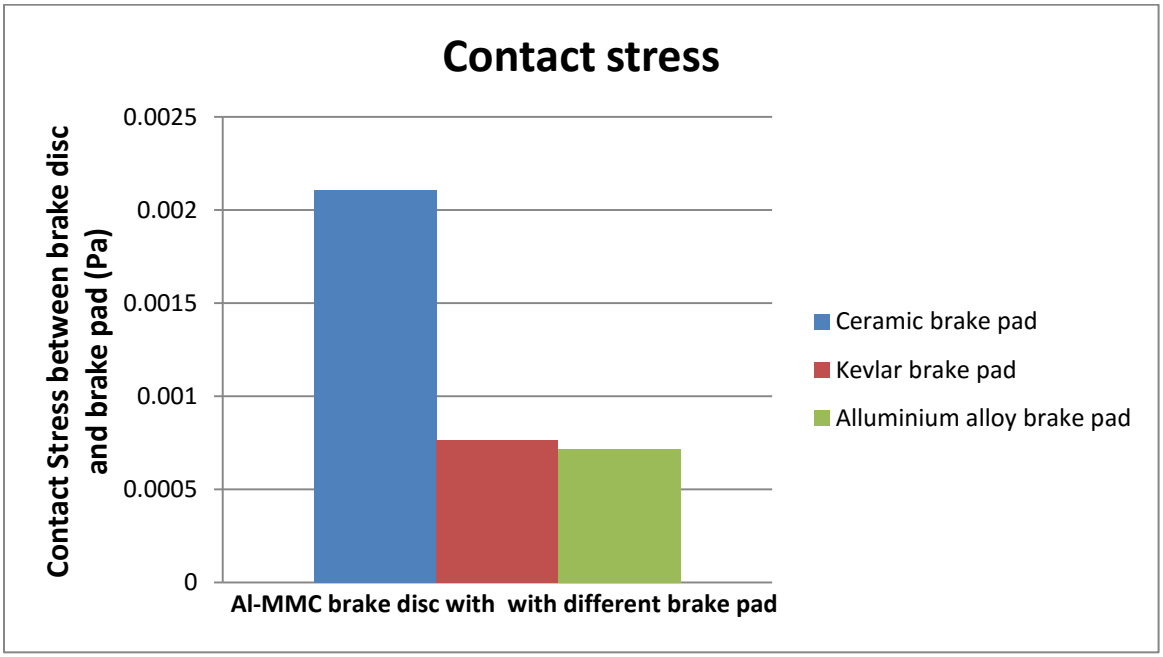

Figure 4.5: Interpretation of contact stress of brake pads with brake disc interface

4.5. Life time Estimation of brake pad strength with Al-MMC brake disc

The life estimation for the material is analyzed for stress life with Goodman Mean stress Correction theories and the stress component is Equivalent (Von-Mises) stress with the life units in Cycle.

A) Life span Estimation for Kevlar brake pad strength with Al-MMC brake disc

Table 4-6: Life span Estimation for Kevlar brake pad strength with Al-MMC brake disc

Alternating Stress (MPa)		No of Cycles	
Kevlar brake pad	**Al-MMC brake disc**	**Kevlar brake pad**	**Al-MMC brake disc**
$8.50x10^{-10}$	$4.25x10^{-10}$	$5.80x10^{-14}$	$2.41x10^{+09}$
$7.55x10^{-10}$	$3.78x10^{-10}$	$6.16x10^{-09}$	$7.85x10^{+11}$
$6.61x10^{-10}$	$3.30x10^{-10}$	$6.55x10^{-04}$	$2.56x10^{+14}$
$5.66x10^{-10}$	$2.83x10^{-10}$	69.55	$8.34x10^{+16}$
$4.72x10^{-10}$	$2.36x10^{-10}$	$7.39x10^{+06}$	$2.72x10^{+19}$
$3.78x10^{-10}$	$1.89x10^{-10}$	$7.85x10^{+11}$	$8.86x10^{+21}$
$2.83x10^{-10}$	$1.42x10^{-10}$	$8.34x10^{+16}$	$2.89x10^{+24}$
$1.89x10^{-10}$	$9.44x10^{-11}$	$8.86x10^{+21}$	$9.41x10^{+26}$
$9.44x10^{-11}$	$4.72x10^{-11}$	$9.41x10^{+26}$	$3.07x10^{+29}$
$3.81x10^{-15}$	$1.90x10^{-15}$	$1.00x10^{+32}$	$1.00x10^{+32}$

Factor of safety: a factor of safety is with respect to fatigue failure at a given design life. The maximum safety factor is 15, but for this analysis the minimum safety factor is **1.0169.**

The S–N curve (stress amplitude versus logarithm cycles to failure) for Al-MMC brake disc with Kevlar brake pad is plotted using these data obtained from analysis results.

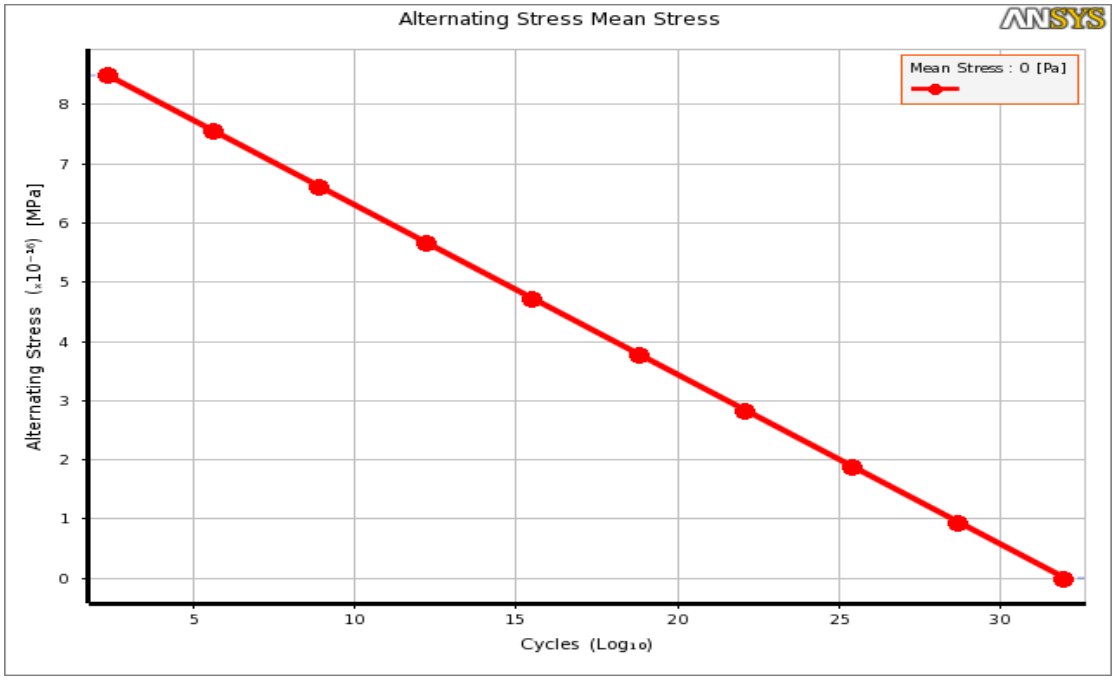

Figure 4.6: The S–N curve of Kevlar brake pad

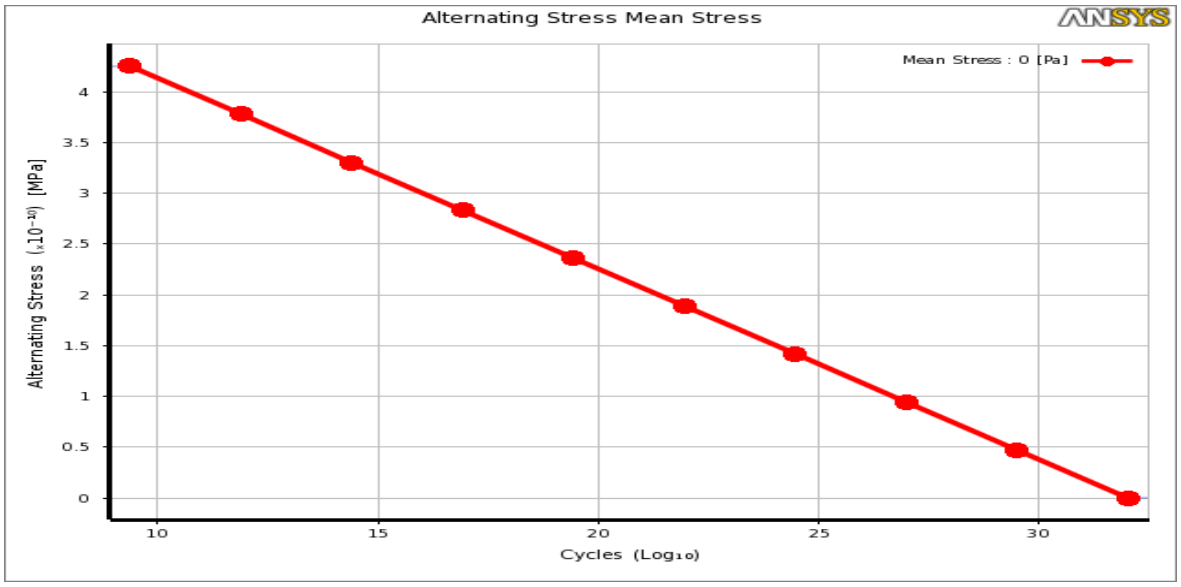

Figure 4.7: The S–N curve of Al-MMC brake disc interface with Kevlar brake pad

From those graph, the number of cycle of the material is depend on fatigue strength of the material, thus as fatigue strength of the material is decrease the number of cycle to failure is increase. Under this analysis of brake disc with brake pad; the maximum fatigue strength of Kevlar brake pad at $5.80 \text{ X } 10^{-14}$ Cycle is $8.50 \text{ X } 10^{-10}$ Mpa and the minimum fatigue strength at $1 \text{ x } 10^{+32}$ Cycle is $3.81 \text{ x } 10^{-15}$ Mpa. And the maximum fatigue strength of Al-MMC brake disc with the interface of Kevlar brake pad at $2.41 \text{ X } 10^{+9}$ Cycle is $4.25\text{X } 10^{-10}$ Mpa and the minimum fatigue strength at $1 \text{ x } 10^{+32}$ Cycle is $1.9 \text{ x } 10^{-15}$ Mpa.

The fatigue sensitivity of the material indicates the fatigue results change as a function of the loading at the critical location on the model and model available life of Al-MMC brake disc with interface of Kevlar brake pad strength if the FE load was 50% of current load, 75% of current load, and 150% of the current load (alternating stress). Sensitivity can be found for life, damage and safety factor. Thus, the graph of fatigue sensitivity is plotted in the figure 4.8.

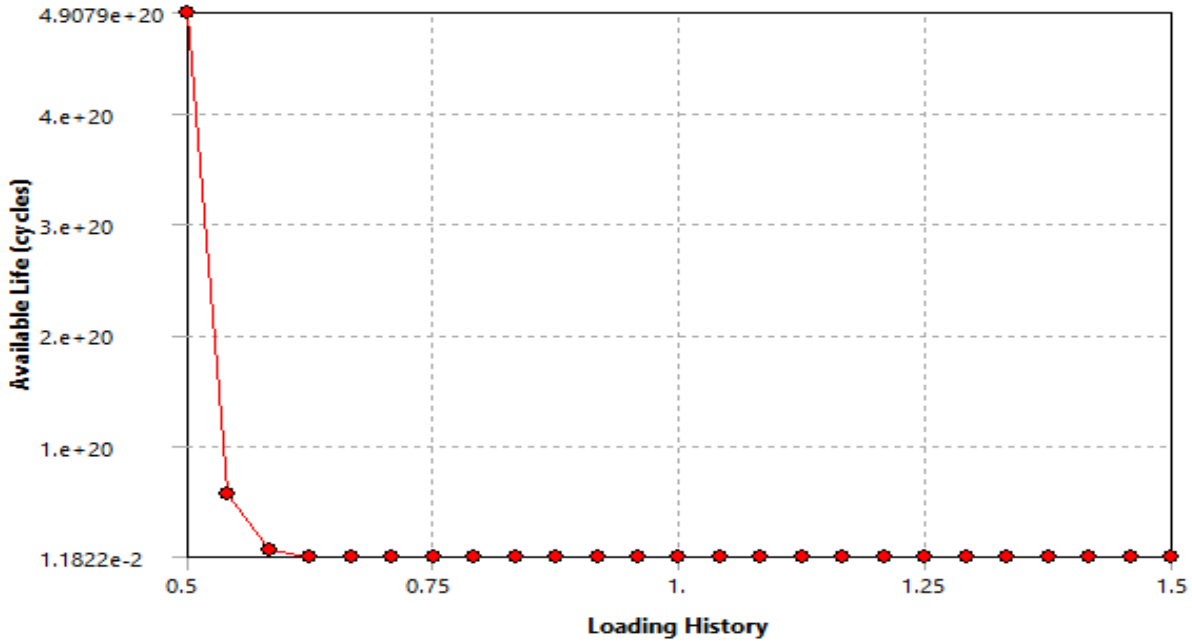

Figure 4.8: Fatigue Sensitivity for available life of Al-MMC brake disc with Kevlar brake pad

B) Life span Estimation for Aluminum alloy brake pad strength with Al-MMC brake disc

The S–N curve (stress amplitude versus logarithm cycles to failure) is plotted from the table 4.7.

Table 4-7: Life span Estimation for Aluminum alloy brake pad strength with Al-MMC brake disc

Alternating Stress (MPa)		No of Cycles	
Aluminum alloy brake pad	**Al-MMC brake disc**	**Aluminum alloy brake pad**	**Al-MMC brake disc**
$8.34x10^{-10}$	$4.16x10^{-10}$	234.8	$1.53x10^{+17}$
$7.41x10^{-10}$	$3.70x10^{-10}$	$4.60x10^{+05}$	6.7810^{+18}
$6.48x10^{-10}$	$3.24x10^{-10}$	$9.02x10^{+08}$	$3.00x10^{+20}$
$5.56x10^{-10}$	$2.78x10^{-10}$	$1.77x10^{+12}$	$1.33x10^{+22}$
$4.63x10^{-10}$	$2.32x10^{-10}$	$3.46x10^{+15}$	$5.88x10^{+23}$
$3.70x10^{-10}$	$1.85x10^{-10}$	$6.78x10^{+18}$	$2.60x10^{+25}$
$2.78x10^{-10}$	$1.39x10^{-10}$	$1.33x10^{+22}$	$1.15x10^{+27}$
$1.85x10^{-10}$	$9.26x10^{-11}$	$2.60x10^{+25}$	$5.10x10^{+28}$
$9.26x10^{-11}$	$4.63x10^{-11}$	$5.10x10^{+28}$	$2.26x10+^{30}$
$4.08x10^{-15}$	$2.04x10^{-15}$	$1.00x10^{+32}$	$1.00x10^{+32}$

Factor of safety: a factor of safety is with respect to fatigue failure at a given design life. The maximum safety factor is 15, but for this analysis the minimum safety factor is **1.5525.**

The S–N curve (stress amplitude versus logarithm cycles to failure) for Aluminum alloy brake pad and Al-MMC brake disc interface is plotted using these data obtained from analysis results.

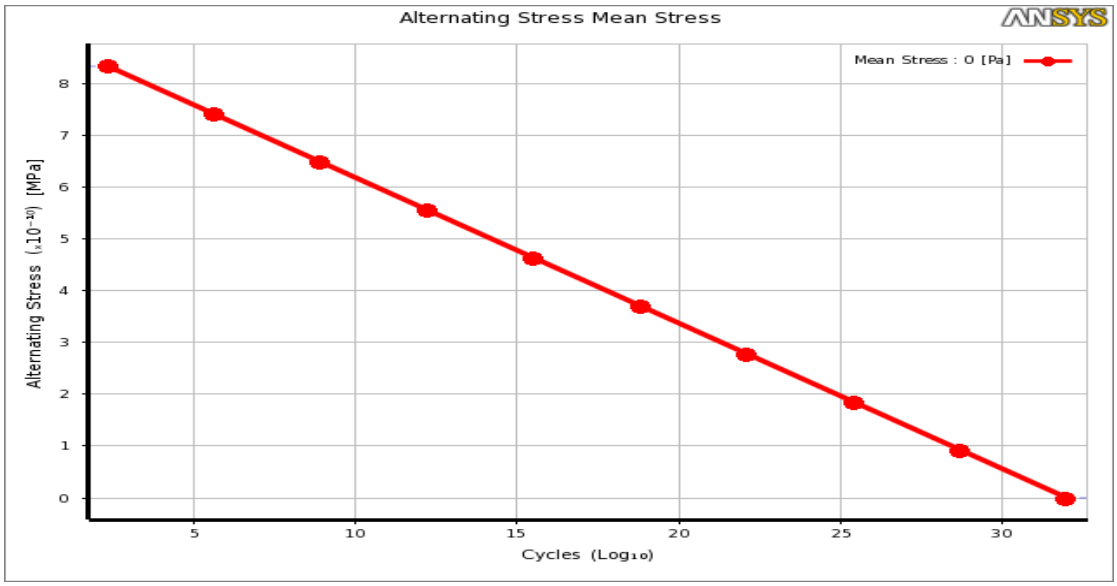

Figure 4.9 : the S–N curve of aluminum alloy brake pad

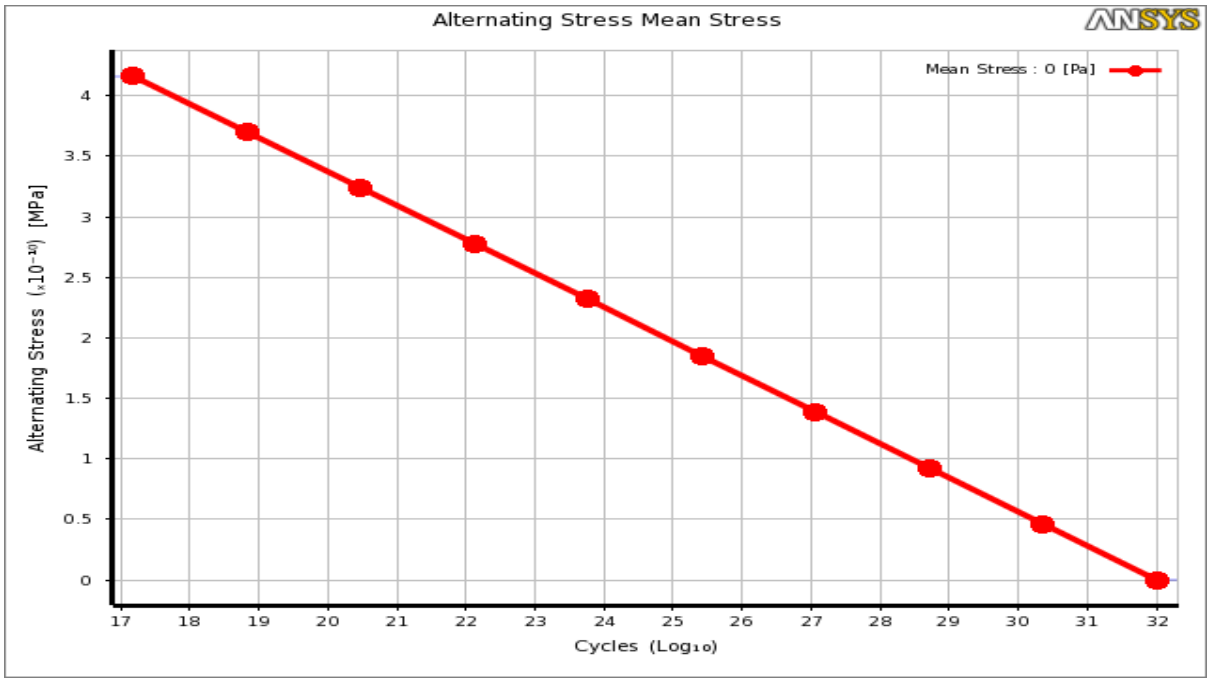

Figure 4.10: The S–N curve of Al-MMC brake disc with interface of aluminum alloy brake pad

From this graph I discuss that, the number of cycle of the aluminum alloy brake pad material is depend on fatigue strength of the material, thus as fatigue strength of the material is decrease the number of cycle to failure is increase. Under this analysis of brake disc with brake pad; the maximum fatigue strength of aluminum alloy brake pad at 234.8 Cycle is 8.34 X 10^{-10} Mpa and the minimum fatigue strength at 1 x 10^{+32} Cycle is 4.08 x 10^{-15} Mpa. And the maximum fatigue strength of Al-MMC brake disc with interface of aluminum alloy brake pad at 1.53x10^{+17} Cycle is 4.16 X 10^{-10} Mpa and the minimum fatigue strength at 1 x 10^{+32} Cycle is 2.04 x 10^{-15} Mpa.

Find sensitivity of available life of Al-MMC brake disc with interface of aluminum alloy brake pad if the FE load was 50% of current load, 75% of current load, and 150% of the current load (alternating stress). Sensitivity can be found for life, damage and safety factor. Thus, the graph of fatigue sensitivity is plotted in the figure 4.11.

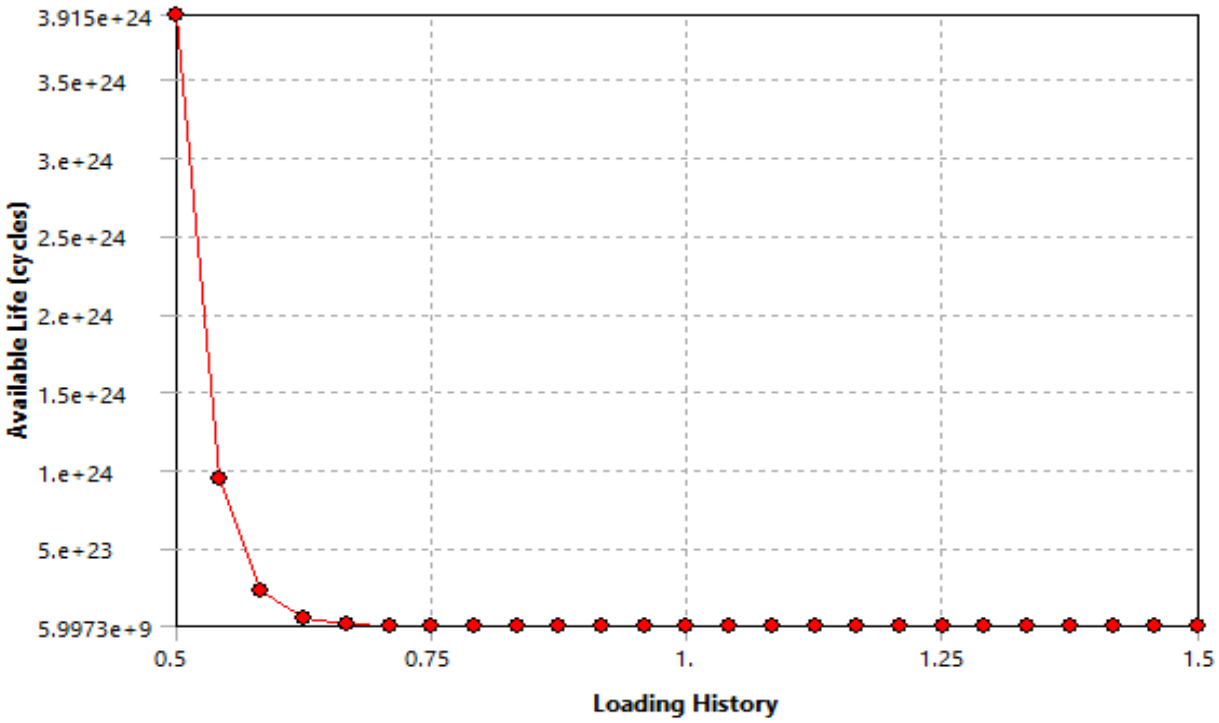

Figure 4.11: Fatigue sensitivity of Al-MMC brake disc with aluminum alloy brake pad

C) Life span Estimation for Ceramic brake pad strength with Al-MMC brake disc

The S–N curve (stress amplitude versus logarithm cycles to failure) is plotted from table 4.8.

Table 4-8: Life span Estimation for Ceramic brake pad strength with Al-MMC brake disc

Alternating Stress (MPa)		No of Cycles	
Ceramic brake pad	**Al-MMC brake disc**	**Ceramic brake pad**	**Al-MMC brake disc**
$3.16x10^{-09}$	$1.58x10^{-09}$	234.8	$1.53x10^{+17}$
$2.81x10^{-09}$	$1.41x10^{-09}$	$4.60x10^{+05}$	$6.78x10^{+18}$
$2.46x10^{-09}$	$1.23x10^{-09}$	$9.02x10^{+08}$	$3.00x10^{+20}$
$2.11x10^{-09}$	$1.05x10^{-09}$	$1.77x10^{+12}$	$1.33x10^{+22}$
$1.76x10^{-09}$	$8.79x10^{-10}$	$3.46x10^{+15}$	$5.88x10^{+23}$
$1.41x10^{-09}$	$7.03x10^{-10}$	$6.78x10^{+18}$	$2.60x10^{+25}$
$1.05x10^{-09}$	$5.27x10^{-10}$	$1.33x10^{+22}$	$1.15x10^{+27}$
$7.03x10^{-10}$	$3.51x10^{-10}$	$2.60x10^{+25}$	$5.10x10^{+28}$
$3.51x10^{-10}$	$1.76x10^{-10}$	$5.10x10^{+28}$	$2.26x10^{+30}$
$4.20x10^{-15}$	$2.10x10^{-15}$	$1.00x10^{+32}$	$1.00x10^{+32}$

Factor of safety: a factor of safety is with respect to fatigue failure at a given design life. The maximum safety factor is 15, but for this analysis the minimum safety factor is **1.5525.**

The S–N curve (stress amplitude versus logarithm cycles to failure) for Ceramic brake pad is plotted using these data obtained from analysis results.

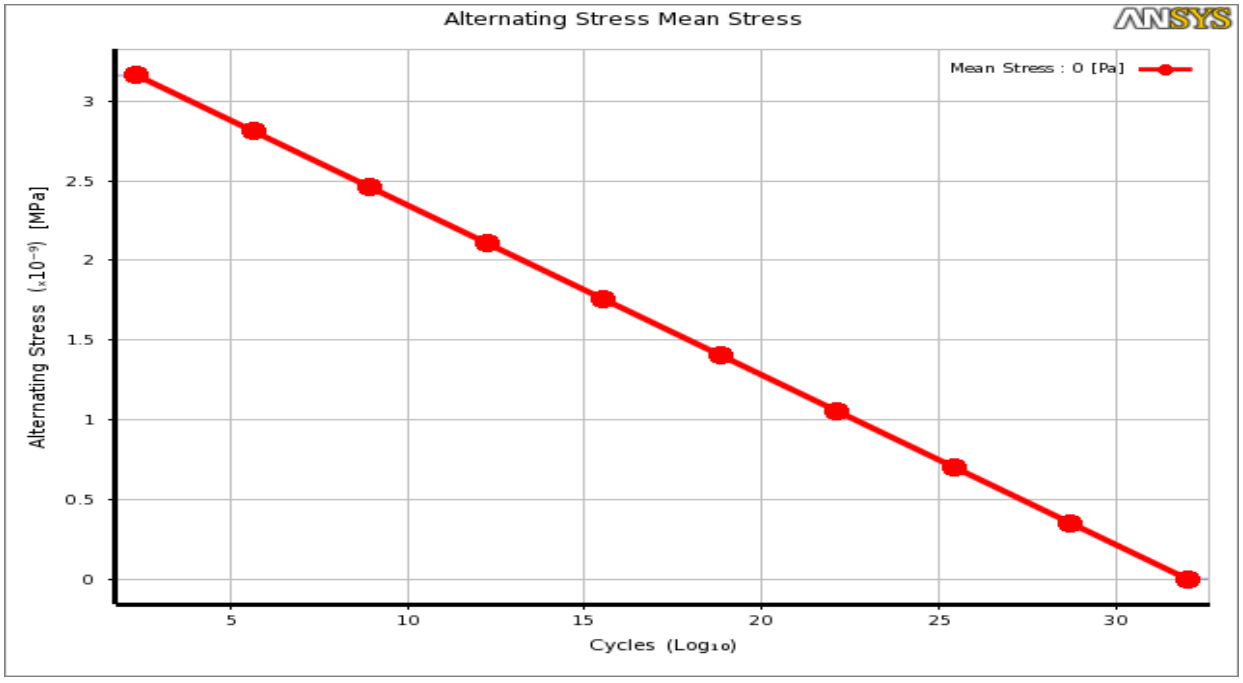

Figure 4.12: The S–N curve of ceramic brake pad

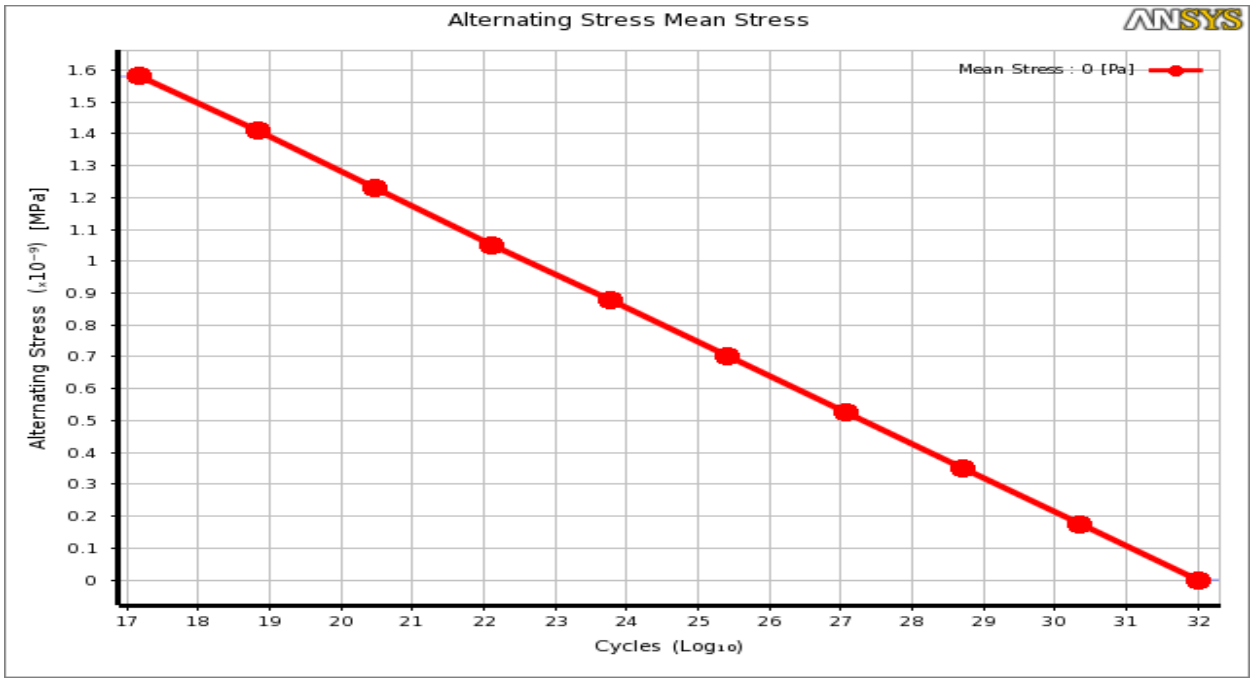

Figure 4.13: The S–N curve of Al-MMC brake disc with interface of ceramic brake pad

Under this analysis of brake disc with brake pad of Ceramic friction material; the maximum fatigue strength of ceramic brake pad at 234.8 Cycle is $3.16x10^{-9}$ Mpa and the minimum fatigue strength at 1 x 10^{+32} Cycle is $4.2x10^{-15}$ Mpa. And the maximum fatigue strength of Al-MMC brake disc with interface of ceramic brake pad at $1.53x10^{+17}$ Cycle is $1.58x10^{-9}$ Mpa and the minimum fatigue strength at 1 x 10^{+32} Cycle is $2.1x10^{-15}$ Mpa. Which is implies that as the fatigue strength of the material is decrease, the number of cycle is increase.

Model fatigue sensitivity of available life for Al-MMC brake disc with interface of ceramic brake pad if the FE load was 50% of current load, 75% of current load, and 150% of the current load (alternating stress). Sensitivity can be found for life, damage and safety factor. Thus, the graph of fatigue sensitivity is plotted in the figure 4.14.

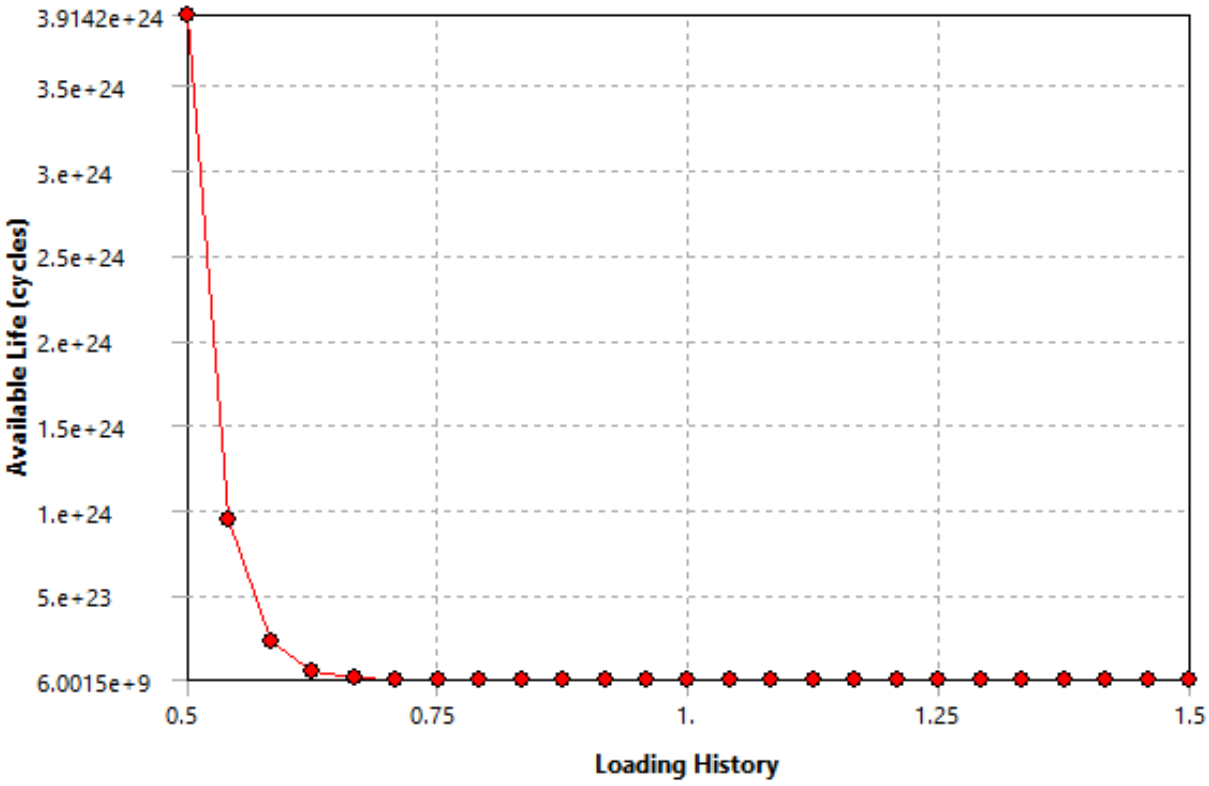

Figure 4.14: Fatigue sensitivity of Al-MMC brake disc with interface of ceramic brake pad

4.6. Total heat flux produced during repeated braking with temperature produced between the interfaces.

The energy generated at the repeated braking between brake disc and brake pad is illustrated. The kind of energy generated is heat energy produced by the effect of temperature that is heat flux. The result of total heat flux with temperature variation obtains from ANSYS software analysis was illustrated in table 4.9.

Table 4-9: Total heat flux produced with temperature between the interfaces.

Temperature (^{0}C)	Total heat Flux (w/mm^2)
31.718	6.94x10^{-5}
40.177	0.0001365
50.891	0.00026837
64.462	0.00052764
81.652	0.0010374
103.43	0.0020396
131.01	0.00401
165.94	0.007894
210.2	0.015501
266.25	0.030475

The heat energy generated at interface of disc brake and brake pad during braking applied is shown by the graph in the figure 4.15.

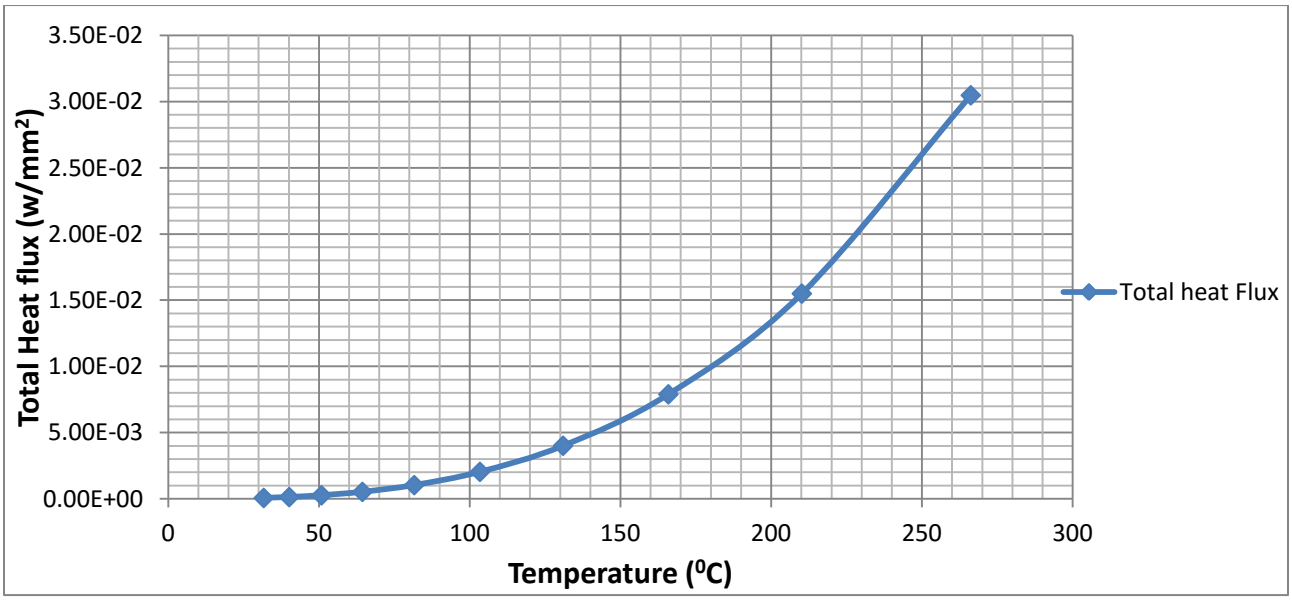

Figure 4.15: Heat energy generated at interface of disc brake with brake pad

The graph indicate that the relation of Total heat flux with Temperature, that means the heat energy is increased with the increment of temperature that produced in the interface of brake disc and brake pad.

Variation of heat flux during vehicle speed decreases with times.

The boundary condition that use for analysis of heat flux is convection coefficient of 1.24x10-6w/mm^2.^{o}C at ambient temperature of 22^{o}C and the disc type is ventilated disc. The interpretation is given in figure 4.16.

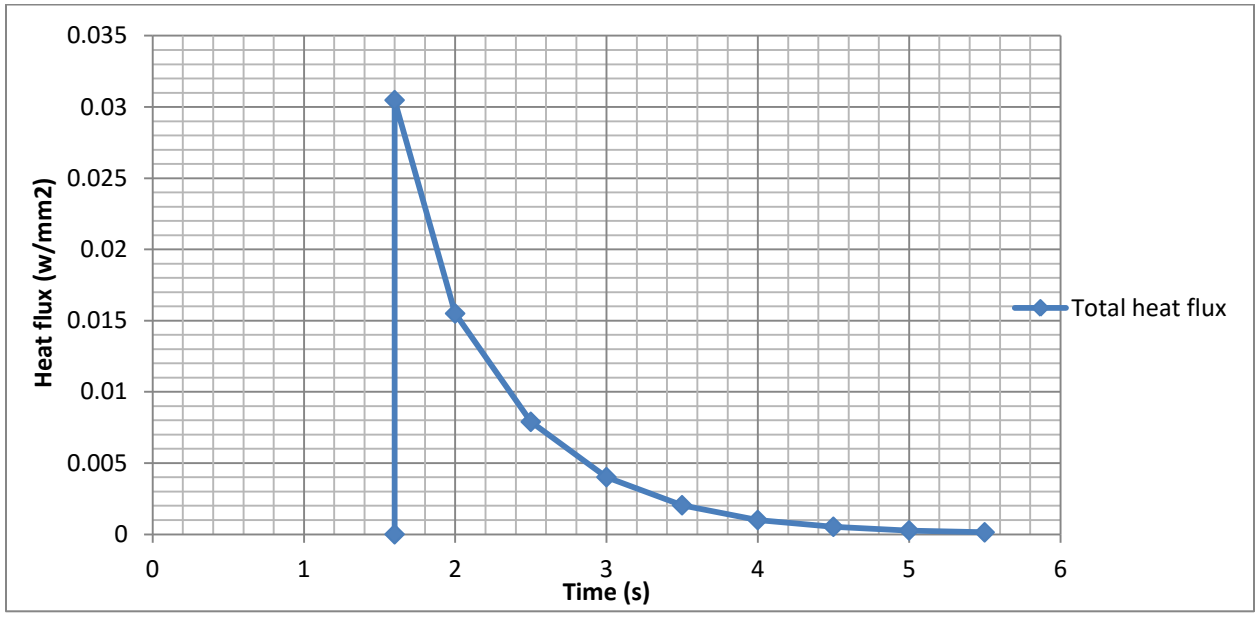

Figure 4.16: Heat flux variation with time

From the graph description the maximum heat flux 0.030475 w/mm^2 occurred is occurred at inner side of the disc with at maximum temperature 266.2^{o}C occurred that brake pad contact with the disc.

From International Journal of Mechanical Engineering and Technology **(IJMET) by Rakesh Jaiswal, et.al B**., Department of Mechanical Engineering, NIT Durgapur, India and by Rabindra **Nath Barman** Assistant Professor, Department of Mechanical Engineering, NIT Durgapur, India on Title of **Structural and thermal analysis of disc brake using solid works and ansys; [41]** The compression of my original thesis work with this journal is listed in table 4-10.

Table 4-10: Result from Literature for Compression

S.No	**Parameter**	**Maximum Value**	**Minimum Value**
1	Equivalent Elastic Strain	3.379e-6 (m/m)	2.8938e-8 (m/m)
2	Directional Deformation	1.7817e-7 (m)	-1.7876e-7 (m)
3	Equivalent (Von Mises) Stress	2.3097e5 (pa)	1178.8 (pa)
4	Maximum Principal Stress	3.4436e5 (pa)	-41599 (pa)
5	Strain Energy	7.4752e-8 (J)	3.7812e-14 (J)
6	Total Deformation	2.4467e-7 (m)	0 (m)
7	Temperature	210.64 (^{o}C)	207.61 (^{o}C)

The above result Journal of thermal and structural analysis of disc brake using solid works and ANSYS software with the aluminum 6262-T9 disc material and corresponding brake pad was analyzed with above result. But, the result of my work analyzed by ANSYS software and by laboratory result with Al-MMC brake disc material and alternative candidate brake pads like Aluminum alloy brake pad, Ceramic brake pad and organic Kevlar brake pad analyzed for TOYOTA HIACE minibus 5L that have 12 seats chairs and used in Ethiopia City taxi was better output when I compare the my result obtain through mechanical result of Al-MMC brake disc with the three alternative candidate brake pad material corresponding to equivalent Elastic Strain, Directional Deformation, equivalent (Von Mises) Stress, maximum Principal Stress, Strain Energy, Total Deformation and Temperature listed in table 4.1, table 4.2, table 4.3 and table 4.9.

CHAPTER FIVE: CONCLUSION AND RECOMMENDATION

5.1. Conclusion

From study of this kind of specified subject, the mechanical properties of automotive disc brake such as contact stress, deformation, strain energy, equivalent strain, equivalent stress, alternative stress, life cycle, fatigue sensitivity for model available life and the rate of energy generated between the brake disc and brake pad that is total heat flux is analyzed by static analysis of finite element method with ANSYS software and studies by experimental result the effect of composition of friction material of brake pad that interface with brake disc. For working this research the Ethiopian city taxi TOYOTA-HIACE minibus 12 seats is taken as a sample. Thus, the Conclusion for this study is pointed as the following clue:

- The friction material of brake pad composition that used in Ethiopian city taxi automotive is investigated experimentally; as the result obtains from laboratory result the highest amount of ingredient in the friction material of brake pad that used in Ethiopian city taxi is Copper. Hence, Copper is naturally it produce high heat transfer and it produce more noises, thus due to produce more to and noise can be damage. Also it produces dusts; the dust scratched from the pad during braking time on the road is moved by rainfall a mixed with water (river, lakes, etc) affect the aquatic life and affect human health.
- The deformation of Al-MMC brake disc during braking is applied with brake pads material is analyzed; thus the total deformation of Al-MMC brake disc with interface of organic Kevlar brake pad is $1.7553x10^{-12}$ mm, the total deformation of Al-MMC brake disc with interface of Ceramic brake pad is $1.5832x10^{-12}$ mm and the total deformation of Al-MMC brake disc with interface of Aluminum alloy brake pad is $1.7787x10^{-12}$ mm, thus among three friction material of brake pad model with interface of Al-MMC brake disc, the total deformation of Al-MMC brake disc with interface of ceramic brake pad is relatively better.
- Among three brake pad model with interface of Al-MMC brake disc, the stress at Al-MMC brake disc with interface Ceramic brake pad has relatively high strength than the others, that means the equivalent stress of Al-MMC brake disc with interface of ceramic brake pad is $3.1627x10^{-9}$ Mpa, the equivalent stress of Al-MMC brake disc with

interface of Kevlar brake pad is $8.4974x10^{-10}$ Mpa and the equivalent stress of Al-MMC brake disc with interface of aluminum alloy brake pad is $8.3353x10^{-10}$ Mpa.

- The maximum contact stress of Al-MMC brake disc with organic Kevlar brake pad is $7.6336x10^{-10}$ Mpa, with interface of ceramic brake pad the maximum contact stress is $2.1663x10^{-9}$ Mpa and with interface of aluminum alloy brake pad the maximum contact stress is $7.1502x10^{-10}$ Mpa, thus the highest maximum contact stress of the Al-MMC brake disc is occurred with ceramic brake pad.
- The service life of brake pad is increase with decreasing fatigue strength , thus among three brake pad model with brake disc the ceramic brake pad has relatively highest lifecycle, that means the life cycle of ceramic brake pad at highest fatigue strength of $3.16x10^{-9}$ Mpa has the minimum life cycle of 234.8 cycle. And the maximum fatigue strength of Al-MMC brake disc with interface of ceramic brake pad at $1.581x10^{-9}$ Mpa has $1.53x10^{+17}$ cycle.
- In the case of modeling the fatigue sensitivity for available life, the ceramic brake pad interface with Al-MMC brake disc has services long life rather than other brake pad interface when reduce the current load (fatigue strength) by 50%. That means when reduce the current load by 50% of current load the minimum available life model is $3.9142x10^{+24}$, that means improves minimum available life of Al-MMC brake disc with interface of ceramic brake pad from $1.53x10^{+17}$ cycle to $3.9142x10^{+24}$ cycles.
- The total heat flux generated between the interface of brake disc and brake pad is increased with increasing temperature, that means the maximum heat flux at maximum temperature of 266.25^{0}C is generate maximum heat energy of $0.030475w/mm^{2}$.
- In general, from the result of analysis the performance of Al-MMC brake disc with interface of ceramic brake pad is better for automotive baking system rather than other interfaces and as theoretical study, the performance of Al-MMC brake disc with interface of ceramic brake pad has good quit braking without noising, it uses at hot environmental conditions and has good heat resistance.

5.2. Recommendation

Studying of this paper is very significant for automotive braking performance, thus the effect of brake pad composition in automotive braking system is determine the performance of braking system; hence the Ethiopian City taxi specifically TOYOTA-HIACE 12 seat should have use brake pad friction material that contain low (or) free of copper in their composition of friction materials. The ministry of transport authority of Ethiopia should give attention and awareness on environmental pollution of dust produced come from interface between brake disc and brake pad that used in Ethiopian City taxes.

As the finite element analysis by ANSYS software, the friction materials of brake pad for automotive brake discs are semimetal brake pad for all environmental condition as get result from laboratory in case of brake pad that used in Ethiopian City taxi, hence The driver of Ethiopian City taxi should select types of brake pad with respect to area of environmental condition (Cold, warm) in order to safe wear and damage of brake disc and for keeping accident. The mechanical characteristics occurred between the interface of Al-MMC brake disc and Ceramic brake pads of automobiles are good characteristics for braking performance, thus a driver use those material will get luxuries braking performance during braking for its quit braking, service long life, for its strength, for its good for environmental condition.

5.3. Future Work

In this studying of subject other influencing factor between brake disc and brake pad of material were not studied, thus the idea investigated in the future work is;

- Fatigue analysis of Anti lock braking system (ABS) Control for modern vehicle by Finite Element method (FEM)
- Development of Brake pad friction material using Composite materials
- Effect of the composition of brake pad materials on friction and wear properties of automotive disc brake
- Mechanical properties and wear behavior analysis on changing and maintenance of surface of friction materials of brake pad materials in case of Ethiopia
- Material Selection and Production for brake pad materials of automobiles at Cold-Worked and Hot worked

REFERENCE

1. Characterization of brake pads by variation in composition of friction materials. Nagesh S. N., Siddarayu C., prakash S. V., Ramesh M. R. procedia : Materials Science, 2014, 5,. p. 295-302.

2. Auto technology, theory and service. Bono S.G., Dekyrger W.J, New york, : DELMAR publishers, 1990.

3. surajshandilya. braking-system. htt://www.slideshare.net. [Online]

4. Dowson, D. History of Tribology. Bury St Edmunds : Professional Engineering Publishing, 1998.

5. Surface characterisation of brake pads after running under silent and squealing conditions, Wear. Eriksson, M., Bergman, F., Jacobson, S. (1999), Vol. 232. 163-167.

6. Bergman, F., Eriksson, M., Jacobson, S. Influence of disc topography on generation of brake squeal, Wear. (1993). 621-628.

7. Generalized Theory of Brake Noise, Proceedings of the Institute of Mechanical Engineers. Nishiwaki, M. (1993), Vol. 207. 195-202..

8. Manfred "Fahrwerktechnik: Bremsdynamik und Pkw-Bremsanlagen. Burckhardt. s.l. : Prof. Dipl.-Ing. Jörnsen Reimpell (Editor),, Vols. Vogel Fachbuch Kraftfahrzeugtechnik,.

9. Copper Substitution and Noise Reduction in Brake Pads: Graphite Type Selection. Raffaele Gilardi 1, Luigi Alzati 1, Mamadou Thiam 2, Jean-François Brunel 2,.

10. Impact of Brake Pad Structure on Temperature and Stress Fields of Brake Disc. Fu, Guoshun Wang and Rong. s.l. : School of Mechanical Engineering, Dalian Jiaotong University, Dalian, Liaoning 116028, China, 2013, Vol. 872972. 9.

11. MODELING FRICTION AND WEAR OF BRAKE SYSTEM. OSTERMEYER, G. P. GERMANY : Institute of Dynamics and Vibrations, Technische Universität Braunschweig, Schleinitzstrasse 20,.

12. Strength Analysis of Disc Brake Assembly & Dynamic Pad Pressure. Chowdary, Prasanna. Mando Softtech India Pvt. Ltd. : s.n.

13. Du_our, Philippe. Noise generation in vehicle brakes. Jesus College, Cambridge : Engineering Department, 2002.

14. HARSHVARDHAN ZULA, 2N.D GHETIYA, 3DIPALI PANDYA. DEVELOPMENT OF FRICTION PAD AND STUDY OF ITS WEAR CHARACTERISTICS. Nirma University : 1,2,3Mechanical Engg. Department, Institute of Technology.

15. Degenstein, Thomas, Winner, Hermann. DYNAMIC MEASUREMENT OF THE FORCES IN THE FRICTION AREA OF A DISC BRAKE DURING A BRAKING PROCESS. s.l. : Institute of Automotive Engineering Department at Technische Universität Darmstadt,Germany.*

16. Jaeho Kwak, Bin Yao, and Anil Bajaj. ANALYTICAL MODEL DEVELOPMENT AND MODEL REDUCTION FOR ELECTROMECHANICAL BRAKE SYSTEM. USA, West Lafayette, : School of Mechanical Engineering, Purdue University. 47907.*

17. Sadiq Sius LAWAL, Katsina Christopher BALA, and Abdulkareem Tunde ALEGBEDE. Development and production of brake pad from sawdust composite. Niger State, Nigeria : Mechanical Engineering Department, Federal University of Technology, P.M.B. 65, Minna,.*

18. S. Oberst, J.C.S. Lai. Numerical prediction of brake squeal propensity using acoustic power calculation. Canberra, Australia : The University of New South Wales, Australian Defence Force Academy,. 2600.

19. Belhocine, A. Finite Element Analysis of Automotive Disc Brake and Pad in Frictional Model Contact. Algeria : Department of Mechanical Engineering, University of Science and Technology USTO Oran,.*

20. Test Approach for Dynamic Groan Noise. Gil-hyoung Lee1, Dong-kyu Lee2 and Jia Chen3, 1Test Team, Saeronautomotive Co.,. 361-763, koria, china : 2Dept. of Engineering Chemistry, Chungbuk National University, 3Department of Computer Science and Engineering, Tianjin University of Technology, Tianjin.

*21. Contact analysis for a passenger car disc brake. Samie, F. and Sheridan, D**. C.** s.l. : SAE, Technical Paper Series, 1990. 900005,.*

22. A Study of Disc Brake Squeal Propensity Using a Parametric Finite Element Model", Vehicle Noise and Vibration. Lee, Y. S., Brooks, P. C., Barton, D. C. and Crolla, D. A. s.l. : IMechE Conference Transactions, 1998. C521/009/98.

23. Sheet cast disc-brake disc innovation through functional integration. Lathwesen, T. Deichmann and H. 16 - 18, Dresden, Germany : Proceedings of the Eurobrake, 2012.

24. Investigation of Product Performance of Al-Metal Matrix Composites Brake Disc using Finite Element Analysis. N Fatchurrohman, C D Marini, S Suraya, AKM Asif Iqbal. Pahang, Pekan, Pahang, Malaysia : Faculty of Manufacturing Engineering, Universiti Malaysia , 2016. 26600.

25. (http://www.dehs.umn.edu/asbestos/]. [Online]

26. [http://www.performancefriction.com/pages/pad_type.htm]. [Online]

27. Feist, Jared. Finite Element Modeling of Brake Pad Materials Performance. Connecticut : Rensselaer polytechnic Institute Hartford, December, 2014.

28. Kelly D. Moran, PhD. brake pad copper reduction- Metrics for tracking Progress. California : CASQA, December 1, 2014. 79.

29. www.toyota.dreamhosters.com/pages/hiace/specs.php. [Online]

30. www.toyota.co.mz/wp-content/uploads/2014/04/Toyota-Hiace.pdf. [Online]

31. Gillespie, Thomas D. fundamental of Vehicle dynamics . s.l. : Sosiety of Automotive Engineer(SAE). 15096.

32. Mathematical Modeling & Analysis of Brake Pad for Wear Characteristics. S. R. Kakad1, R.M. More2, Dr. D. N. Kamble3. 6, s.l. : 1Prof. S. R. Kakad, Department of Mechanical Engineering, SKNCOE, Pune, 2Prof. R.M. More, Department of Mechanical Engineering, SKNCOE, Pune, 3Dr.D.N.Kamble, Department of Mechanical Engineering, SAOE, kondhwa Pune, dnkamble81@gmail.com, 2017, Vol. 5. 2321-8169.

33. Ferdinand P. Beer, E. Russell Johnston, Jr., John T. DeWolf, David F. Mazurek. Mechanics of Materials,Seventh edition. New York : McGraw-Hill Education, 2 Penn Plaza, 2012, 2009, 2006, and 2002. 10121.

34. Rice, James R. SOLID MECHANICS. Harvard University, Cambridge, USA : School of Engineering and Applied Sciences, and Department of Earth and Planetary Sciences, Original version: October 1994, This revision: February 2010. 02138.

35. School of Engineering and Applied Sciences, and Department of Earth and Planetary Sciences. SOLID MECHANICS. [book auth.] James R. Rice. Cambridge University, USA : Harvard University, MA 02138 , October 1994. February 2010.

36. (www.engr.mun.ca/~katna/5931/Theories%20of%20Failure2.pdf). [Online]

37. (web.mae.ufl.edu/nkim/eas4200c/VonMisesCriterion.pdf). [Online]

38. PETER ANDRESEN, BRUCE ANTOLOVICH,STEPHEN D. ANTOLOVICH, ET,AL. fatigue and fracture. United States of America : ASM Handbook, 1996. ISBN 0-87170-385-8.

39. [https:// www.efatigue.com/glossary/]. [Online]

40. [https:/www.efatigue.com]. [Online]

41. International journal of Mechanical Engineering and technology, volume 7, issue date jan-fab 2016;

Structural and thermal analysis of Disc brake using solid works and ANSYS: Rakesh Jaiswal, Anupam Raj Jha, Anush Karki, Debayan Das, Pawan Jaiswal, Saurav Rajgadia and Ankit Basnet

42. [Sites: https://www.toyota.com.au/hiace/specifications/long-wheelbase-crew-van-diesel-auto]. [Online]

43. Sit: https://www.carsguide.com.au/toyota/hiace/price/2017/lwb?id=BdTMRlVV. [Online]

APPENDIX

Appendix I: Simulation Result

A) Al-MMC brake disc with Kevlar brake pad

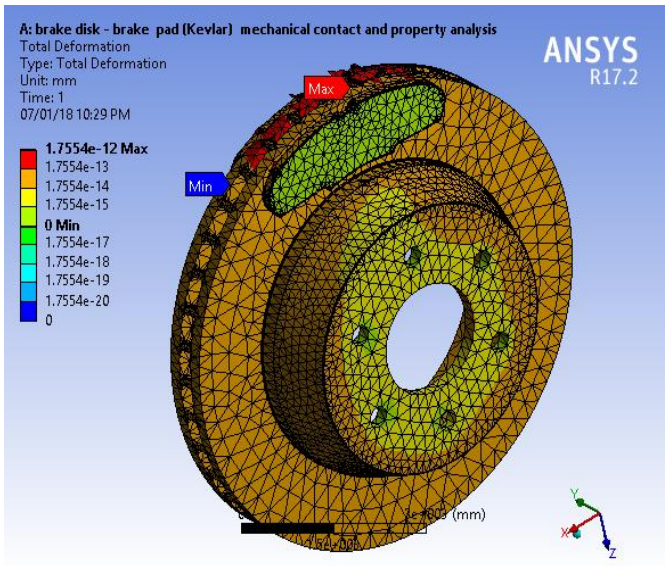

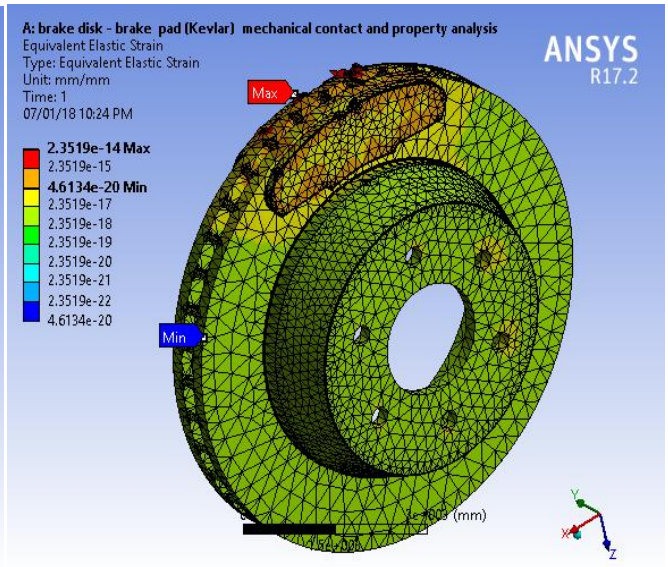

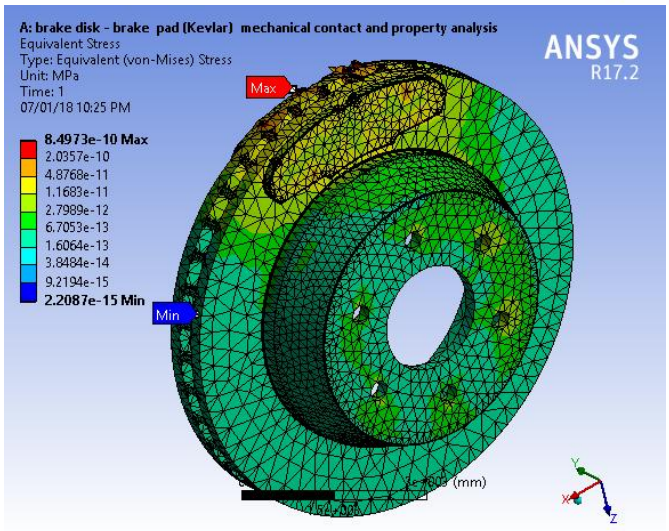

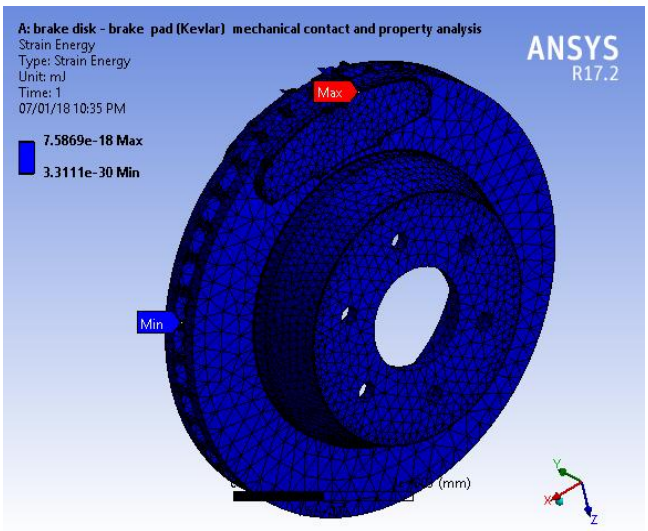

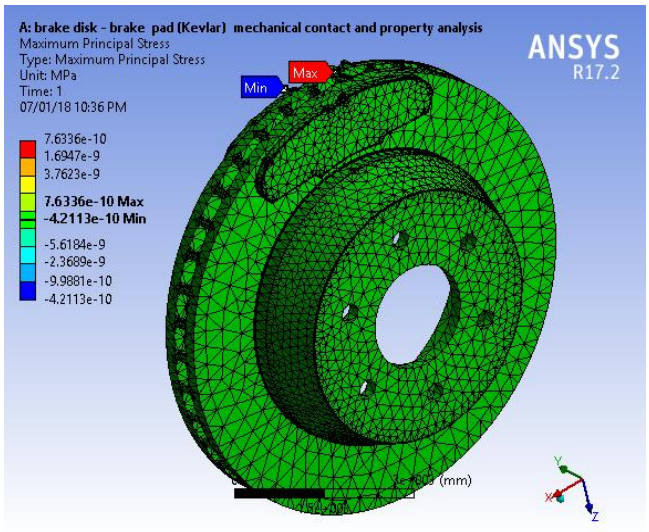
A: brake disk - brake pad (Kevlar) mechanical contact and property analysis
Maximum Principal Stress
Type: Maximum Principal Stress
Unit: MPa
Time: 1
07/01/18 10:36 PM
7.6336e-10
1.6947e-9
3.7623e-9
7.6336e-10 Max
-4.2113e-10 Min
-5.6184e-9
-2.3689e-9
-9.9881e-10
-4.2113e-10
ANSYS
R17.2
Max
Min
(mm)

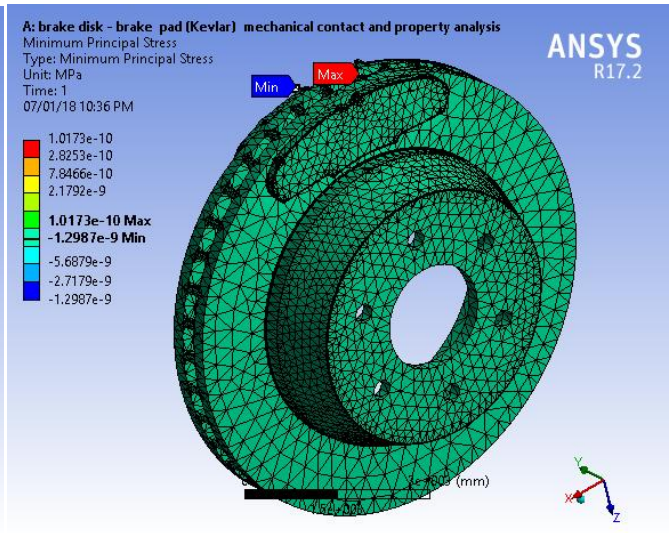
A: brake disk - brake pad (Kevlar) mechanical contact and property analysis
Minimum Principal Stress
Type: Minimum Principal Stress
Unit: MPa
Time: 1
07/01/18 10:36 PM
1.0173e-10
2.8253e-10
7.8466e-10
2.1792e-9
1.0173e-10 Max
-1.2987e-9 Min
-5.6879e-9
-2.7179e-9
-1.2987e-9
ANSYS
R17.2
Min
Max
(mm)

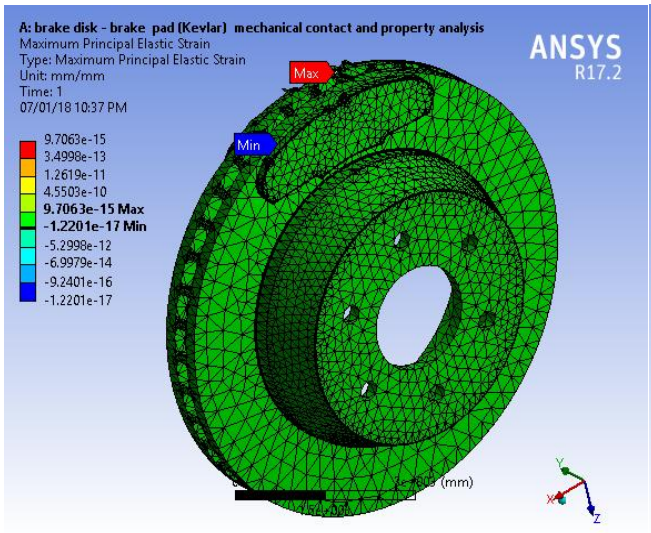
A: brake disk - brake pad (Kevlar) mechanical contact and property analysis
Maximum Principal Elastic Strain
Type: Maximum Principal Elastic Strain
Unit: mm/mm
Time: 1
07/01/18 10:37 PM
9.7063e-15
3.4998e-13
1.2619e-11
4.5503e-10
9.7063e-15 Max
-1.2201e-17 Min
-5.2998e-12
-6.9979e-14
-9.2401e-16
-1.2201e-17
ANSYS
R17.2
Max
Min
(mm)

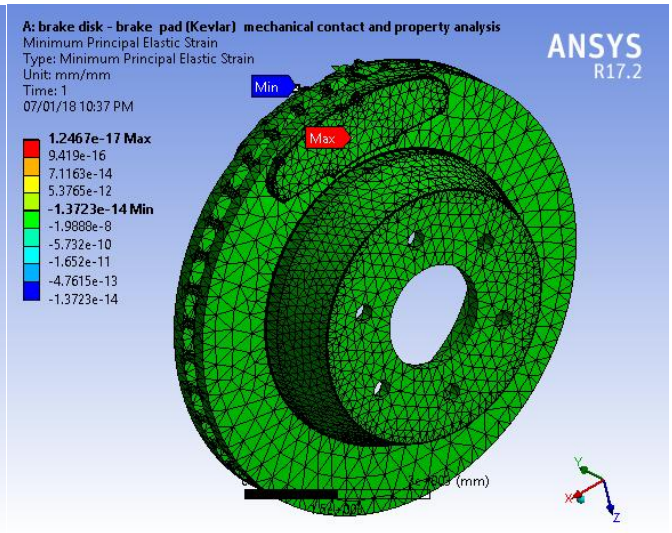
A: brake disk - brake pad (Kevlar) mechanical contact and property analysis
Minimum Principal Elastic Strain
Type: Minimum Principal Elastic Strain
Unit: mm/mm
Time: 1
07/01/18 10:37 PM
1.2467e-17 Max
9.419e-16
7.1163e-14
5.3765e-12
-1.3723e-14 Min
-1.9888e-8
-5.732e-10
-1.652e-11
-4.7615e-13
-1.3723e-14
ANSYS
R17.2
Min
Max
(mm)

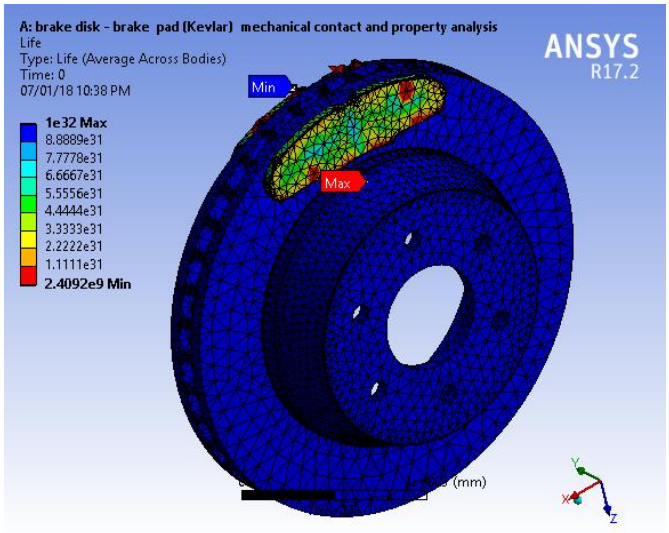
A: brake disk - brake pad (Kevlar) mechanical contact and property analysis
Life
Type: Life (Average Across Bodies)
Time: 0
07/01/18 10:38 PM
1e32 Max
8.8889e31
7.7778e31
6.6667e31
5.5556e31
4.4444e31
3.3333e31
2.2222e31
1.1111e31
2.4092e9 Min
ANSYS
R17.2
Min
Max
(mm)

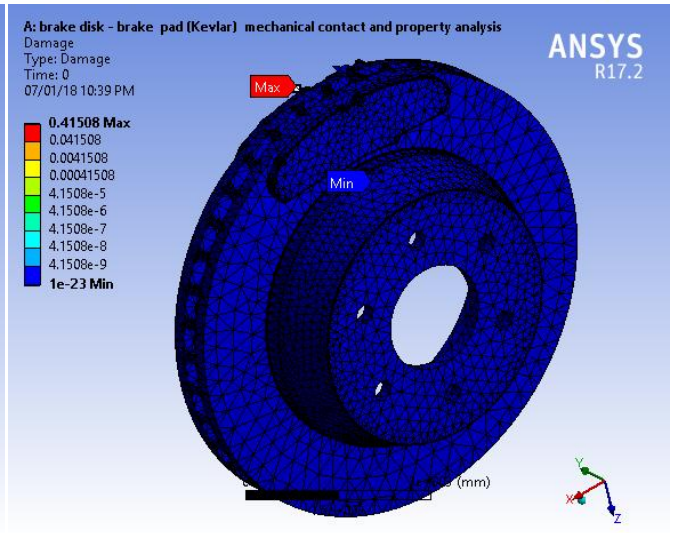
A: brake disk - brake pad (Kevlar) mechanical contact and property analysis
Damage
Type: Damage
Time: 0
07/01/18 10:39 PM
0.41508 Max
0.041508
0.0041508
0.00041508
4.1508e-5
4.1508e-6
4.1508e-7
4.1508e-8
4.1508e-9
1e-23 Min
ANSYS
R17.2
Max
Min
(mm)

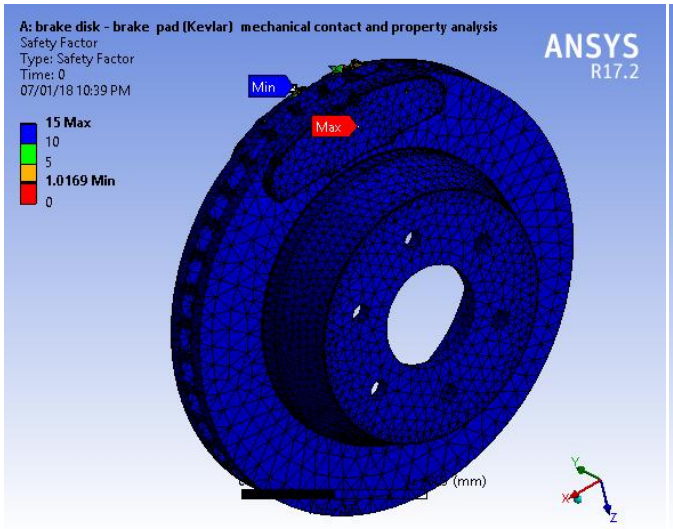

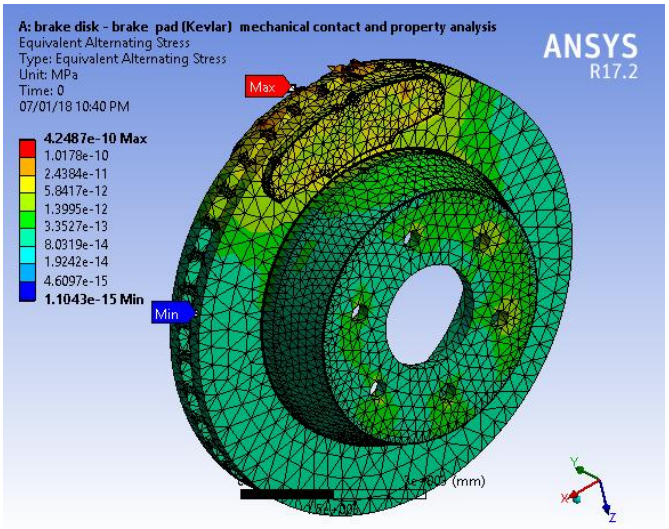

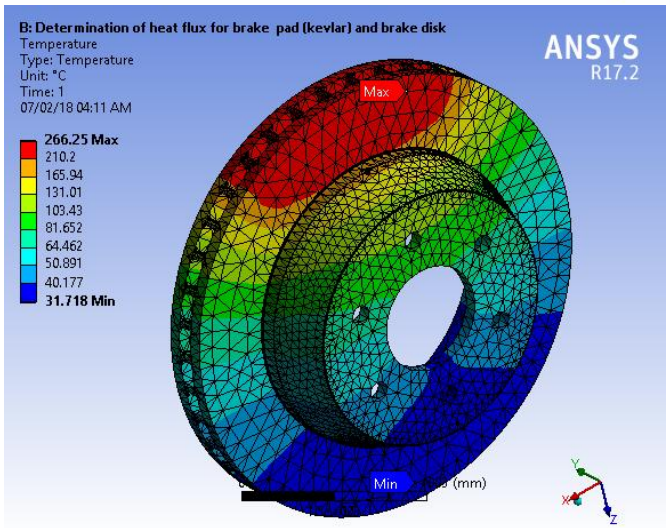

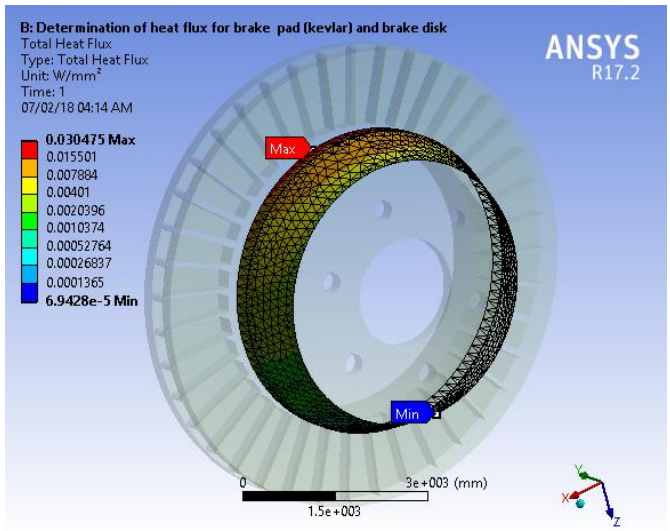

B) Al-MMC brake disc with Ceramic brake pad

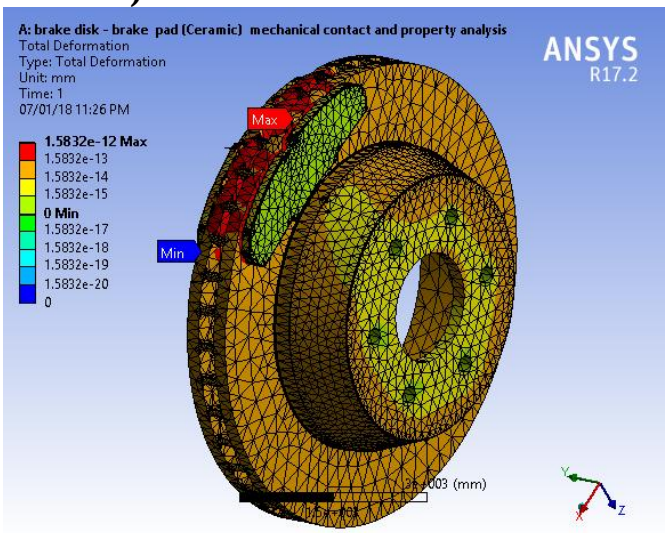

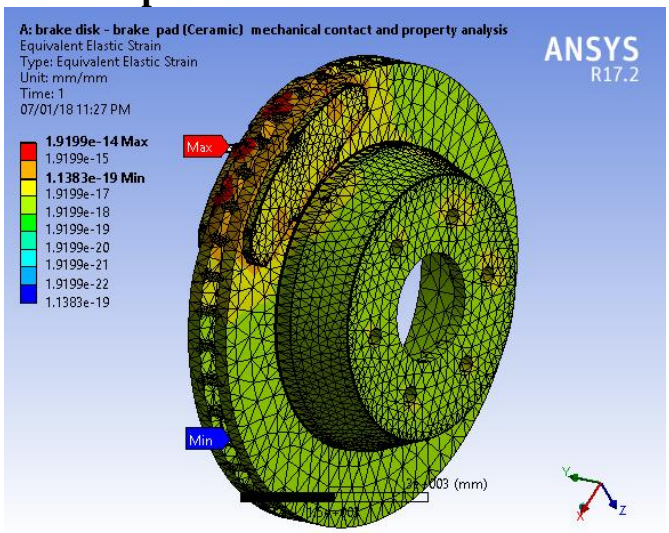

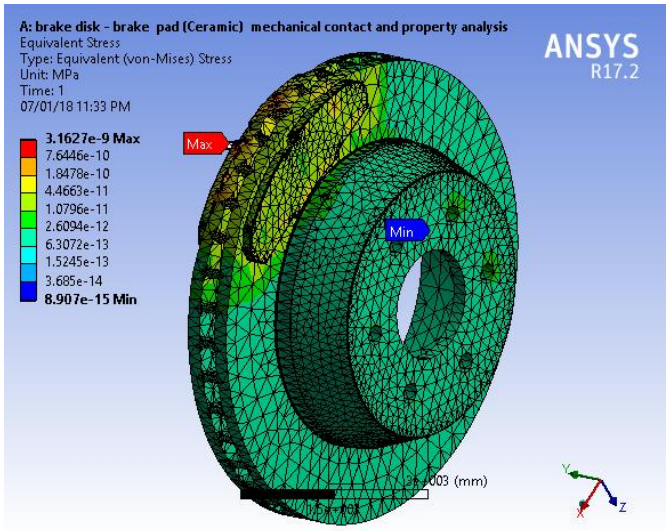
A: brake disk - brake pad (Ceramic) mechanical contact and property analysis
Equivalent Stress
Type: Equivalent (von-Mises) Stress
Unit: MPa
Time: 1
07/01/18 11:33 PM
3.1627e-9 Max
7.6446e-10
1.8478e-10
4.4663e-11
1.0796e-11
2.6094e-12
6.3072e-13
1.5245e-13
3.685e-14
8.907e-15 Min
Max
Min
ANSYS
R17.2

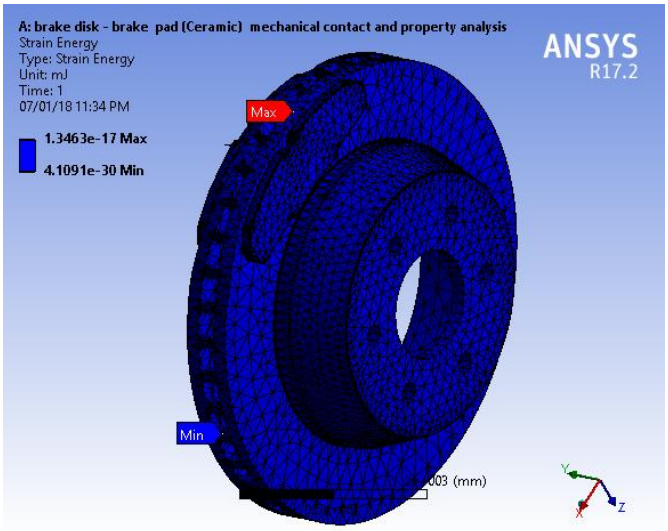
A: brake disk - brake pad (Ceramic) mechanical contact and property analysis
Strain Energy
Type: Strain Energy
Unit: mJ
Time: 1
07/01/18 11:34 PM
1.3463e-17 Max
4.1091e-30 Min
Max
Min
ANSYS
R17.2

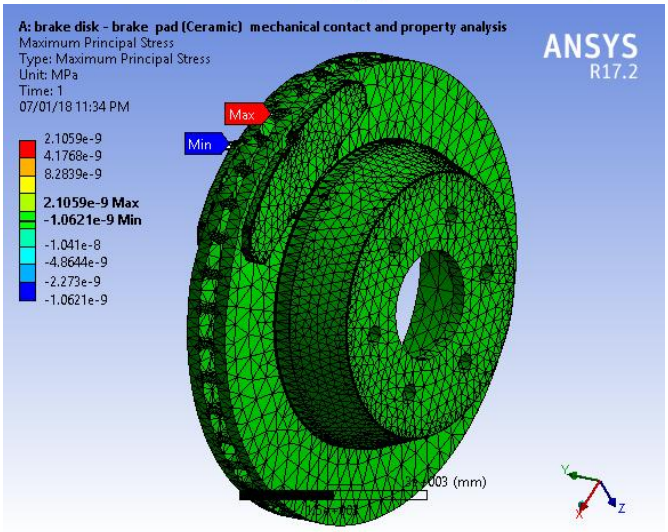
A: brake disk - brake pad (Ceramic) mechanical contact and property analysis
Maximum Principal Stress
Type: Maximum Principal Stress
Unit: MPa
Time: 1
07/01/18 11:34 PM
2.1059e-9
4.1768e-9
8.2839e-9
2.1059e-9 Max
-1.0621e-9 Min
-1.041e-8
-4.8644e-9
-2.273e-9
-1.0621e-9
Max
Min
ANSYS
R17.2

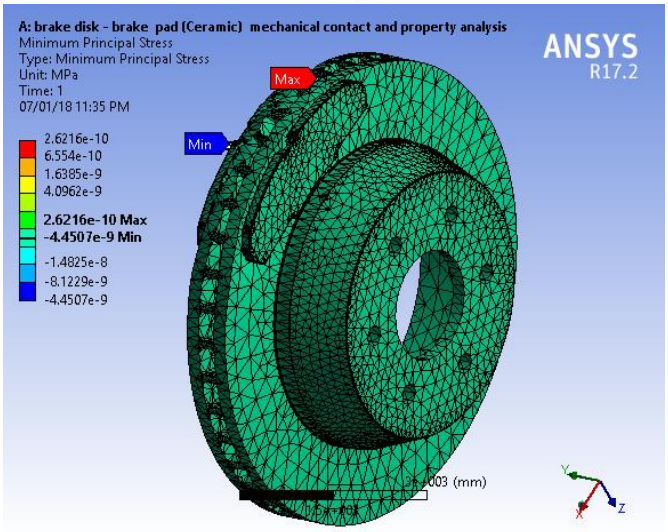
A: brake disk - brake pad (Ceramic) mechanical contact and property analysis
Minimum Principal Stress
Type: Minimum Principal Stress
Unit: MPa
Time: 1
07/01/18 11:35 PM
2.6216e-10
6.554e-10
1.6385e-9
4.0962e-9
2.6216e-10 Max
-4.4507e-9 Min
-1.4825e-8
-8.1229e-9
-4.4507e-9
Max
Min
ANSYS
R17.2

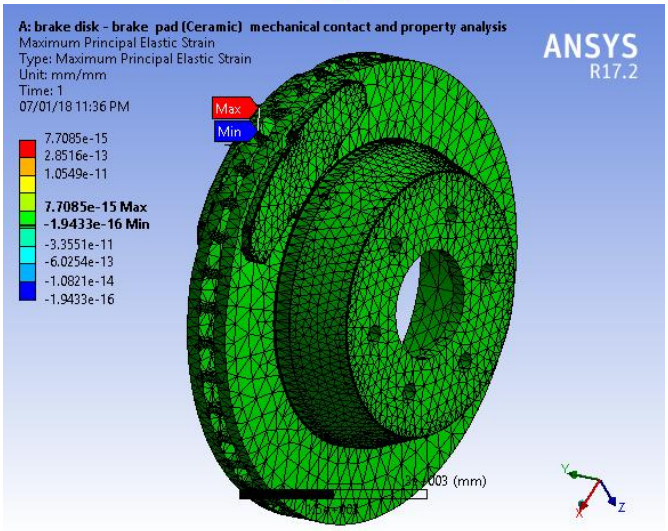
A: brake disk - brake pad (Ceramic) mechanical contact and property analysis
Maximum Principal Elastic Strain
Type: Maximum Principal Elastic Strain
Unit: mm/mm
Time: 1
07/01/18 11:36 PM
7.7085e-15
2.8516e-13
1.0549e-11
7.7085e-15 Max
-1.9433e-16 Min
-3.3551e-11
-6.0254e-13
-1.0821e-14
-1.9433e-16
Max
Min
ANSYS
R17.2

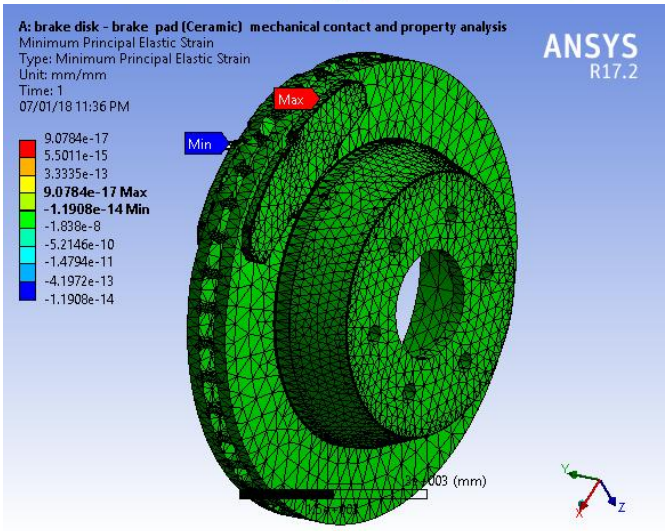
A: brake disk - brake pad (Ceramic) mechanical contact and property analysis
Minimum Principal Elastic Strain
Type: Minimum Principal Elastic Strain
Unit: mm/mm
Time: 1
07/01/18 11:36 PM
9.0784e-17
5.5011e-15
3.3335e-13
9.0784e-17 Max
-1.1908e-14 Min
-1.838e-8
-5.2146e-10
-1.4794e-11
-4.1972e-13
-1.1908e-14
Max
Min
ANSYS
R17.2

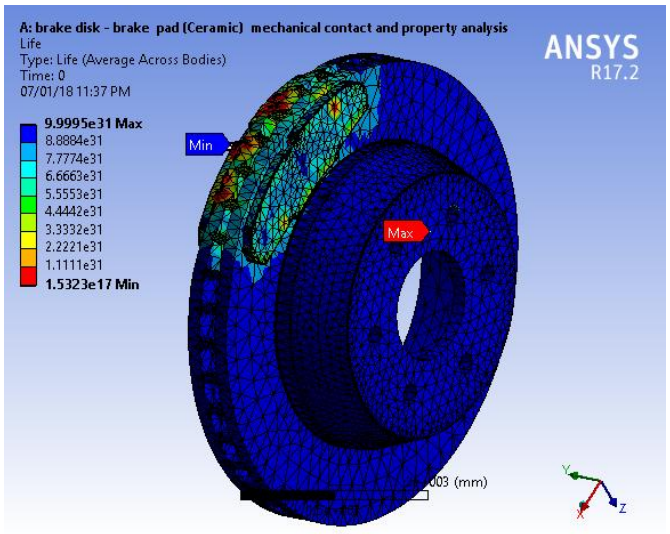
A: brake disk - brake pad (Ceramic) mechanical contact and property analysis
Life
Type: Life (Average Across Bodies)
Time: 0
07/01/18 11:37 PM
9.9995e31 Max
8.8884e31
7.7774e31
6.6663e31
5.5553e31
4.4442e31
3.3332e31
2.2221e31
1.1111e31
1.5323e17 Min
Min
Max
ANSYS
R17.2

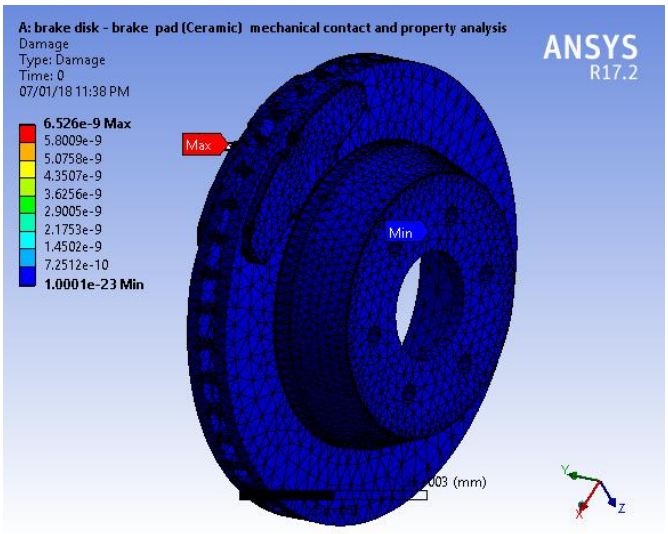
A: brake disk - brake pad (Ceramic) mechanical contact and property analysis
Damage
Type: Damage
Time: 0
07/01/18 11:38 PM
6.526e-9 Max
5.8009e-9
5.0758e-9
4.3507e-9
3.6256e-9
2.9005e-9
2.1753e-9
1.4502e-9
7.2512e-10
1.0001e-23 Min
Max
Min
ANSYS
R17.2

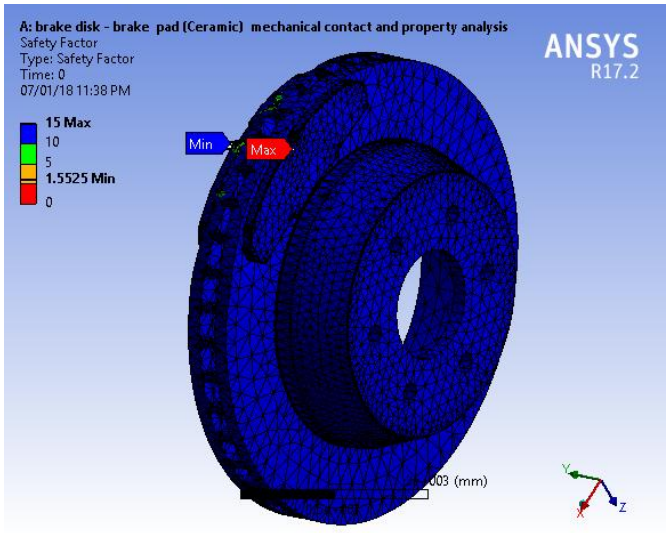
A: brake disk - brake pad (Ceramic) mechanical contact and property analysis
Safety Factor
Type: Safety Factor
Time: 0
07/01/18 11:38 PM
15 Max
10
5
1.5525 Min
0
Min
Max
ANSYS
R17.2

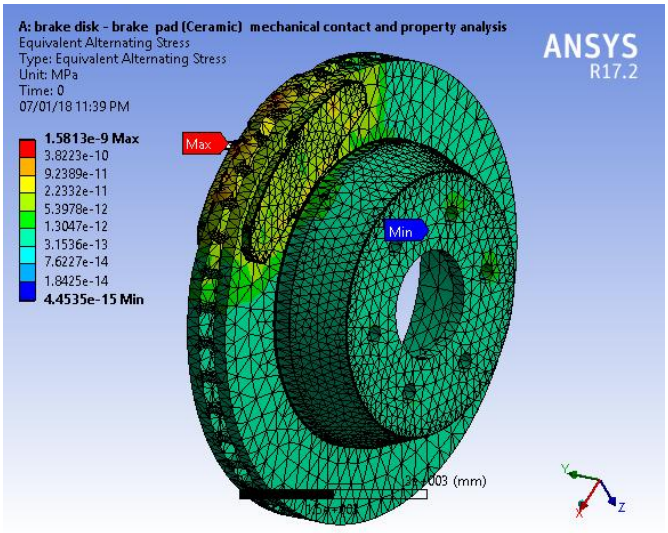
A: brake disk - brake pad (Ceramic) mechanical contact and property analysis
Equivalent Alternating Stress
Type: Equivalent Alternating Stress
Unit: MPa
Time: 0
07/01/18 11:39 PM
1.5813e-9 Max
3.8223e-10
9.2389e-11
2.2332e-11
5.3978e-12
1.3047e-12
3.1536e-13
7.6227e-14
1.8425e-14
4.4535e-15 Min
Max
Min
ANSYS
R17.2

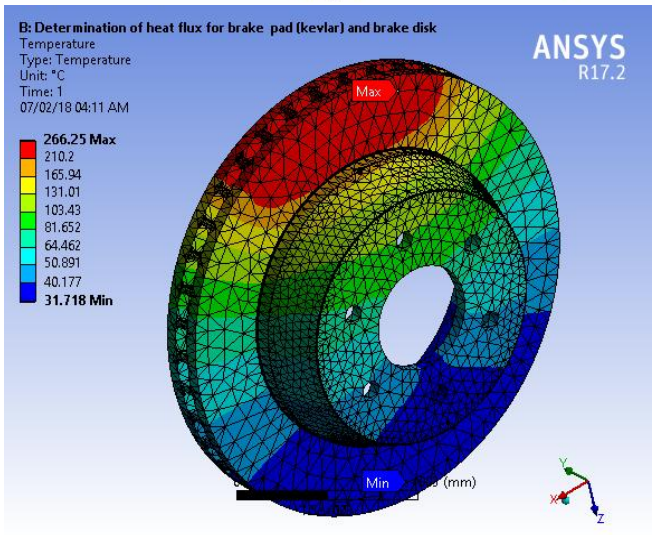
B: Determination of heat flux for brake pad (kevlar) and brake disk
Temperature
Type: Temperature
Unit: °C
Time: 1
07/02/18 04:11 AM
266.25 Max
210.2
165.94
131.01
103.43
81.652
64.462
50.891
40.177
31.718 Min
Max
Min
ANSYS
R17.2

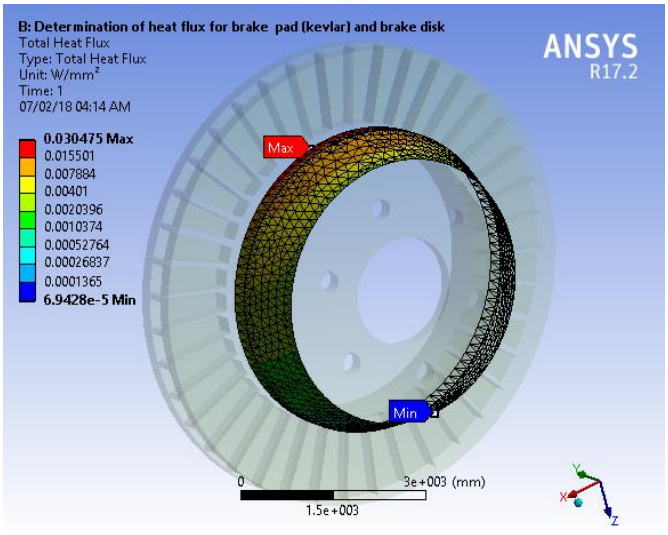
B: Determination of heat flux for brake pad (kevlar) and brake disk
Total Heat Flux
Type: Total Heat Flux
Unit: W/mm²
Time: 1
07/02/18 04:14 AM
0.030475 Max
0.015501
0.007884
0.00401
0.0020396
0.0010374
0.00052764
0.00026837
0.0001365
6.9428e-5 Min
Max
Min
0
3e+003 (mm)
1.5e+003
ANSYS
R17.2

C) Al-MMC brake disc with Aluminum alloy brake pad

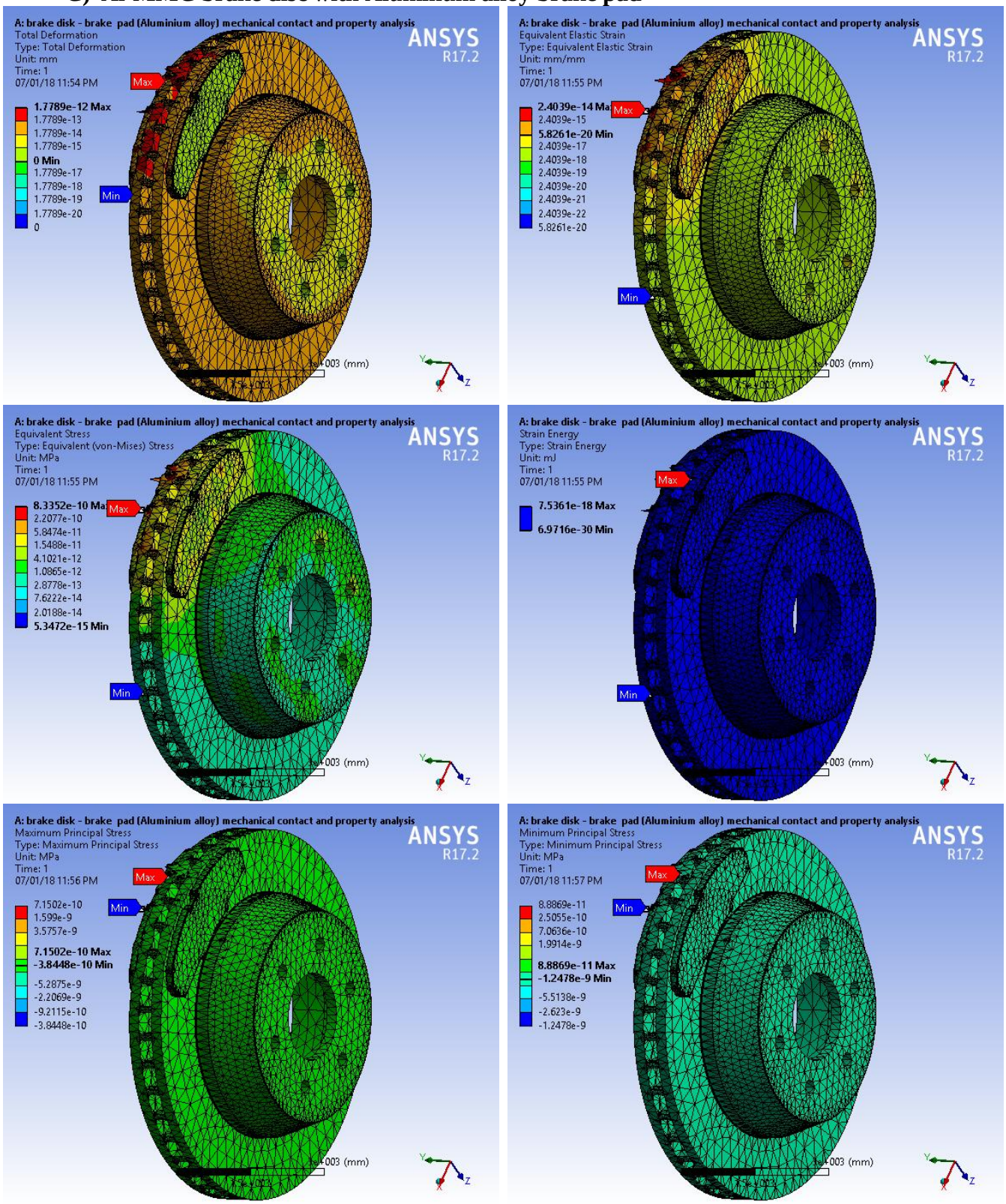

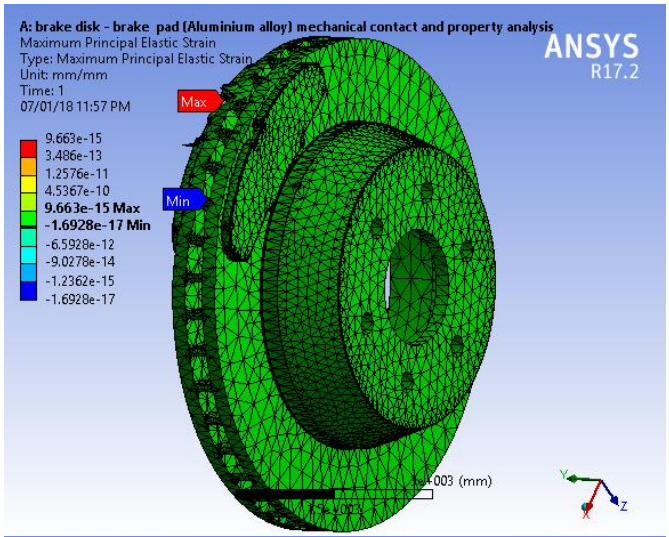
A: brake disk - brake pad (Aluminium alloy) mechanical contact and property analysis
Maximum Principal Elastic Strain
Type: Maximum Principal Elastic Strain
Unit: mm/mm
Time: 1
07/01/18 11:57 PM
9.663e-15
3.486e-13
1.2576e-11
4.5367e-10
9.663e-15 Max
-1.6928e-17 Min
-6.5928e-12
-9.0278e-14
-1.2362e-15
-1.6928e-17
Max
Min
ANSYS
R17.2
003 (mm)

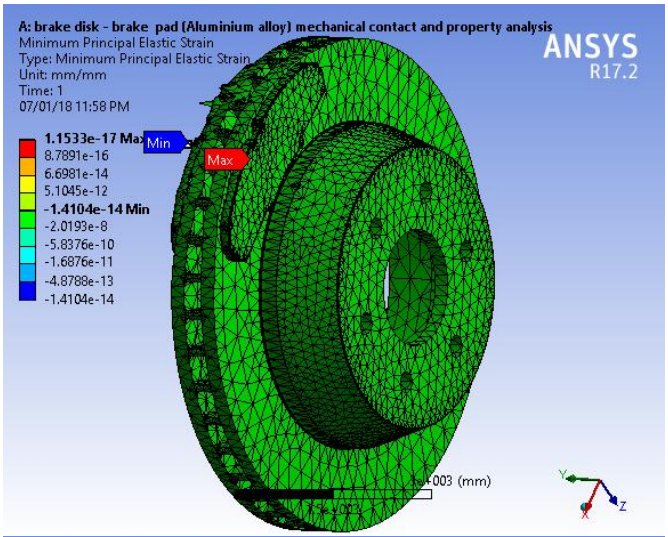
A: brake disk - brake pad (Aluminium alloy) mechanical contact and property analysis
Minimum Principal Elastic Strain
Type: Minimum Principal Elastic Strain
Unit: mm/mm
Time: 1
07/01/18 11:58 PM
1.1533e-17 Ma
8.7891e-16
6.6981e-14
5.1045e-12
-1.4104e-14 Min
-2.0193e-8
-5.8376e-10
-1.6876e-11
-4.8788e-13
-1.4104e-14
Min
Max
ANSYS
R17.2
003 (mm)

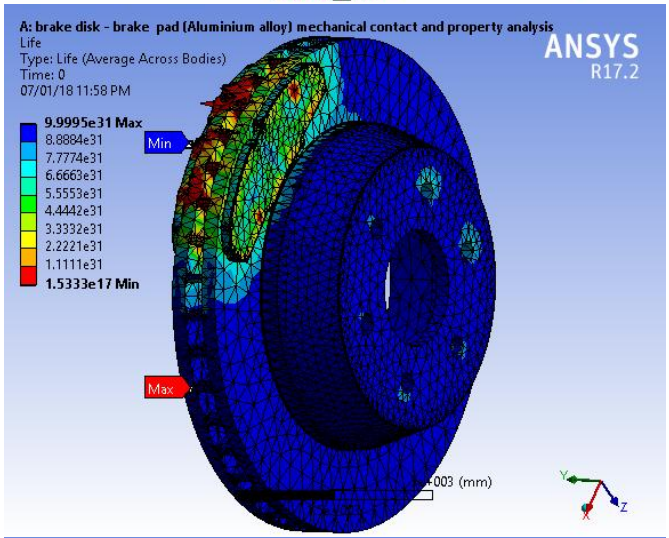
A: brake disk - brake pad (Aluminium alloy) mechanical contact and property analysis
Life
Type: Life (Average Across Bodies)
Time: 0
07/01/18 11:58 PM
9.9995e31 Max
8.8884e31
7.7774e31
6.6663e31
5.5553e31
4.4442e31
3.3332e31
2.2221e31
1.1111e31
1.5333e17 Min
Min
Max
ANSYS
R17.2
003 (mm)

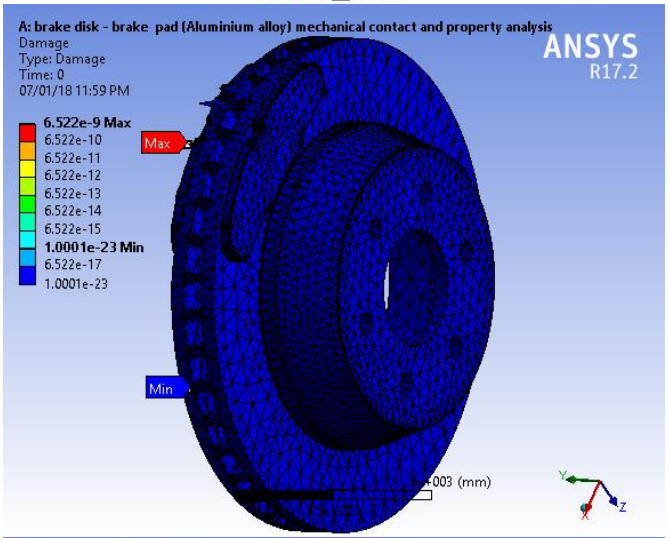
A: brake disk - brake pad (Aluminium alloy) mechanical contact and property analysis
Damage
Type: Damage
Time: 0
07/01/18 11:59 PM
6.522e-9 Max
6.522e-10
6.522e-11
6.522e-12
6.522e-13
6.522e-14
6.522e-15
1.0001e-23 Min
6.522e-17
1.0001e-23
Max
Min
ANSYS
R17.2
003 (mm)

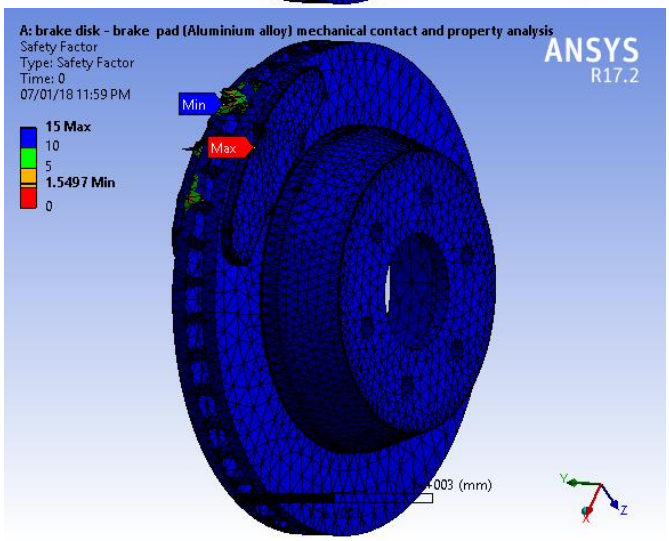
A: brake disk - brake pad (Aluminium alloy) mechanical contact and property analysis
Safety Factor
Type: Safety Factor
Time: 0
07/01/18 11:59 PM
15 Max
10
5
1.5497 Min
0
Min
Max
ANSYS
R17.2
003 (mm)

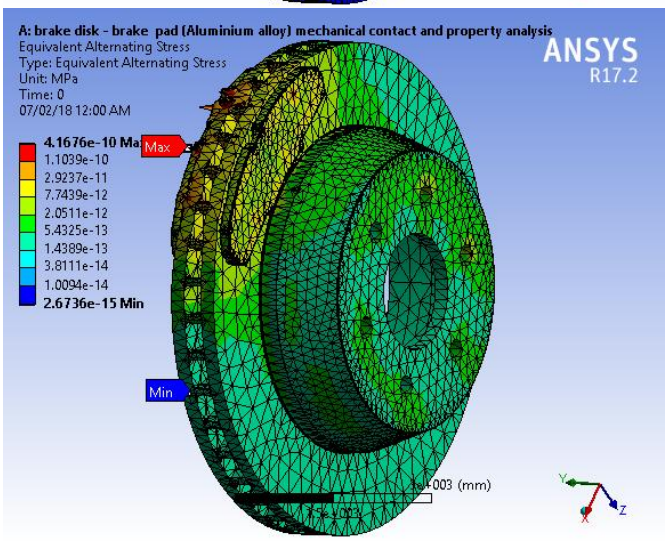
A: brake disk - brake pad (Aluminium alloy) mechanical contact and property analysis
Equivalent Alternating Stress
Type: Equivalent Alternating Stress
Unit: MPa
Time: 0
07/02/18 12:00 AM
4.1676e-10 Ma
1.1039e-10
2.9237e-11
7.7439e-12
2.0511e-12
5.4325e-13
1.4389e-13
3.8111e-14
1.0094e-14
2.6736e-15 Min
Max
Min
ANSYS
R17.2
003 (mm)

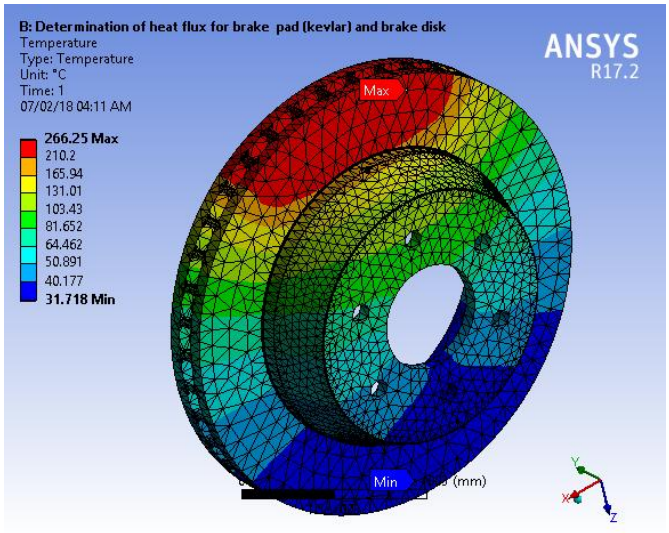
B: Determination of heat flux for brake pad (kevlar) and brake disk
Temperature
Type: Temperature
Unit: °C
Time: 1
07/02/18 04:11 AM
266.25 Max
210.2
165.94
131.01
103.43
81.652
64.462
50.891
40.177
31.718 Min
ANSYS
R17.2
Max
Min
(mm)

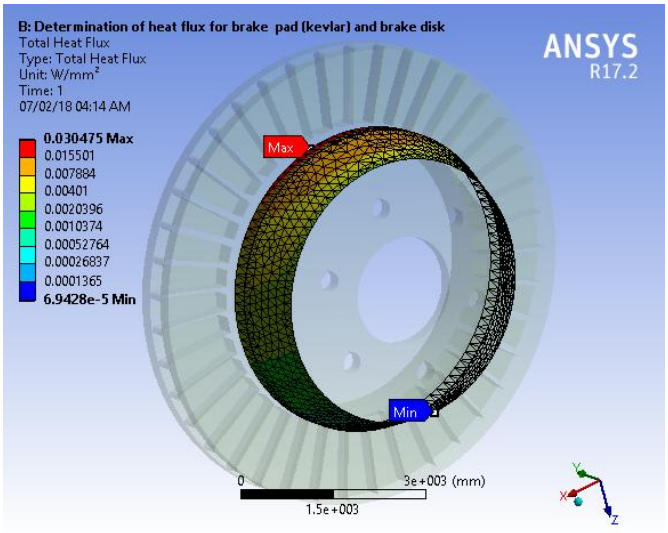
B: Determination of heat flux for brake pad (kevlar) and brake disk
Total Heat Flux
Type: Total Heat Flux
Unit: W/mm²
Time: 1
07/02/18 04:14 AM
0.030475 Max
0.015501
0.007884
0.00401
0.0020396
0.0010374
0.00052764
0.00026837
0.0001365
6.9428e-5 Min
ANSYS
R17.2
Max
Min
0
3e+003 (mm)
1.5e+003

Appendix II: Experimental Result

	GEOLOGICAL SURVEY OF ETHIOPIA	Doc.Number GLD/F5.10-2	Version No: 1
	GEOCHEMICAL LABORATORY DIRECTORATE		Page 1 of 1
Document Title:	Base Metal Analysis Report	Effective Date:	May, 2017

Issued Date: 16/04/2018

Originator: - Oliyadi Dereje

Request No; GLD/TR//0154/18

Sample type: - Rock

Report No: - GLD/TR/0211/18

Date Submitted: - 23/03/2018

Sample Preparation: - 200 Mesh

Analytical Result: - ppm

Number of Sample: - One (1)

Analytical Method: - Four acid attack (HCl, HNO3, HClO4, HF) and AAS finish.

Collector's Code	Cu(ppm)	Zn(ppm)	Pb(ppm)	Co(ppm)	Ni(ppm)
O.D-01	13,360.00	686.40	<0.01	58.60	30.00

N.B:

- ppm: parts per million
- Cu for Copper, Zn for Zinc, Pb for Lead, Co for Cobalt and Ni for Nickel
- Dup Duplicate

Analysts

Dessalew Bitew
Almaz Eticha
Derara Gabissa

Checked By

for Gethet Zeleke

Quality Control

Awash Yirga

Geological Survey of Ethiopia Central Geological Laboratory

Geochemical Laboratory Directorate
Tell: +251113204161

Appendix III: Specification of Toyota Hiace

SPECIFICATION OF TOYOTA-HIACE MINIBUS 12 SEATS, [**42**], [**43**].

EXTERIOR DIMINESIONS	**280 SWB**
Overall length (mm)	4,795
Overall width (mm)	1,800
Overall height (mm)	2,000
Front track/real track (mm)	1,560/1,540
Front overhang (mm)	870
Rear overhang (mm)	940
INTERIOR DIMINESIONS	
Load length (mm)	2,335
Load width (mm)	1,650
Load height (mm)	1,420
ENGINE	**2.5 D-4D 95**
Type	4 cylinders in-line
Fuel type	Diesel
Valve mechanism	DOHC 16-Valve
Exhaust System	Turbocharger
Intake System	Intercooler, swirl control Vale
Capacity (cc)	2,494
Bore X Stroke (mm)	92.0 x 93.8
Compression ratio	17.4:1
Max Power (bhp @ rpm)	94 @ 3,600
Max power (NM @ rpm)	230 @ 1,400-2800
PERFORMANCE	
Max Speed (mph)	91
Acceleration 0-62mph (sec)	22.4
Combined fuel consumption (mpg)	32.1
CO_2 emissions (combined)	221
WHEELS	
Wheel size (in)	15
Tyre size	195/70 R15
BRAKES	
Front (diameter mm)	Ventilated discs (285)
Real (diameter mm)	Drums (270)
WEIGHT	**2.5-D4D-95**
Gross Vehicle weight (kg)	2,800
STEERING	
Type	Rack and pinion
Ratio	20.6:1
Turns lock-to-lock	4.0
Minimum turning radius tyre (m)	5.5